Report Prepared by:

Michael T. Walsh
Alberto A. Sagüés

FINAL REPORT

Durability Performance of Submerged Concrete Structures - Phase 2

Contract No. BDV25 977-12

Final Report to Florida Department of Transportation

A. A. Sagüés
Principal Investigator
Department of Civil and Environmental Engineering

UNIVERSITY OF SOUTH FLORIDA
COLLEGE OF ENGINEERING

Tampa, FL 33620
September 2015

DISCLAIMER

The opinions, findings, and conclusions expressed in this publication are those of the authors and not necessarily those of the State of Florida Department of Transportation.

UNIVERSAL CONVERSION TABLE

SI* (MODERN METRIC) CONVERSION FACTORS

APPROXIMATE CONVERSIONS TO SI UNITS

Symbol	When You Know	Multiply By	To Find	Symbol
		LENGTH		
in	inches	25.4	millimeters	mm
ft	feet	0.305	meters	m
yd	yards	0.914	meters	m
mi	miles	1.61	kilometers	km
		AREA		
in^2	square inches	645.2	square millimeters	mm^2
ft^2	square feet	0.093	square meters	m^2
yd^2	square yard	0.836	square meters	m^2
ac	acres	0.405	hectares	ha
mi^2	square miles	2.59	square kilometers	km^2
		VOLUME		
fl oz	fluid ounces	29.57	milliliters	mL
gal	gallons	3.785	liters	L
ft^3	cubic feet	0.028	cubic meters	m^3
yd^3	cubic yards	0.765	cubic meters	m^3
	NOTE: volumes greater than 1000 L shall be shown in m^3			
		MASS		
oz	ounces	28.35	grams	g
lb	pounds	0.454	kilograms	kg
T	short tons (2000 lb)	0.907	megagrams (or "metric ton")	Mg (or "t")
		TEMPERATURE (exact degrees)		
°F	Fahrenheit	5 (F-32)/9 or (F-32)/1.8	Celsius	°C
		ILLUMINATION		
fc	foot-candles	10.76	lux	lx
fl	foot-Lamberts	3.426	$candela/m^2$	cd/m^2
		FORCE and PRESSURE or STRESS		
lbf	poundforce	4.45	newtons	N
lbf/in^2	poundforce per square inch	6.89	kilopascals	kPa

APPROXIMATE CONVERSIONS FROM SI UNITS

Symbol	When You Know	Multiply By	To Find	Symbol
		LENGTH		
mm	millimeters	0.039	inches	in
m	meters	3.28	feet	ft
m	meters	1.09	yards	yd
km	kilometers	0.621	miles	mi
		AREA		
mm^2	square millimeters	0.0016	square inches	in^2
m^2	square meters	10.764	square feet	ft^2
m^2	square meters	1.195	square yards	yd^2
ha	hectares	2.47	acres	ac
km^2	square kilometers	0.386	square miles	mi^2
		VOLUME		
mL	milliliters	0.034	fluid ounces	fl oz
L	liters	0.264	gallons	gal
m^3	cubic meters	35.314	cubic feet	ft^3
m^3	cubic meters	1.307	cubic yards	yd^3
		MASS		
g	grams	0.035	ounces	oz
kg	kilograms	2.202	pounds	lb
Mg (or "t")	megagrams (or "metric ton")	1.103	short tons (2000 lb)	T
		TEMPERATURE (exact degrees)		
°C	Celsius	1.8C+32	Fahrenheit	°F
		ILLUMINATION		
lx	lux	0.0929	foot-candles	fc
cd/m^2	$candela/m^2$	0.2919	foot-Lamberts	fl
		FORCE and PRESSURE or STRESS		
N	newtons	0.225	poundforce	lbf
kPa	kilopascals	0.145	poundforce per square inch	lbf/in^2

*SI is the symbol for the International System of Units. Appropriate rounding should be made to comply with Section 4 of ASTM E380.

TECHNICAL REPORT DOCUMENTATION PAGE

<table>
<tr><td colspan="2">1. Report No.</td><td>2. Government Accession No.</td><td colspan="2">3. Recipient's Catalog No.</td></tr>
<tr><td colspan="3" rowspan="2">4. Title and Subtitle
Durability Performance of Submerged Concrete Structures - Phase 2</td><td colspan="2">5. Report Date
September 2015</td></tr>
<tr><td colspan="2">6. Performing Organization Code</td></tr>
<tr><td colspan="3">7. Author(s)
M.T. Walsh and A.A. Sagüés</td><td colspan="2">8. Performing Organization Report No.</td></tr>
<tr><td colspan="3" rowspan="2">9. Performing Organization Name and Address
Department of Civil and Environmental Engineering
University of South Florida (USF)
Tampa, FL 33620</td><td colspan="2">10. Work Unit No. (TRAIS)</td></tr>
<tr><td colspan="2">11. Contract or Grant No.
BDV25 977-12</td></tr>
<tr><td colspan="3" rowspan="2">12. Sponsoring Agency Name and Address
Florida Department of Transportation
605 Suwannee St. MS 30 Tallahassee, Florida 32399
(850)414-4615</td><td colspan="2">13. Type of Report and Period Covered
Final Report 02/10/2011 - 09/30/2015</td></tr>
<tr><td colspan="2">14. Sponsoring Agency Code</td></tr>
<tr><td colspan="5">15. Supplementary Notes</td></tr>
<tr><td colspan="5">16. Abstract: This project determined that severe corrosion of steel can occur in the submerged portions of reinforced concrete structures in marine environments. Field studies of decommissioned pilings from Florida bridges revealed multiple instances of strong corrosion localization, showing appreciable local loss of steel cross-section. Quantitative understanding of the phenomenon and its causes has been developed, and a predictive model was created based on that understanding. Corrosion rate estimates and the extent of corrosion localization from the field observations were consistent with the results of the predictive model. The most likely explanation for the phenomenon is that cathodic reaction rates under oxygen diffusional limitation that are negligible in cases of uniform corrosion can support substantial corrosion rates in cases of localized corrosion. Modeling projected that, with use of sacrificial anode cathodic protection, corrosion in the submerged zone could be virtually eliminated, together with significant reduction of the rate of corrosion damage progression in the low elevation zone above water. Continuation work should be conducted to define an alternative limit state other than visible external cracks and spalls for submerged reinforced concrete, and for determination of the possible structural consequences of this form of corrosion, as well as to assess the technical feasibility and cost/benefit aspects of incorporating protective anodes in new pilings.</td></tr>
<tr><td colspan="2">17. Key Words
Reinforced concrete, submerged, corrosion, damage, modeling, reinforcing steel, durability, concrete.</td><td colspan="3">18. Distribution Statement
No Restriction
This report is available to the public through the NTIS, Springfield, VA 22161</td></tr>
<tr><td>19. Security Classif. (of this report)
Unclassified</td><td colspan="2">20. Security Classif. (of this page)
Unclassified</td><td>21. No. of Pages 107</td><td>22. Price</td></tr>
</table>

ACKNOWLEDGEMENT

The assistance of personnel at the Florida Department of Transportation (FDOT) State Materials Office in conducting the field investigations is gratefully acknowledged. The assistance of student participants in the University of South Florida, College of Engineering Research Experience for Undergraduates, is also acknowledged.

EXECUTIVE SUMMARY

The Florida Department of Transportation (FDOT) has more than 3,000 bridges on salt water, most with concrete with steel reinforcing bars, pre-tensioned or post-tensioned steel, or other embedded steel. Corrosion of the embedded steel, triggered by chloride ion intrusion, forms expansive products that cause spalling and cracks on the concrete cover. The damage is most evident in the portion of the substructure above water, especially at low elevations in the splash-evaporation zone, where evaporative chloride concentration is most severe. Because external signs of damage are seen earliest there, much of the corrosion control effort has focused on above-water corrosion, for which FDOT has successfully adopted the use of highly impermeable concrete and a thick concrete cover. In contrast with the attention given to the above-water zone, potentially severe corrosion in the submerged portion has remained comparatively unattended in Florida and worldwide. Part of the reason for that limited attention is the theoretical expectation of lower corrosion there because of reduced oxygen supply. However, the near absence of reports of underwater corrosion reflects in part the lower frequency of inspection of that zone, which is harder to access and where features like cracks and spalls can be easily hidden by deposits and marine growth. Moreover, corrosion products there may be fluid and not cause concrete cracking, but still extensive steel cross-section loss could exist undetected. Recent advances in knowledge of basic corrosion issues of steel in concrete have reopened concern about possible submerged zone corrosion by noting that lowered oxygen supply to the steel surface in submerged concrete does not guarantee uniformly low corrosion rates there. Even if oxygen supply was restricted to the submerged zone, in cases where steel activation is limited to a few spots, the cumulative extent of oxygen reduction over a much larger steel area in immersed concrete could result in severe concentrated corrosion. Such concerns are of special relevance as ambitious durability goals for FDOT structures are now in place, and ever longer design life is being considered. Damage rates that might have been tolerable with shorter service life goals now have many decades to proceed, possibly undetected given the limited information available on corrosion behavior in the submerged zone. This investigation was conducted in order to resolve the underlying questions in submerged concrete corrosion, to assist in improving future design, and to guide decisions on corrosion control of existing structures.

The investigation was conducted by means of assessment of corrosion in decommissioned field piles and an existing submerged footer chamber and formulation of predictive modeling based on the field findings and basic corrosion science. The model was then applied to evaluate the possible extent of corrosion in typical FDOT pilings and the feasibility of corrosion control by means of sacrificial cathodic protection anodes.

Field assessment included study of sixty-year-old bridge piles, both pre-stressed and conventional rebar-reinforced, from the decommissioned Sunshine Skyway Bridge

Fishing Pier, the Pinellas Bayway Drawbridge, and the Sunrise Key Bridge, as well as submerged footers in the present Sunshine Skyway Bridge. The most notable finding from the field examination of piles was the evidence of severe localized corrosion in the submerged zone of the piles, substantiating concerns indicated above. The corrosion was limited to relatively short segments (e.g., 10% or less) of the steel length, while the large majority of the rest of the steel showed little evidence of wastage. In the corroding sections, the steel experienced sometimes severe loss of cross-section (e.g., 20% to 30%). A limited survey of the Sunshine Skyway footer chamber revealed one instance of localized corrosion of epoxy-coated rebar at a preexisting concrete crack location. The survey involved evaluating epoxy coating adhesion and corrosion status of rebar exposed by coring. Adhesion was poor in all three of the three sites evaluated. Two of the three sites were situated on pre-existing cracks and the rebar in one of the two crack sites was actively corroding.

Corrosion modeling was based on a generic substructure column with above- and below-water sections to explore the integral behavior of the system. Concrete model input parameters were assigned values representing a broad range of conditions encountered in Florida bridges, from older structures with high concrete permeability and low electric resistivity, such as that encountered in some of the Florida Keys bridges that experienced early corrosion in the 1980s, to much more impervious modern design approaching conditions encountered with the use of FDOT Class V concrete with low water-to-cement ratio, high cement content, and pozzolanic admixtures. The model output projected the extent of damage as a function of structure age, over a nominal 100-year period. Consistent with field observations of above-water corrosion from previous studies, the model output indicated that the high permeability concrete structures were expected to begin showing some signs of deterioration at times on the order of one decade, while those with very low permeability would start showing damage at times between several decades and more than 100 years of age. For the submerged region and for high permeability concrete as that in the field pile examinations, the model predicted damage on the order of that actually observed, supporting the validity of the modeling approach. For the modern, highest quality concretes in sound condition, the model prognosis indicated some concern for submerged zone corrosion only at ages on the order of the present 75-year design service life. However, it is noted that those projections have not evaluated the case of cracked concrete. If cracks were to occur for example during pile driving, chloride penetration and hence corrosion initiation at the crack/steel intersection could happen very fast. Thus, the possibility of topical severe corrosion at the spots affected by cracking could not be ignored even though concrete permeability was very low. Importantly, the model calculations showed that under some circumstances eliminating corrosion in the evaporative/splash zone could increase corrosion vulnerability of steel in the submerged region, as otherwise beneficial protective electrochemical coupling would no longer exist.

The modeling projected also that with use of sacrificial anode cathodic protection (SACP), corrosion in the submerged zone could be virtually eliminated, together with

significant reduction of the rate of corrosion damage progression in the low elevation zone above water.

For consideration as a path forward, the results of this project indicate a need for defining an alternative limit state (i.e., other than visible external cracks and spalls) for submerged reinforced concrete and for determination of the possible structural consequences of this form of corrosion in future work. Continuation work should be conducted to assess the technical feasibility and cost-benefit aspects of incorporating anodes or provisions for anode placement in future specification guidelines for bridge piling and other submerged elements. Field investigations should be extended to include modern piling.

It is also recommended that a next-generation modeling tool be developed in continuation work for more accurate assessment of the extent and consequences of corrosion in submerged substructure. New features of importance to be incorporated should include effect of preexisting cracking, statistical dispersion of more system properties, and three-dimensional representation of the system.

TABLE OF CONTENTS

LIST OF FIGURES

LIST OF TABLES

LIST OF SYMBOLS

C	oxygen concentration
C_{SO}	oxygen concentration at the steel surface
C_O	oxygen concentration at the external concrete surface
C_s	chloride surface concentration
C_{sB}	chloride surface concentration at bottom of column
C_{sP}	chloride surface concentration at the waterline i.e., “peak” concentration
C_{sT}	chloride surface concentration at top of column
C_T	critical chloride threshold
C_{T0}	baseline chloride threshold value at E_{T0}
D	oxygen diffusion coefficient
D_{Cl}	apparent chloride diffusion coefficient
D_L	oxygen diffusion coefficient below the waterline
D_H	highest value of oxygen diffusion coefficient above the waterline
DF	damage function
E	potential
E_0	nominal equilibrium potential
E_{0a}	nominal equilibrium potential for the anodic reaction
E_{0c}	nominal equilibrium potential for the cathodic reaction
E_{Prot}	operating galvanic anode potential
E_S	steel potential
E_{T0}	baseline steel potential value at C_{T0}
F	Faraday constant
i_{0a}	nominal exchange current density for the anodic reaction

i_{0c}	nominal exchange current density for the cathodic reaction
i_a	anodic current density
i_c	cathodic current density
i_p	steel passive current density
L	column length
P_{CRIT}	critical local steel corrosion penetration
PDT	potential-dependent threshold or chloride threshold dependent on steel potential
SCE	saturated calomel electrode
SF	steel placement density factor
V_T	threshold potential value at which the calculated value of ia is less than i_p
X_C	concrete cover
β_a	anodic Tafel slope
β_c	cathodic Tafel slope
β_{CT}	slope of the straight line corresponding to eq. 6 when plotted in an E-logC_T representation. Also called the cathodic prevention slope
Φ	column diameter
ρ	concrete resistivity
ρ_T	concrete resistivity – top of the column
ρ_S	concrete resistivity – submerged portion of the column
ρ_H	concrete resistivity – highest value
ρ_L	concrete resistivity – lowest

1 INTRODUCTION AND OBJECTIVES

1.1 Background

The Florida Department of Transportation (FDOT) has more than 3,000 bridges on salt water, most with concrete with steel reinforcing bars, pre-tensioned or post-tensioned steel, or other embedded steel. Corrosion of the embedded steel, triggered by chloride ion intrusion, forms expansive products that cause visible deterioration in the form of spalling and cracks on the concrete cover. The damage is most evident in the portion of the substructure above water, especially at low elevations in the splash-evaporation zone. In that zone there is a strong combination of adverse factors, including evaporative accumulation of chloride salts on the concrete surface, ready local or nearby oxygen access to the steel surface, galvanic cell formation that accelerates local corrosion, and formation of solid corrosion products that promote early cracking [1,2].

Because external signs of damage are seen earliest in the splash-evaporation zone, much of the corrosion control effort by FDOT and other stakeholders has concentrated in forecasting, diagnosing, preventing, and repairing above-water corrosion. For corrosion control in that zone in new structures, the FDOT has adopted the use of concrete with low water-to-cementitious content ratio, with pozzolanic and slag cement replacement material, plastic control chemical admixtures, and a thick concrete cover. That approach has resulted in significant progress in controlling corrosion and has been the basis for deterioration forecasting and maintenance decisions by the state.

In contrast with the attention given to the above-water zone, potentially severe corrosion in the submerged portion has remained comparatively unattended in Florida and worldwide. This situation has resulted from generally few investigations of corrosion in the submerged zone and from theoretical expectations of lower corrosion there because of reduced oxygen supply. However, those considerations can be misleading, as discussed next.

The near absence of reports of underwater corrosion reflects in part the lower frequency of in-depth inspection of that zone, which is inherently harder to access and where features like cracks and spalls can be easily hidden by deposits and marine growth. Detailed examination of submerged structural elements after decommissioning of a bridge is possible but rarely conducted [3] given priorities elsewhere. Corrosion underwater is harder to detect also because fluid corrosion products, which are more likely to develop in those high humidity conditions, may not induce telltale concrete cracking. The absence of cracking could nevertheless decrease the possibility of discovering extensive steel cross-section loss and associated bond loss with the surrounding concrete. It is also possible that symptoms are absent because corrosion in the submerged zone has been somewhat suppressed by galvanic coupling with reinforcement in the tidal and evaporation zones, if steel in these zones started corroding earlier in the life of the structure. That coupling tends to make the potential of the submerged steel more negative than otherwise, elevating the corrosion threshold and thus retarding the initiation of corrosion below water (cathodic prevention) [4,5]. Mitigation of the corrosion below water would continue even after eventual initiation

there because of ordinary corrosion protection coupling with the corroding steel above. In both instances the extent of corrosion above water would be increased while corrosion in the submerged zone would be less. However, the advent of successful corrosion control measures for the tidal and evaporation zones lessens the likelihood of this protective mechanism for the submerged zone and proportionally increases the chances of corrosion there.

Lowered oxygen supply to the steel surface in submerged concrete does not guarantee low corrosion rates there either. Oxygen diffusivity tends to be dramatically lower in water saturated than in atmospherically exposed concrete, so the rate of arrival of oxygen molecules to the steel surface in submerged concrete can be very small even if the oxygen concentration at the external concrete surface were to remain relatively high. The traditional argument is that since the cathodic oxygen reduction reaction at the steel surface is thus limited, then the matching anodic iron oxidation reaction (corrosion) is similarly limited to a very small value [4]. That argument is generally applicable if corrosion is fairly uniform and only the immersed zone provides a site for the cathodic reaction. However, steel in the submerged zone often is in electronic contact with the rest of the steel assembly which extends to the atmospheric region. Oxygen supply is plentiful above water and could galvanically make up for deficiency below water, as has been illustrated by computer models of corrosion distribution in marine piles [6]. Even if oxygen supply were restricted to the submerged zone, in cases where steel activation is limited to a few spots the cumulative extent of oxygen reduction over a much larger steel area in immersed concrete could result in severe concentrated corrosion, even if oxygen reduction proceeded at a very low average rate. Strong corrosion localization at small active zones have been examined experimentally [7] and by detailed modeling [8,5]. These concerns are supported by the observation of severe localized corrosion in an early investigation by Beaton et al. [3]. In that work the continuously submerged portion of 37-year old piles from a bridge replacement in San Francisco Bay were autopsied. Almost half of the piles had heavy corrosion pitting of steel, much of it taking place near the mudline where detection during service would have been very difficult. Investigations elsewhere, oriented toward offshore oil platforms [9,10] have shown no tendency for severe corrosion in the submerged zone. However, the relatively small number of surveys of corrosion in the submerged zone limits the extent of any assurance that can be derived from negative observations.

The potential severity of underwater corrosion depends on other issues not satisfactorily resolved at the beginning of this investigation. Those include knowing the effective value of the chloride content at the surface of submerged concrete, which may be strongly affected by the presence of surface deposits, of the chloride ion diffusivity in the water-saturated pore network (which, opposite to the case of oxygen, increases with respect to the case of non-saturated concrete), and of the oxygen concentration at the concrete surface, which may be affected by biofilms that could create an anoxic interface. Unique to submerged concrete, the effect of hydrostatic pressure driven penetration of chlorides and its ruling parameters merits consideration as well. Each of those parameters is are affected by uncertainty, but each could greatly increase or

decrease the timing and extent of corrosion that could take place. The presence of local concrete deficiencies like cracks in piles or walls introduces added concern.

The above considerations are of special relevance as renewed interest exists in the potential for corrosion in the submerged zone. This interest arises because ambitious durability goals for FDOT structures are now in place, such as the 75 years design life requirement [11]. Damage rates that might have been tolerable with shorter service life goals now have many decades to proceed, possibly undetected given the limited information available on corrosion behavior in that zone.

The issue of corrosion in the submerged zone concerns most FDOT marine bridge substructures, and importantly also the Miami Port Tunnel, where one side of the wall is in a submerged condition while the other is exposed atmospherically a short distance away. Need for resolution there is acute given the unusually long 150 year service life goal. Investigations addressing these conditions are relatively few and corrosion monitoring methods are still evolving [12]. An investigation on submerged concrete for an undersea tunnel [13] showed low corrosion in uncracked concrete but strong corrosion localization at a crack, underscoring the need for careful assessment of the possible modes of corrosion.

The above observations show the scarcity of research directly related to corrosion in submerged portions of reinforced concrete structures. FDOT design for long term corrosion control in the submerged zone of bridge components and other structures such as underwater tunnels has had to rely on that limited evidence and associated theoretical assumptions.

1.2 Project Objectives and Approach

1.2.1 Objectives

This investigation was conducted to determine the extent to which submerged zone corrosion is present in FDOT substructures, the mechanism of that corrosion if present, and means for its control.

1.2.2 Approach

The investigation was conducted by means of assessment of corrosion in decommissioned field piles and an existing submerged footer chamber and formulation of predictive modeling based on the field findings and basic corrosion science. The model was then applied to evaluate the possible extent of corrosion in typical FDOT piling and the feasibility of corrosion control by means of sacrificial cathodic protection anodes. The following chapters detail the execution of each of the approach items and the corresponding project outcomes.

For the purposes of this report the submerged zone is defined as the part of the pile or substructure element that extends from the bottom end of the element up to the highest elevation of the marine-organism coated region, hereafter called the waterline. That

elevation is approximately coincident with the mean high tide level in typical Florida marine locations, where the tidal span is only on the order of 2 ft (0.6 m). Hence, conditions have been abstracted here for field assessment and modeling as representing a simple transition between submerged and atmospheric regimes, recognizing that other geographic locations may require detailed treatment to account for an extended tidal zone. The submerged zone includes the portions directly in contact with seawater and also any part of the overall length of the element that is buried in the bottom soil, a level hereafter named the mudline. The atmospheric regime includes at its lowest elevations the splash zone where evaporative chloride buildup is most prominent.

2 FIELD ASSESSMENT

2.1 General Approach

The corrosion condition of reinforcing steel was assessed for elements in the following structures:

1. Bridge Pilings
    a. Sunshine Skyway Fishing Pier
    b. Pinellas Bayway Drawbridge
    c. Sunrise Key Bridge
2. Submerged Footers - Sunshine Skyway Bridge

The first three assessments concerned partially submerged piles from decommissioned FDOT bridges/structures. The fourth addressed in-service pier footers.

Field assessment was conducted to make determinations as to presence of corrosion related phenomena such as:

- Long-term stability of the passive regime of steel embedded in submerged concrete structures.
- Extent of corrosion macrocell activity in partially submerged piles.
- Effective loss of rebar cross-sectional area.
- Expansive character and mobility of corrosion products.
- Visible corrosion indicators on exterior surfaces of structures and components.
- Elevation and distribution of corroded and non-corroded regions.

The individual studies made use of both non-destructive and destructive test techniques such as visual inspection, potential mapping/surveying, chloride concentration profiling, pore water pH determination, and rebar section loss quantification. These techniques enabled detection of structural damage and active corrosion, assessment and quantification of environmental factors, and calculation of affected steel surface area.

2.2 Structures Examined

2.2.1 Sunshine Skyway Fishing Pier

2.2.1.1 Background

Two piles, designated as pile #1 and #2, were taken out of service from the north end of the South Skyway Fishing Pier, and transferred to the University of South Florida (USF) Corrosion Laboratory. These particular piles were extracted on 09-27-2011 and arrived at USF on 11-04-2011. While neither the precise bent number nor information regarding bent location was available, it is known that both piles were removed from the northbound span of the original Sunshine Skyway Bridge (Bridge Identification Number:

139002; built in 1952). The piles, as received, measured approximately 23 ft and 25 ft in length and were, as expected, 20 inches by 20 inches in cross-section in the main region. Both piles had conventional jackets (33 inches by 33 inches in cross-section) and both retained some of their original sub-mudline length (Figures 1 and 2). Each of the piles contained a central steel H beam ~ 10 inch wide that had been cut off during the process of extraction from the bridge. As visible in Figure 2, the concrete part of the pile started with chamfers at that cut off point. The embedded H beam extended upwards into the pile sections for an undetermined distance from the cut end.

The environment of the pile extraction site has been classified as *extremely aggressive* based on the parameters contained in the FDOT Structures Design Guidelines. In 2002, inspectors observed that more than 85% of the jackets on the older south (east) portion of the bridge (139002; Skyway Fishing Pier) showed cracks, spalls, and iron rust staining on several faces. They also performed core tests and recorded chloride content levels at the reinforcement depth that "greatly exceed(ed) the critical chloride content threshold of 1.2 lb/yd^3 (0.71 kg/m^3)." Half-cell potential measurements made at the same time indicated high probability of corrosion. In 1993, structural jackets that consisted of concrete filler material and epoxy-coated rebar were installed on all of the piles of bridge 139002. Prior to this point, pile damage repair was limited to concrete patching on beams and caps [14].

Upon arrival at USF, dimensions were recorded, photographs were taken, and provisions were made to both maintain surface wetness and protect the surface water from evaporation. The piles were covered upon arrival and, at periodic intervals (average interval: one week), the cover was removed, the exterior surfaces of the piles were sprayed with water from a hose to retain a high moisture content approaching the submerged condition, and the cover was reinstalled.

Figure 1. Piles resting side-by-side on horizontal concrete columns. Note jackets on upper area (left) of piles and H-beams visible at each pile bottom end (right).

Figure 2. Piles, end view. Note marine organisms and muck accumulation on each pile's exterior surface everywhere except area below the mudline (foreground).

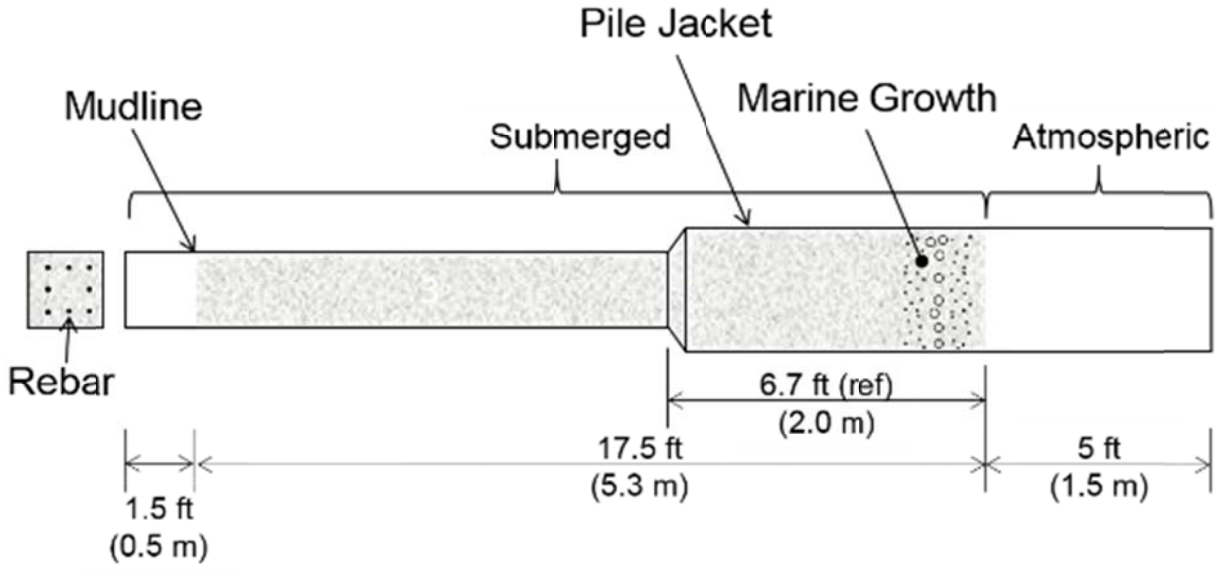

Figure 3. Typical configuration and dimensions of the two Skyway Fishing Pier piles.

2.2.1.2 Methods and Results

2.2.1.2a Visual Inspection

No concrete cracks or spalls were visible/apparent on the external surface of the piles.

2.2.1.2b Reinforcing Steel Condition Assessment

The rebar cage in each pile consisted of eight #8 bars arranged vertically in a cage of approximate square dimensions as shown in Figure 4. The H beam was not included in the assessment, which focused on the reinforcing bars as those were closest to the external pile surface and subject to the most aggressive conditions. The bar that appears in the upper left corner of Figure 4 was designated “bar 1” and was chosen as the first bar to be analyzed. In order to assess the condition of the surface of bar 1, concrete cover was removed along the pile edge from the bottom of the concrete portion of the pile to a point approximately 11 feet above the bottom. That point coincided with the bottom end of the jacket, ~6.7 ft below waterline. Concrete removal involved making a vertical cut from the “top” surface of the pile and a horizontal cut from the “side” of the pile and then using a hammer and chisel to fracture the concrete and debond it from the rebar (Figure 5). This method effectively exposed as much as half of the circumference of Bar 1 (an arc of approximately 135° to 180°) along the length of the 11 ft long region.

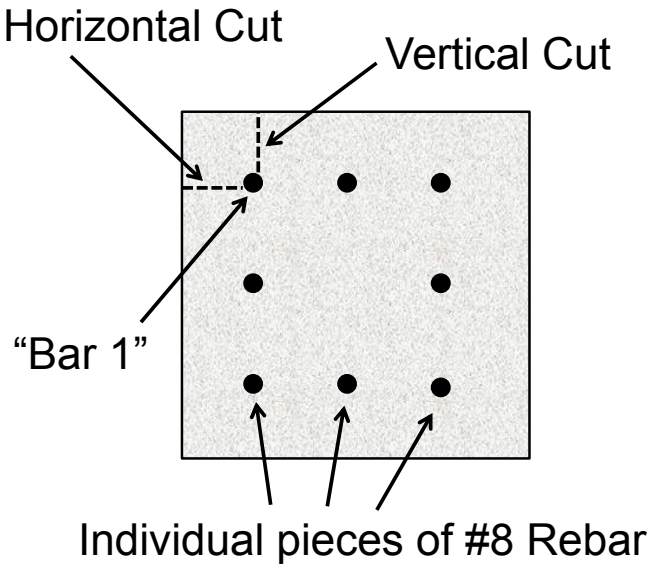

Figure 4. Cross-section of Pile #2 showing vertical and horizontal saw cuts. H beam not shown.

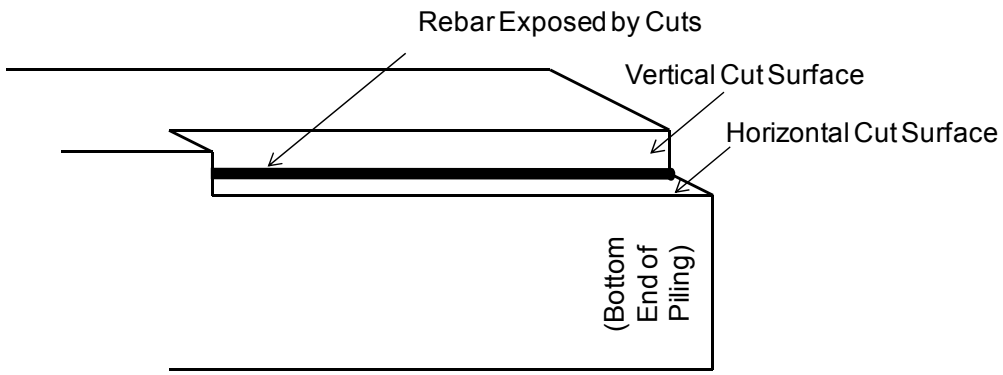

Figure 5. Rebar exposed by 11′-long vertical and horizontal saw cuts (not to scale).

Most of the exposed region of bar 1 was free of visible corrosion but several portions, with a combined surface area that amounted to approximately 19% of the total, showed evidence of corrosion. The approximate locations of corroded regions are shown in Figure 6. The corrosion was sufficient to leave a distinct rust-colored trace on portions of the removed concrete (Figure 7).

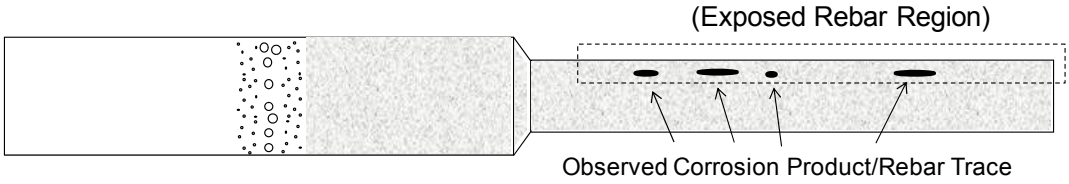

Figure 6. Approximate locations of observed corrosion products and rust trace on removed concrete bar 1.

Figure 7. Rebar rust trace on portion of concrete removed from Pile #1. Tape measure indicates distance from bottom of pile.

Concrete removed from the pile was retained to provide specimens for porosity and chloride content. Newly exposed concrete surfaces were evaluated for resistivity and carbonation.

Detailed Steel Examination

Initially, two 11 ft-long rebar segments were removed from one of the piles to facilitate the implementation of a technique that would enable approximate quantification of rebar section loss due to corrosion. The two segments i.e., the previously mentioned bar #1 and a second bar hereafter referred to a bar #2, came from the region of the pile that was continuously submerged throughout its entire service life, including a small length below the mudline. The two saw cuts (one vertical, one horizontal) made near the corner of the submerged portion of the pile are shown in Figure 8. The saw cuts extended from the bottom of the pile to the bottom of the jacket.

Figure 8. Vertical and horizontal saw cuts in the submerged portion of Pile #2.

A hammer and chisel were then used to fracture the concrete beyond the saw cut and expose the embedded bar. As the concrete cover was fractured and removed, several oxide-stained regions were observed as shown in Figures 9 and 10.

Figure 9. Oxide stains in concrete cover observed during removal of embedded bar.

Figure 10. Close-up view of oxide stains in concrete cover observed during removal of embedded bar. Note that a small portion of the bar itself can be seen in the center of the photo.

The exposed bar (in each case) showed some areas of apparent significant section loss as shown in Figure 11. The corrosion products appeared to have spread into corrosion-induced cracks that radiated from the bar, although some extent of corrosion product penetration was present also in the bulk of the concrete near the bar.

Figure 11. Rebar in situ following removal of the concrete shown in Figures 9 and 10.

A saw was used to cut the stirrups and to cut the bar itself near the lower end of the jacket. (Note that the jacket's geometry prevented cutting into this portion of the pile with the saw.) Adhesion between the concrete and the bar in each case was very low. As can be seen in the photos, very little concrete maintained adhesion with the surface of the bars and very little effort was needed to separate the bars from the concrete. The bars were taken into the lab, inspected, and photographed. Two regions with apparent significant corrosion are shown in Figure 12.

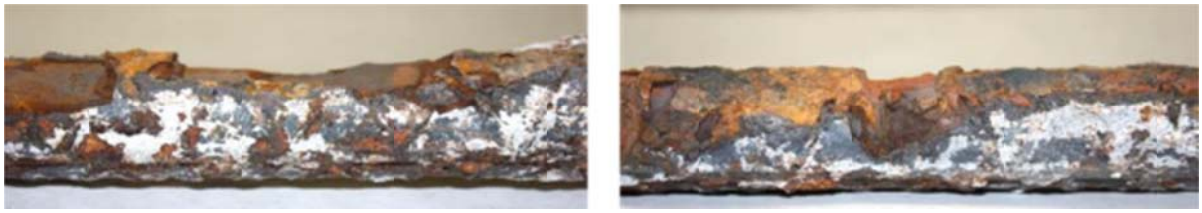

Figure 12. Apparent corrosion-related cross-section loss observed in bar #1.

The bar extraction and analysis operations were intended to detect any corrosion present in the submerged region and, if corrosion was observed, to estimate the rate at which it had propagated. As the actual duration of the initiation period was indeterminable, this period was assigned zero length and corrosion rates were based on the service life of the piles (~60 years). This represents a simplification that effectively yields the lowest corrosion rates that would have been observed over the entire pile service life. Estimating the corrosion rate over equispaced intervals along the length of each bar involved quantifying the loss of rebar cross-sectional area in each interval and converting it to a bar radius change (as described below), and then dividing by the time-in-service.

In order to quantify section loss, an experimental procedure was developed wherein changes in electrical resistance along the length of the bar could be used as indicators of changes in the effective diameter of the bar itself. First, low resistance electrical contact points were made by grinding spots on the surface of each bar at 2-inch intervals along its length. Next, as a DC current of 10 amperes was passed through the bar, the voltage drop over each 2-inch segment was measured at the contact points and recorded. (Note that voltage drop was measured in both forward and reverse polarities/orientations of the dual-electrode instrument.) As is indicated in Figure 13, electrical resistance (as indicated by voltage drop) varied along the length of each bar and some regions showed substantial elevated resistance. Visual inspection of the bars verified that the regions of high resistance corresponded with regions of high visible section loss.

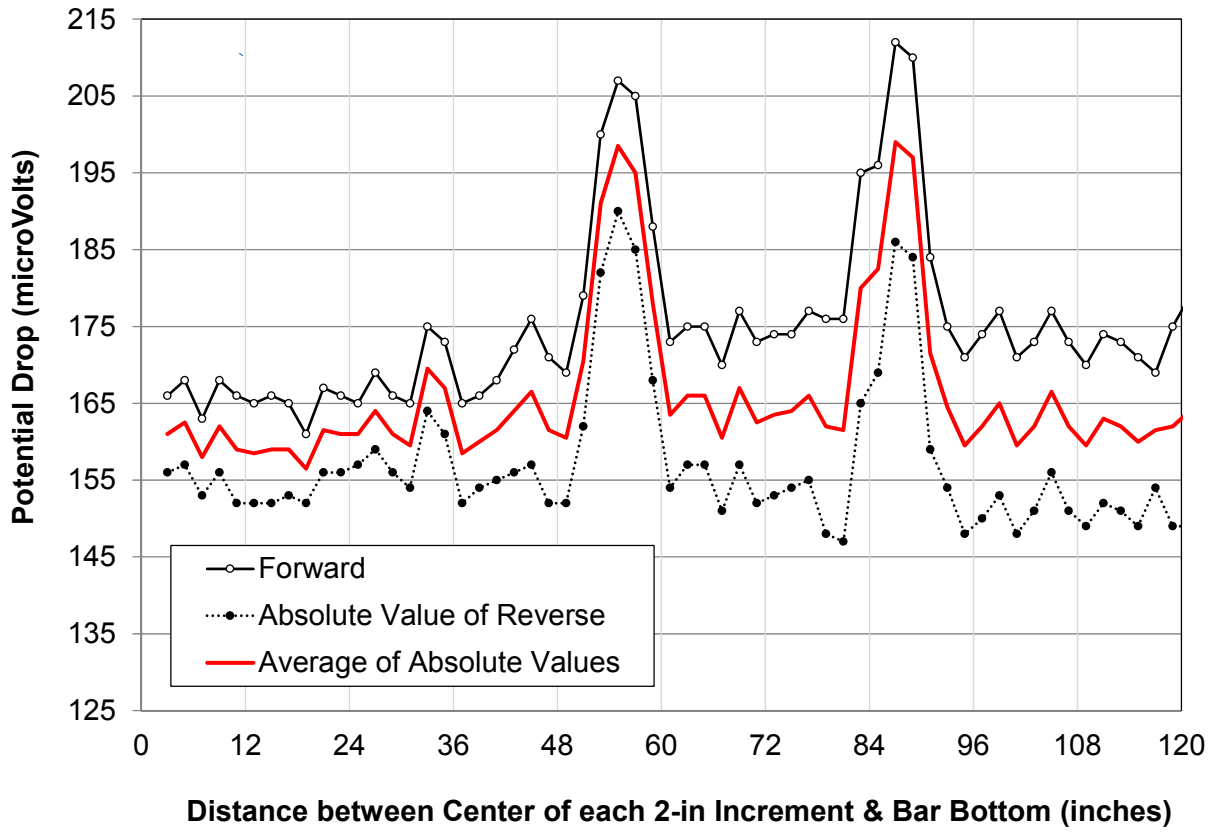

Figure 13. Cross-section loss survey. Voltage Drop at 2-inch intervals along the length of Bar #1 with DC current of 10 amperes.

Per the basic relationships between voltage drop, resistance/conductance, and the cross-sectional area of the bar, it can be shown that the effective radius of the bar is inversely proportional to the square root of the voltage drop over a particular length of bar.

Accordingly, the effective radius of the bar can be estimated with consideration of the actual measured voltage drop in each 2-in segment. Evaluating the ratio of the difference between the original radius of the bar and the effective radius of the bar to the time in service, corrosion rate as a function of position on the bar can be plotted as shown in Figure 14. Any negative values in this and subsequent graphs, are usually small and the result of computation uncertainty.

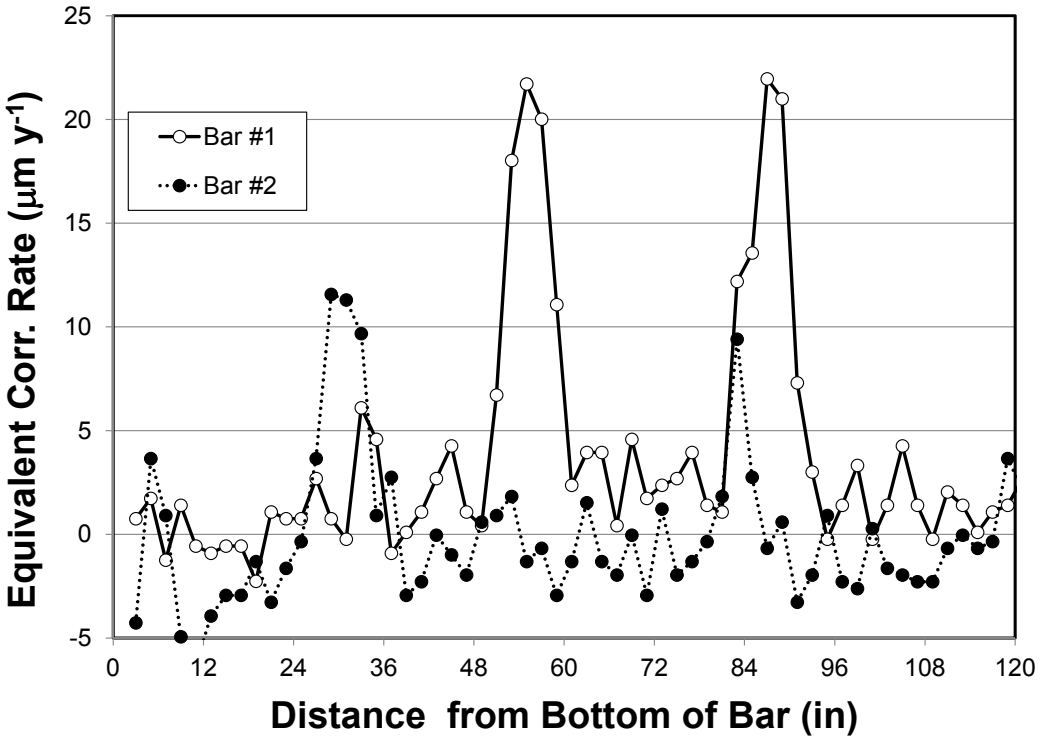

Figure 14. Equivalent corrosion rate as a function of the distance between the vertical midpoint of a 2-inch increment and the bottom of the bar.

Regarding corrosion rate values less than 7 μm/yr as indicative of baseline conditions, each bar was observed to have approximately 8% of its total observed area undergoing active corrosion. This analysis revealed localized corrosion rates as high as 22 μm/yr and an average corrosion rate of approximately 16 μm/yr in the affected areas. These results indicated a corrosion rate on the same order of magnitude as data collected via predictive modeling of a similar system (see Predictive Modeling below).

Extended evaluation

In a second set of tests, four more bars (two from Pile #2 and two from Pile #1; bar #s 5 and 6, 3 and 4 respectively) were extracted from the same elevation range as for bar #s 1 and 2 and analyzed. Corrosion-related section loss of the type and degree described earlier for bars # 1 and 2 was found in one bar (# 5) of the second set of four bars. The affected segment of bar # 5 was significantly corroded in the region that faced “outward” toward the concrete surface but much less corroded on the reverse side as can be seen in Figure 15. The rebar trace associated with the less corroded underside of bar # 5 in the affected region is shown in Figure 16. Only minor surface corrosion was observed on the other three bars.

Figure 15. Corrosion-related cross-section loss in Bar #5.

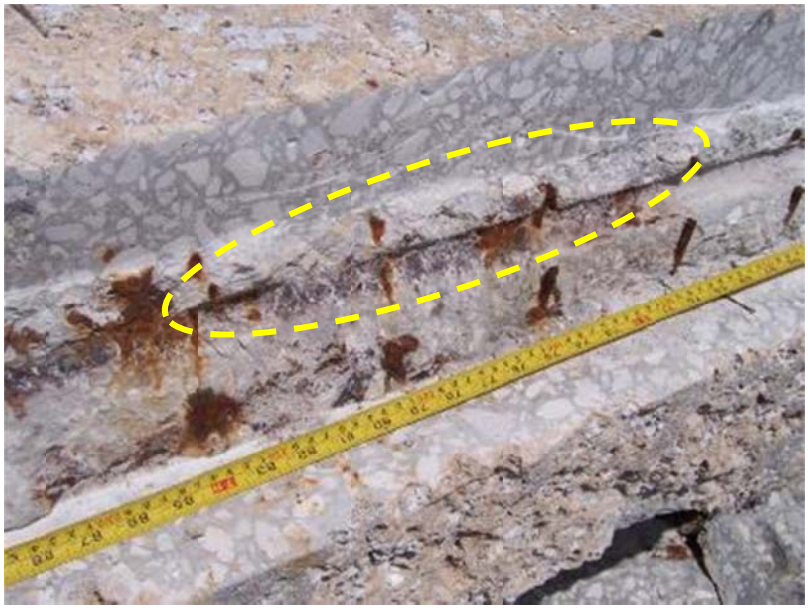

Figure 16. Rebar trace corresponding to underside of the corroded region of Bar #5. Marked zone corresponds approximately to bar segments pictured in Figure 15.

Changes in electrical resistance along the length of each bar were also measured for this second set and converted into estimated corrosion rates. This additional evaluation included also exploratory half-cell potential measurements of the second set of bars and had also been done for bar #2 (bar #1 had been extracted before reliable methodology was established). Before cutting into the concrete, stainless steel screws were installed on exposed pieces of reinforcing steel at both ends of both piles to serve as low resistance electrical contact points. The half-cell electrical potential (vs $Cu/CuSO_4$ reference electrode) was measured according to ASTM C 876. Two potential maps were made. One map followed a line parallel to the corner edge of the pile (offset by approximately 4 inches) along the "top" surface of the pile and the other map followed a similar line along the "side" surface of the pile.

Figure 17 (a, b, c, d, and e) presents the corrosion rate estimated from the resistance measurements (assuming as before a nominal 60-year interval) and the half-cell potential results along the length of each bar. The regions with high estimated corrosion rate for bar #5 corresponded with regions of high visible section loss, as was noted earlier too for the case for bar #s 1 and 2. Bar #5 showed estimated local corrosion rates that reached a peak value of 33 μm/y. Estimated corrosion rates for all the other bars in the second set were low, consistent with their lack of visible appreciable corrosion.

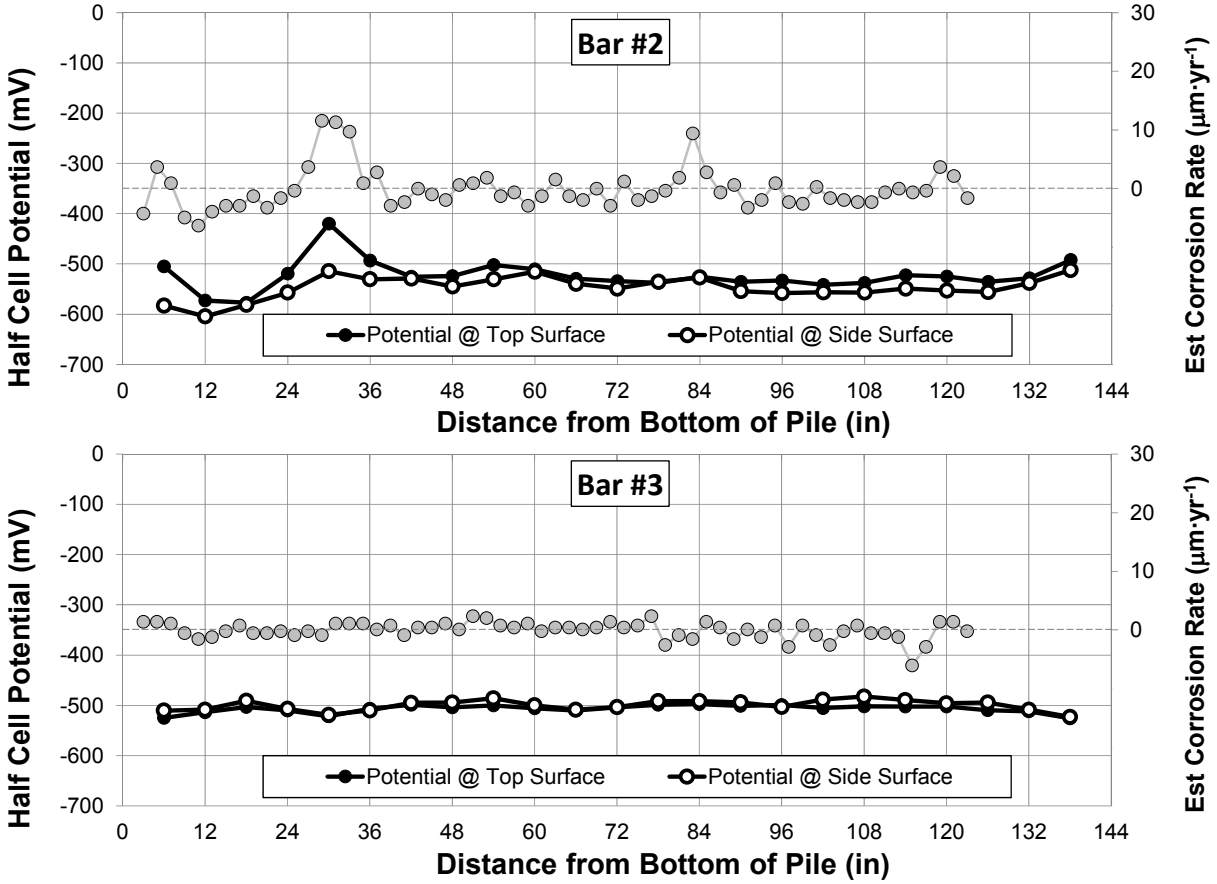

Figure 17 a and b. Half-cell Potential at 6-inch intervals and estimated corrosion rate (average decrease in radius divided by 60 years) at 2-inch intervals along the length of Bar #s 2 and 3 respectively.

As can be seen in the figure, all half-cell potential values where highly negative, consistent with an expectation of active corrosion of the steel. There was some apparent minor correlation between potential variations and the location of the highly corroding spots. However, the correlation is in the opposite of the expected direction (which would have resulted in somewhat more negative potentials in the area of greatest corrosion). The reason for these local discrepancies has not been established. It can be speculated nevertheless that the presence of corrosion products and pH variations in the highly corroded regions may have introduced local junction potentials that acted to result in a small excursions toward less negative values [15]. Notably considering the 6-decade long service, the original dark mill scale, apparently undisturbed, was often visible on the bar surface in regions distant from localized corrosion after removing concrete residues.

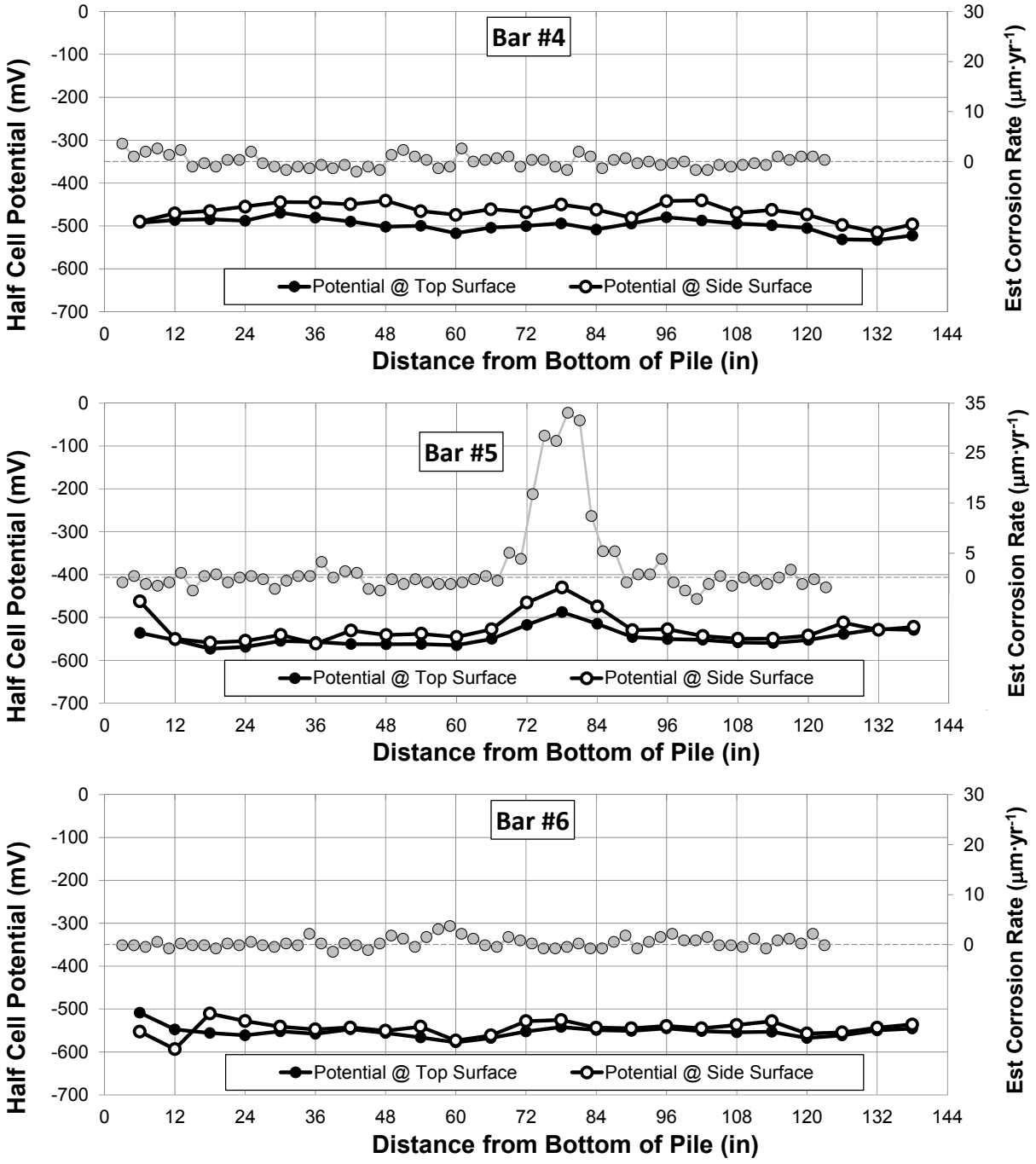

Figure 17 c, d, and e. Half-cell Potential at 6-inch intervals and estimated corrosion rate (average decrease in radius divided by 60 years) at 2-inch intervals along the length of bar #s 4, 5, and 6 respectively. The corroded regions showed the greatest metal loss on the side of the bar closest to the concrete surface, while the inward-facing side (toward the bulk of the concrete) showed little or no corrosion.

2.2.1.2c Concrete Material Assessment

Concrete Resistivity

Resistivity was measured on the freshly cut surfaces of the pile concrete using a C.N.S. RM MkII four-point Wenner array probe. Measurements were made on both the horizontal and vertical exposed surfaces in the exposed rebar region. Measured resistivity values ranged from 3.31 to 4.97 kΩ-cm and averaged 4.24 kΩ-cm. These low observed values are typical of high permeability concrete when saturated with seawater, and consistent with the class of concrete with unblended cement that was used for other FDOT pile applications at the time of construction [16].

Concrete Porosity

Three mass-appropriate specimens were selected from the concrete removed from the pile during the rebar extraction process and were subjected to analysis according to ASTM C642, Standard Method for Density, Absorption, and Voids in Hardened Concrete. The exterior surfaces of the piles, as received, were uniformly covered with organic and inorganic material. This material was removed from the specimens to an extent as great as deemed necessary and reasonable prior to initiation of the analysis. The results of the analysis indicated that the porosity (volume of permeable voids) of the concrete was approximately 16%. This value is comparable to porosity values presented in a previous study of older construction FDOT bridges [16].

Concrete Chloride Content – First set of analyses

Concrete for chloride analysis was selected from various locations on the exterior surface of the pile including: (1) a region where active corrosion as indicated by the presence of iron oxide deposition was observed, and (2) a region that was adjacent to that where iron oxide deposition was observed but was itself devoid of any visible corrosion. The specimen collection process involved securing a piece of concrete on a mill table, drilling into the concrete at precisely marked locations, and collecting the pulverized/powdered concrete via a specialized powder collection system.

Pulverized concrete specimens were collected at multiple depths that represented the outermost region (just below the outer, seawater-exposed surface of the concrete), the innermost region (just above the embedded rebar), and the intermediate region. Average concrete cover thickness measured approximately 75 mm. Each pulverized concrete specimen was divided into three portions of approximately equal mass, and each portion was analyzed according to FM 5-516, Florida Method of Test Determining Low-Levels of Chloride in Concrete and Raw Materials.

Results of the analysis are summarized and presented in Table 1 and Figure 18.

Table 1. Observed chloride concentrations (Note that disintegration of the concrete sample prevented data collection at 5 and 25 mm in the corroded rebar region.)

Average Distance from Outer Surface [mm]	Chloride Concentration [lb/yd^3], Non-corroded Rebar Region	Chloride Concentration [lb/yd^3], Corroded Rebar Region
5	21.3	-
25	16.3	-
45	17.1	19.2
65	27.1	29

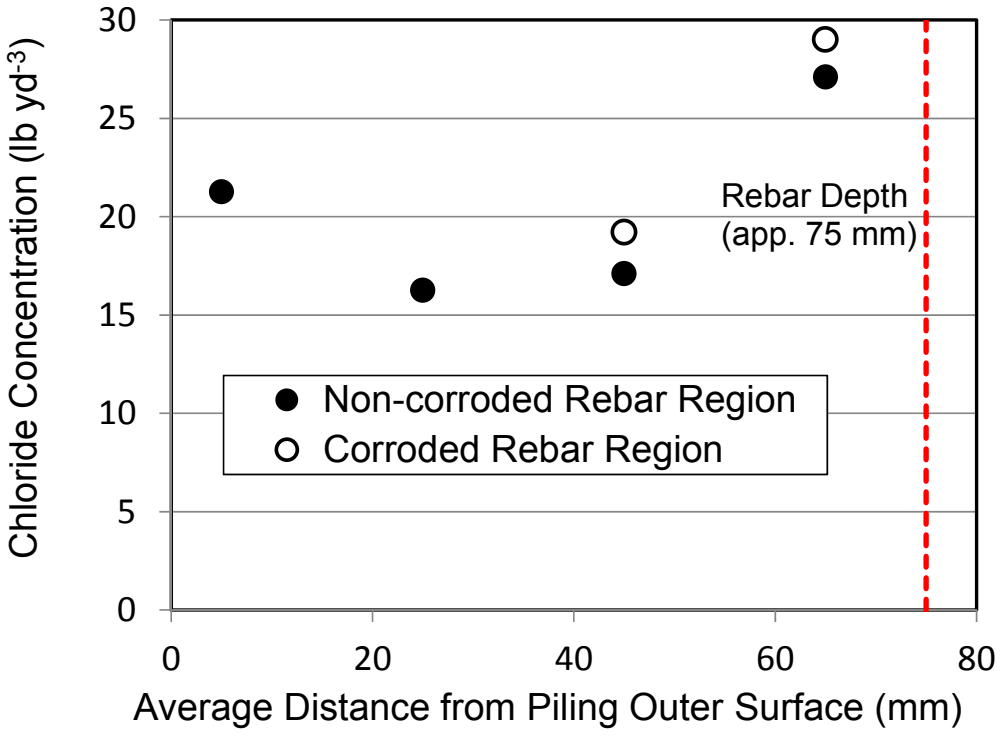

Figure 18. Observed chloride concentrations.

The results indicated that the distribution of chloride did not vary dramatically throughout the concrete cover. This can be attributed to the long seawater exposure duration (approximately 60 years) of the pile. This roughly uniform chloride distribution precluded computation of a concrete apparent diffusion coefficient (D_{Cl}) value. However, it is noted that the value of D_{Cl} must have been significantly greater than the values

associated with modern highly impermeable FDOT concrete formulations which typically yield D~< 0.01 in^2/y (~2×10^{-9} cm^2/sec), and would have resulted in a profile decaying to ~1/2 of the surface concentration at a depth of ~20 mm after 60 years.

These findings are consistent with the expectation that concrete formulations in use several decades ago in applications of this type would have values of D_{Cl} that are one or even two orders greater than those of the modern materials. The higher chloride concentrations observed in Figure 18 for the samples obtained near the rebar could be attributable to transport obstruction effects.

Concrete Chloride Content - Second set of analyses

Two concrete cores were removed from each of the two Sunshine Skyway Fishing Pier piles. In each case, one core was taken from a point approximately 1 foot above the mudline and another core was taken from a point approximately 8 feet above the mudline (which corresponds with the midpoint between the mudline and the waterline). Results, presented in Table 2 and Figure 19 indicated that after the 60-year service period the concrete had substantially reached a state of near chloride saturation through the region reaching down to the rebar depth, consistent with the results obtained for the first set of analyses. The concrete chloride content is in the order of that expected when taking into account the concrete porosity, the chloride content of seawater, and a typical amount of chloride binding by the cement paste [17]. The nearly flat concentration profiles are also consistent with those expected from the time of service and the typical chloride ion diffusivity value (in the order of 10^{-7} cm^2/sec) of concrete that has the low resistivity reported earlier.

Table 2. Chloride content of Sunshine Skyway Fishing Pier core slices

		Chloride Content [pcy]			
		Pile #1 (west pile) (source of bars 3 & 4)		Pile #2 (east pile) (source of bars 1, 2, 5, & 6)	
Slice	Depth of midpoint [in]	Core #1 (1' above mud line)	Core #2 (8' above mud line)	Core #3 (1' above mud line)	Core #4 (8' above mud line)
A	**0.25**	17.1	18.9	21.1	24.7
B	**0.75**	14.3	20.5	18.5	23.2
C	**1.5**	16.2	22.5	23.4	25.6
D	**2.5**	14.6	21.7	22.9	22.5
E	**3.5**	15.7	22.7	19.5	20.7
F	**4.5**		21.4	17.0	
G	**5.25**			17.7	
H	**5.75**			17.0	

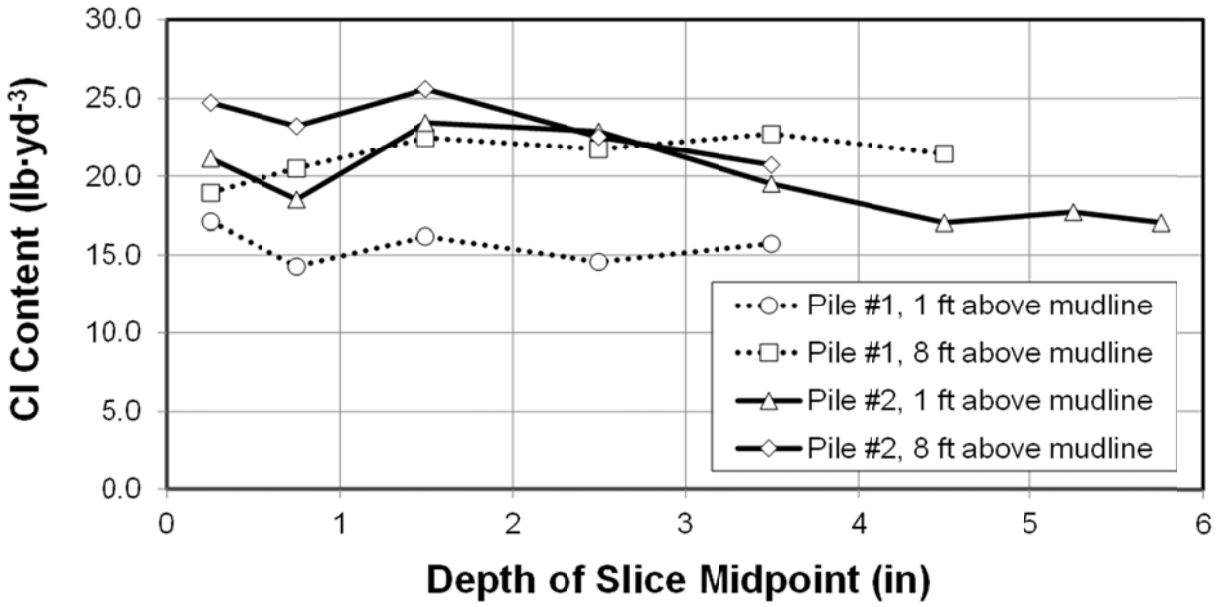

Figure 19. Chloride content as a function of depth from concrete surface for cores taken from Sunshine Skyway Fishing Pier piles.

Concrete Carbonation

Phenolphthalein was sprayed onto the freshly cut concrete surfaces in the exposed rebar region resulting in solid purple coloration on the entire surface. This result indicated, as expected for submerged concrete [18] that no discernible carbonation of the concrete had taken place near the pile surface during the pile service life, or after extraction during the pre-autopsy period when the piles were frequently wetted.

2.2.2 Pinellas Bayway Drawbridge

2.2.2.1 Background

The Pinellas Bayway Drawbridge Structure “C”, which was undergoing demolition in 2013, provided an additional field specimen. The pile, which had been partially submerged for approximately 51 years, was subjected to visual inspection, concrete property (e.g., resistivity, porosity) analysis, and corrosion investigation by actual pile autopsy/strand removal. Photos of the piles are presented in Figures 20, 21, 22, 23, 24. A schematic sketch with cross-section detail is presented in 25.

Figure 20. Atmosphere-exposed (i.e., top) end of extracted pile.

Figure 21. Submerged (i.e., bottom) end of extracted pile, end view. Note that the absolute bottom end of the in-service pile was left in situ and that this pile segment was cut from it.

Figure 22. Submerged (i.e., bottom) end of extracted pile, oblique view. Note that marine growth has been scraped from the surfaces near the corner to facilitate saw cuts.

Figure 23. Marine growth on the submerged regions of two piles. Note that some growth has been removed from the surface of the pile on the left in preparation for autopsy/saw cutting.

Figure 24. Submerged end of pile selected for autopsy. Note that marine growth has been scraped from the surfaces near the corner to facilitate saw cuts.

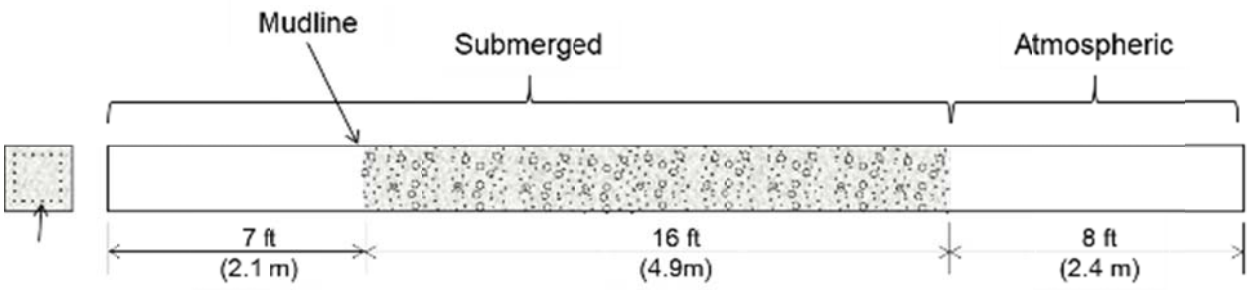

Figure 25. Typical configuration and dimensions of Pinellas Bayway Drawbridge piles.

2.2.2.2 Methods and Results

2.2.2.2a Visual Inspection and NDT

No concrete cracks or spalls were visible/apparent.

2.2.2.2b Reinforcing Steel Condition Assessment

Under field conditions, only a partial pile autopsy was performed and was limited to a single corner of the pile, exposing one of the 20 steel strands in the cross-section by cutting the concrete in a manner similar to that used on the Skyway Fishing Pier pile. The pile had been removed from its in-service location less than three days prior to the autopsy (September 2013) and had been laid on its side on a barge as shown in Figure 26.

Figure 26. Pinellas Bayway Drawbridge pile selected for autopsy. Atmospheric air-exposed end of pile (i.e., top) is in the foreground. Note marine growth between waterline and mudline.

The autopsy involved making two saw cuts, one vertical and one horizontal, near one of the lengthwise corners of the pile as shown in Figure 27. The cuts were initiated at a point approximately two feet below the waterline.

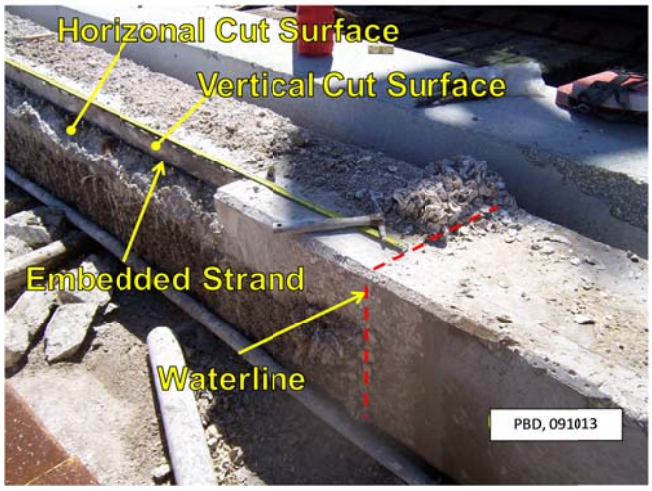

Figure 27. Autopsied pile. Note concrete chunks on deck removed from pile with a hammer and chisel after vertical and horizontal saw cuts were made.

The single strand was exposed between the pile's mudline and a point approximately 2 ft (0.6 m) below the waterline. The strand was visually inspected and the strand cross-section loss was estimated. Most of the exposed strand was free of visible corrosion but five segments typically ~4 in (~10 cm) long showed evidence of reduced cross-sectional area of some of the individual strands and distinct rust-colored stains, as illustrated in Figures 28 and 29. The segments were located at approximately 52, 71, 95, 112 and 138 in (1.3, 1.8, 2.4, 2.8 and 3.5 m) below the waterline with no clear preferential elevation location (no locations below the mud line were surveyed due to on-site time and equipment constraints). The apparent corrosion affected about 12% of the total length of strand examined.

Figure 28. Exposed strand in uppermost region (nearest waterline) of autopsied pile. Note rust stains. (Photo was taken immediately after strand was exposed.)

Figure 29 top, middle, bottom. Three different instances of localized corrosion. Note that the measurement datum for the indicated distances was the waterline.

2.2.2.2c Concrete Material Assessment

Resistivity

Concrete resistivity was measured on-site using the C.N.S. RM MkII four-point Wenner array probe. Measurements were made in different regions, including the concrete exterior surface near the top end of the pile (approximately 8 ft above the waterline) and the freshly cut surfaces in the exposed strand region. Measured resistivity values on the freshly cut surfaces of the submerged region ranged from 1.8 to 3.5 kΩ-cm. The seawater-saturated condition resistivity values and the porosity are comparable to those of the Skyway Fishing Pier piles and similarly indicative of highly permeable concrete, consistent with the construction era practice [16]. For verification of expected trends, resistivity values were also obtained for a region on the pile surface 8 ft (2.5 m) above the waterline. The results were in the 31-47 kΩ-cm range (average 38 kΩ-cm), consistent with the expectation of higher resistivity when the concrete is drier and consequently with lesser electrolytic connectivity.

Concrete removed from the pile was transferred to the USF Corrosion Lab for porosity, chloride content, and pH analysis.

Porosity

Three specimens were selected from the concrete removed from the pile and were subjected to analysis according to ASTM C642, Standard Method for Density, Absorption, and Voids in Hardened Concrete. The exterior surfaces of the pile were initially uniformly covered with marine material. This material was removed from the specimens prior to initiation of the analysis. The results of the analysis indicated that the porosity (volume of permeable voids) of the concrete was approximately 13% of the total concrete volume. This value is comparable to both the results of the Skyway Fishing Pier analysis described above and with porosity values presented in a previous study of older construction FDOT bridges [16].

Chloride Content

Concrete specimens for chloride analysis were taken from regions in close proximity to the exterior surface (depth from exterior concrete surface: 0.375 to 1.0 in) and from regions along the strand trace (depth from exterior concrete surface: 2.75 to 3.5 in) at each of two different depths below the waterline (i.e., 2 ft and 16 ft). Pulverized concrete specimens were collected via a process that involved securing a piece of concrete on a mill table (Figure 30), boring into the concrete at precisely marked locations, and collecting the pulverized/powdered concrete via a specialized powder collection system. The flat, upward-facing surface of the concrete fragment in Figure 30 is a saw-cut surface that resulted from the vertical cut (i.e., perpendicular to the deck of the barge on which the pile rested). The semi-flat vertical surface in the foreground of the figure resulted from the horizontal cut (i.e., parallel to the barge deck). The cutter is positioned near the rebar trace in the figure. Following the boring operation in this location, which was presumed to have a lower chloride content than the concrete

surface, the pulverized concrete was bottled and labeled, the cutter was cleaned and all loose particles and dust were removed. The mill table was then moved toward the foreground of the picture in Figure 30 and a subsequent boring operation was performed at a location near the concrete exterior surface. The specimens were analyzed according to FM 5-516, Florida Method of Test Determining Low-Levels of Chloride in Concrete and Raw Materials at the State Materials Office Corrosion Research Laboratory in Gainesville. Results of the chloride analysis are presented in Table 3.

Figure 30. Pinellas Bayway Drawbridge pile concrete sample mounted on mill table for chloride analysis specimen collection. Note that the measurement datum for the indicated depth was the waterline of the in-service pile.

Table 3. Chloride analysis results

	Average Cl Concentration (lb/yd^3)	
Location:	Near Concrete Surface	Near Strand Trace
16' BWL, Specimen A	31.70	36.46
16' BWL, Specimen B	28.84	31.73
2' BWL, Specimen A	24.93	31.16
2' BWL, Specimen B	19.76	21.38

The chloride content was regarded as being very high. The chloride distribution could be described as either uniform or inverted and, as it was the case for the Skyway Fishing Pier, this precluded computation of a concrete apparent diffusion coefficient (D_{Cl}) value using conventional methods. Higher chloride concentration values near the strand trace might to some extent be attributed to diffusional obstruction effects near the strand. [19] It is noted that, as was the case in the Skyway Fishing Pier concrete chloride analysis, the value of D_{Cl} must have been significantly greater than the values associated with modern highly impermeable FDOT concrete formulations.

Pore Water pH

Pore water pH was estimated via in-situ leaching (ISL). One specimen was prepared using a concrete fragment taken from the region that lies approximately 2 ft below the waterline and another specimen used a concrete chunk taken from a region approximately 16 ft below the waterline. ISL test results indicated pore water pH of approximately 12.5 in each of the two specimens. Note that the indicated pH in both cases was the average of three measured values.

2.2.3 Sunrise Key Bridge

2.2.3.1 Background

A field assessment was conducted on February 20, 2015 at the Sunrise Key Bridge (Bridge No. 423469-1-52-01, Ft. Lauderdale) which was being demolished as part of the FDOT Bridges of the Isle and Sunrise Key project. The bridge, which spanned a seawater canal, was approximately 70 years old and its piles (12” × 12” square cross-section) had been fitted with conventional jackets near the waterline at some point in its service life. The rebar cage in each pile consisted of four #5 bars arranged in a square; cover depth ranged from 3 to 4 inches. The piles were approximately 24 feet long and were driven to a depth below the mudline of 12 to 14 feet. (see Figure 31) The canal is subject to tidal variation and the depth at the time of the assessment was ~4 ft.

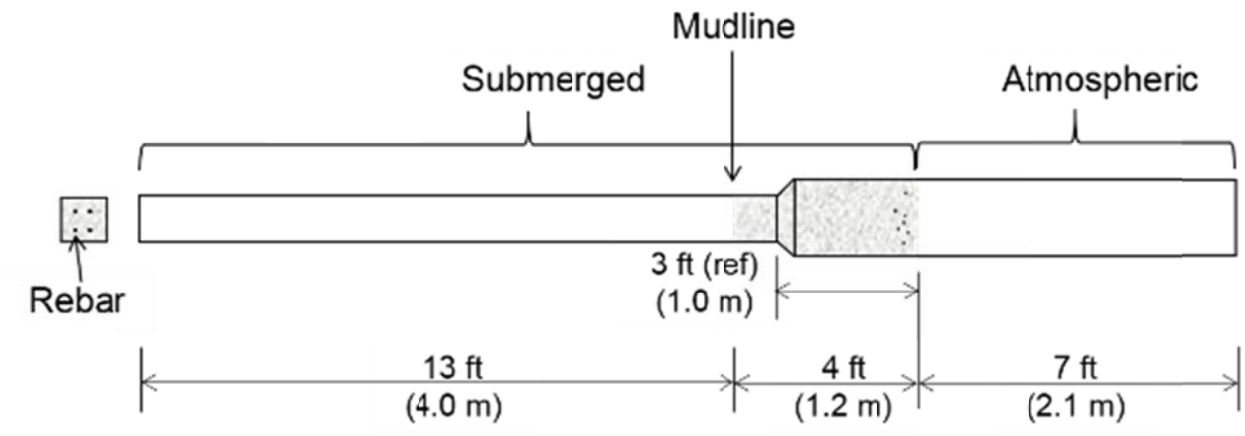

Figure 31. Typical configuration and dimensions of Sunrise Key Bridge piles.

2.2.3.2 Methods and Results

2.2.3.2a Visual Inspection and NDT

Substantial spalling was visible near the splash zone of some of the piles. During extraction of some of the piles, the top half of the pile had broken and separated from the bottom half (see Figure 32). Some of the rebar appeared to have suffered 100% section loss near the waterline.

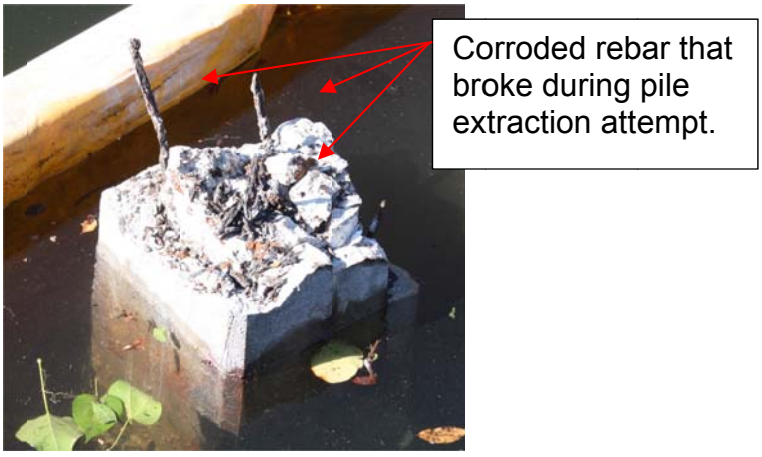

Figure 32. Bottom half of pile left in place as a result of breakage during extraction attempt. Visible rebar corrosion and section loss in splash zone.

After pile extraction, the exterior concrete surfaces in the submerged region were inspected. No concrete cracks or spalls were visible/apparent in this region.

2.2.3.2b Reinforcing Steel Condition Assessment

The demolition crew was able to expose the entire rebar cage of one of the piles that was extracted intact by fracturing the concrete subsequent to extraction and mechanically separating the concrete from the steel. Most of the embedded reinforcing steel was corrosion-free and had presumably remained in a passive condition (see Figure 33). Some evidence of corrosion below the waterline was however present in one region of one vertical bar (see Figure 34). The affected region was approximately ten inches long and was located at an elevation of approximately four feet from the bottom end of the pile, which corresponds to a location approximately ten feet below the mudline. The total steel surface area below the waterline per pile was estimated to be ~10 ft^2 and the total surface area of the corrosion affected region was estimated to be ~0.14 ft^2 (1.4% of the total surface area). A dial caliper was used to directly measure the decreased bar diameter in the corroded portion of the bar. It was estimated that the cross-sectional area of the bar in the affected area had been reduced by approximately 23%. No concrete property data were obtained from this bridge but from the date of construction it is estimated that permeability was high and comparable to that of the other two bridge piles.

The presence of corrosion in the submerged region provides valuable confirmation of the development of local steel corrosion in the completely submerged portions of reinforced concrete structures. The presence and amount of the corrosion was consistent with both that of other field observations made in this project and the outcome of modeling reported later in this report.

Figure 33. Corrosion-free steel in much of the submerged region. Note that pile in photo was lying on its side.

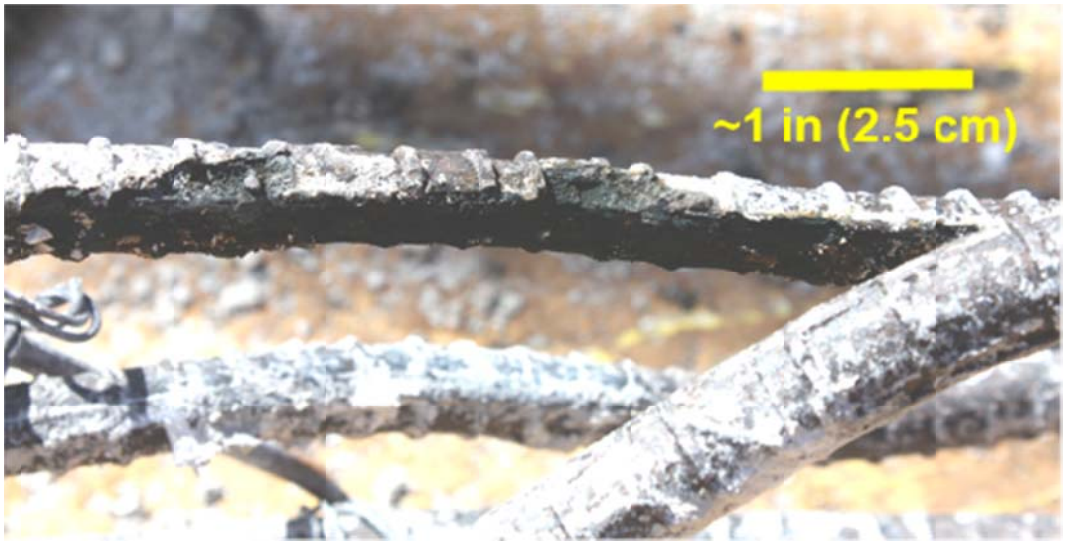

Figure 34. Locally corroded steel in region below mudline. Note corrosion-related cross-sectional area decrease of bar near top of photo.

2.2.4 Sunshine Skyway Bridge Submerged Pier Footers

2.2.4.1 Background and First Field Study (2012)

The first of two Sunshine Skyway Bridge (FDOT Bridge Number 150189) Pier Footer inspections was performed during the week of October 15, 2012, as part of activities coordinated by FDOT District 7. During the week that preceded the inspection, and while the footers were still in their normal flooded condition, dissolved oxygen (DO) content and resistivity of the water in the pier footers were measured with a probe at depth intervals of 3 feet between the datum surface (manhole cover deck) and the bottom (floor) of each pier footer. In addition, pier footer water samples were collected both before and at the commencement of dewatering. During the week of the inspection, which involved removing the water from the pier footers and entering the enclosed space, three cores were extracted by FDOT personnel from the south pier (111) and two cores were extracted from the north pier (112). Half-cell potential measurements were made in the local areas of the core extraction sites and samples of water emerging from the cracks on the interior walls of the pier footers were collected.

2.2.4.2 Methods and Results – First Field Study

Pier Footer Water Analysis

On October 9, 2012, the dissolved oxygen content of the water in both (north and south) pier footers was measured at 3 ft intervals between each respective manhole cover deck and footer bottom (floor) using an Extech DO600 oxygen sensor. The lowest observed oxygen levels (~ 0.05 ppm) were found at the bottom of each pier and the highest observed levels (~0.80 ppm) were found near the top (free) surface. A sample of water was collected at the free surface in each pier footer and subsequently analyzed at the USF Corrosion Laboratory (Table 4).

Table 4. Sunshine Skyway Pier Footer Water Laboratory Analysis Results, 9-9-2012. (Note that the disparity between DO observed on-site and DO observed in the laboratory can likely be attributed to oxygen uptake during sampling and transportation.)

Water Sample Location	pH	Resistivity, ρ (Ω–cm)	Dissolved Oxygen, *on-site* (ppm)	Dissolved Oxygen, *laboratory* (ppm)
Pier 111 (south)	8.31	2,440	0.06	1.93
Pier 112 (north)	8.50	2,630	0.82	1.42

The observed oxygen levels in the pier footers differed significantly from typical oxygen levels in Tampa Bay itself (~ 6 to 8 ppm) and the observed resistivities likewise differed

significantly from expected values (~ 25 Ω-cm). As resistivity is a primary indicator of salinity and salinity affects oxygen content measurement, a plan was implemented wherein resistivity would be measured coincidentally with a second measurement of DO at the same depth intervals as the initial measurements. The measurements were made on October 12, 2012 prior to dewatering and the results are presented graphically in Figure 35.

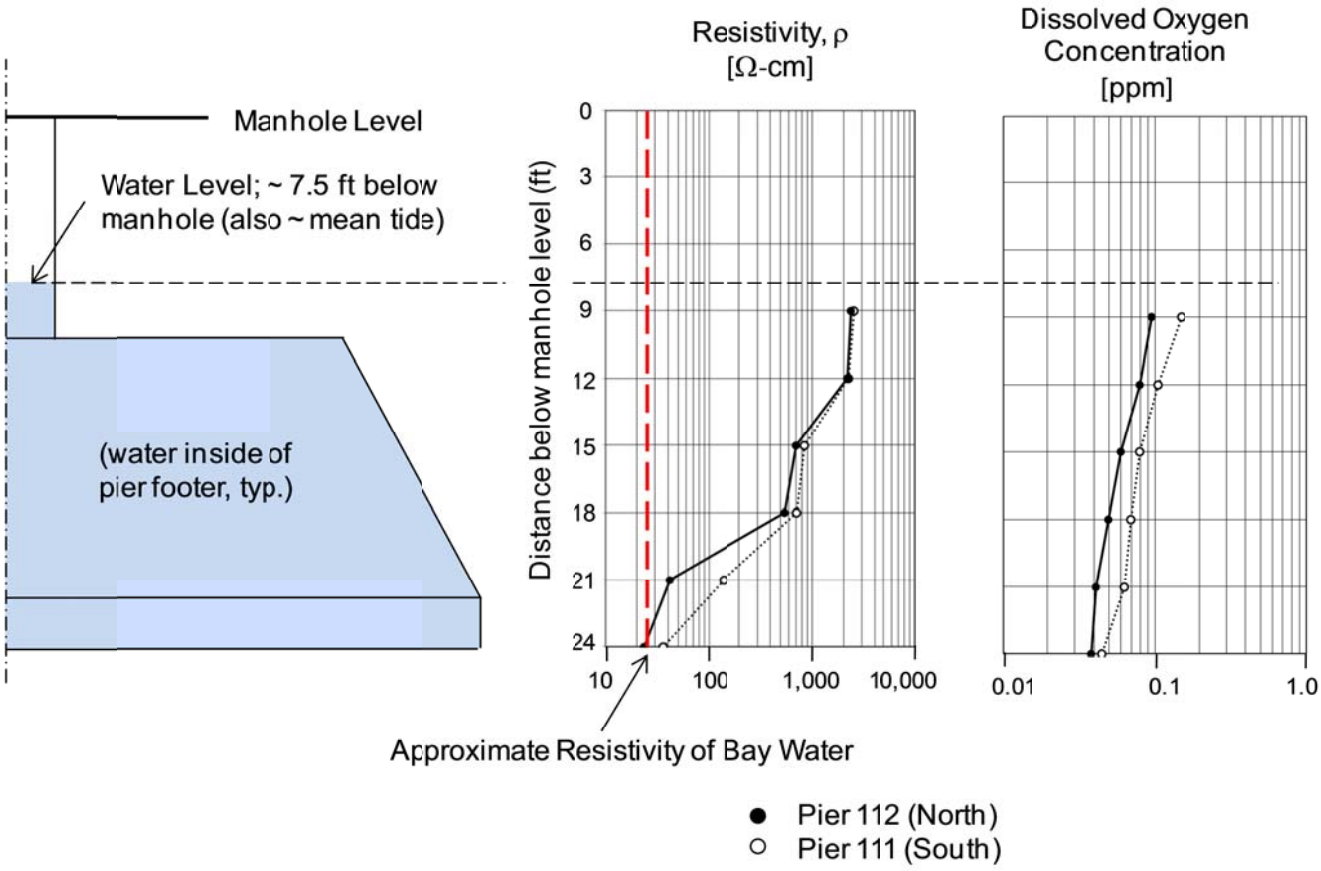

Figure 35. Resistivity and dissolved oxygen profiles; October 12, 2012.

The oxygen values observed on October 12 corresponded with the values observed on October 9 and the resistivity values measured on October 12 reflected an apparent salinity gradient between the free surface of the water and the footer floor. Resistivity values observed at the free surface corresponded with resistivity values typically observed in fresh water while resistivity values observed at each footer floor matched values observed in water in Tampa Bay.

The water in the pier footers, which had been pumped directly into the pier footers from Tampa Bay in 2008, had been expected to show the same properties as water in the local area of the piers but, as indicated, it did not. The observed differences imply that either some chemical or biological mechanism had consumed or was actively consuming the oxygen or that some volume of freshwater had infiltrated the pier footers and had mixed with the contained seawater

It was noted that, as the passivity breakdown of reinforcing steel is caused by the presence of chlorides, low chloride content of the water contained in the pier footers could be regarded as a favorable indicator of structural durability. As oxygen is required to support the cathodic reaction of depassivated steel, it was also noted that low oxygen content could likewise be regarded as favorable.

Post-dewatering Crack Seepage

As indicated above, water that seeped into each pier footer through cracks was collected and analyzed with respect to pH, resistivity, and dissolved oxygen (D.O.) content at the USF Corrosion Lab. The results of the analysis are presented in Table 5.

Table 5. Sunshine Skyway Pier Footer Crack Seepage Water Properties

	pH	**ρ [Ω−cm]**	**D.O. [ppm]**
Bay Water	8.05	24.4	5.52
Crack Seepage, Pier 111 (south), sample A	7.85	500	6.42
Crack Seepage, Pier 111 (south), sample B	9.02	125	6.05
Crack Seepage, Pier 112 (north)	10.94	167	5.25

The observed elevated pH levels reflect a typical alkalinity increase caused by the mixing of crack seepage water with concrete pore water.

Pier Footer Core Analysis

As indicated above, three 3-inch cores were extracted by FDOT personnel from the south pier (111). All cores within a given pier were extracted from positions in close proximity to each other. Core #1 was taken from a point along the centerline of crack #5 at a height of approximately 52 inches above the chamber “floor”. Core #2 was taken from a point offset (to the right) from the centerline of crack #5 by a distance of approximately 18 inches at a height of approximately 52 inches above the chamber “floor”. Core #3 was taken from a point offset (to the right) from the centerline of crack #5 by a distance of approximately 18 inches at a height of approximately 58 inches above the chamber “floor”. The extraction sites for both cores 2 and 3 were crack-free.

In all cases, coring was terminated upon reaching steel reinforcement and in each case, core extraction allowed visual access to the underlying rebar. Adhesion between the epoxy coating and the rebar was evaluated by scraping, to the extent possible with moderate effort, the coating from the bar with a sharp knife. Actual loss of adhesion was indicated by the ease with which the epoxy coating was removed from the exposed bar in the core #1 hole, and the dark colored surface of the bar (Figure 36). The epoxy coating on rebar in the core holes of cores #2 and #3 appeared to be intact, but the disbondment test was not conducted in these sites. Sharp knife tests conducted at the north site revealed poor adhesion in similar apparently intact coating.

Figure 36. Rebar at the bottom of hole at core #1; before and after scraping epoxy coating.

Two 3-inch cores were extracted from the north pier (112). Core #4 was taken from a point offset (to the right) from the centerline of crack #7 by a distance of approximately 6 inches at a height of approximately 72 inches above the chamber floor. The core #4 site was crack-free. Core #5 was taken from a point along the centerline of crack #7 at a height of approximately 76 inches above the chamber floor.

As with cores 1, 2, and 3, coring was terminated upon reaching steel reinforcement. The epoxy coating on bars at the bottom of cores holes #4 and #5 appeared to be continuous and intact but when the epoxy coating on the rebar exposed by core #4 was

cut with a sharp blade knife forming a triangular region, as in the case of core #1, the cut triangle was easily separated from the steel using the knife tip. This observation again indicated poor adhesion/bond between the coating and the rebar itself (Figure 37). Similar observation of poor adhesion was found at the rebar in the core #5 hole (Figure 38).

The findings of poor epoxy coating adhesion and absence of visible corrosion in cores #4 and #5 are consistent with previous determinations with marine epoxy coated rebar bridges in Florida, where coating disbondment was observed for rebar in service after only a few years.

Figure 37. Rebar at core #4 site; Note epoxy cut and easily peeled showing poor adhesion.

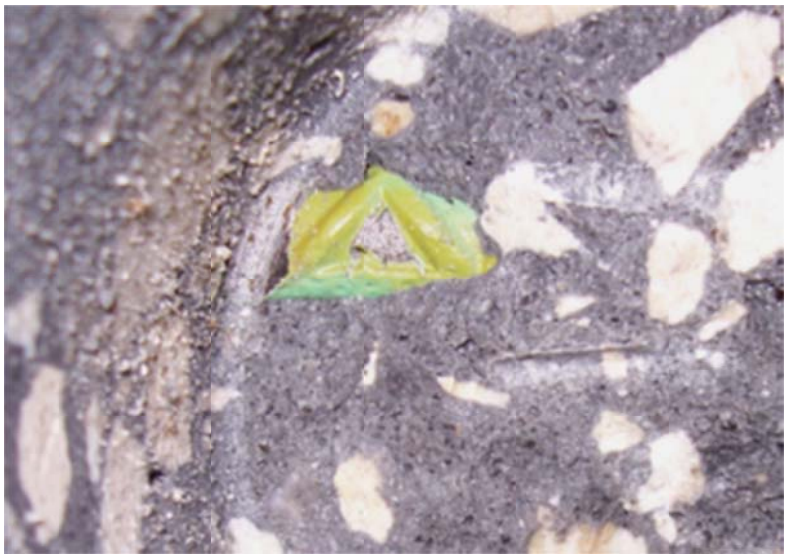

Figure 38. Rebar at core #5 site. Note poor adhesion.

Core Analysis

Core dimensions, extraction site observations, and as-received (native moisture content) surface resistivity values measured with a Wenner array probe are presented in Table 6.

Table 6. Core Data

Pier	FDOT Core #	Elevation Above Floor (in)	Core Length i.e. cover depth (in)	Core Site On Crack	Rebar Corrosion Observed	Epoxy Disbondment Observed	ρ, on line (kΩ-cm)	ρ, 120° CW (kΩ-cm)	ρ, 240° CW (kΩ-cm)
111 (S)	1	52	4.49	Y	Y	Y	26.1	26.2	23.5
111 (S)	2	52	5.24	N	N	N	23.3	27.0	24.8
111 (S)	3	58	5.91	N	N	N	29.7	29.8	26.5
112 (N)	4	72	4.49	N	N	Y	27.3	30.6	29.5
112 (N)	5	78	4.06	Y	N	Y	16.8	21.2	23.7

(Note: The "line" and associated angular offsets indicated in the surface resistivity headers refer to arbitrary measurement locations. Resistivity values reported include correction for finite specimen dimension and probe tip spacing. Y: Yes; N: No)

The concrete resistivity values were typical of those obtained in similar wet bridge substructures in previous surveys of bridges with comparable low permeability concrete [11].

Core Chloride Analysis

The depth at which chloride concentration would reach one half of the value observed at the exposed concrete surface was estimated to be approximately 0.50 inches according to $x_{1/2} \sim (D_{Cl}t)^{1/2}$ where t = nominal length of footer submersion ~25 years and D_{Cl} = 2E-9 cm^2/sec, which was the expected typical chloride diffusivity for fully wet concrete in this Sunshine Skyway Bridge element. To obtain good profile resolution of chloride concentration as a function of depth, a milling scheme was developed to provide thin milling in the first ½ inch and thicker slices at greater depths. The slicing scheme shown is in Figure 39.

A special tiltable mounting jig was constructed to ensure that milling was true to the core face, which deviated somewhat from the core axis perpendicular. The arrangement is shown in Figure 40.

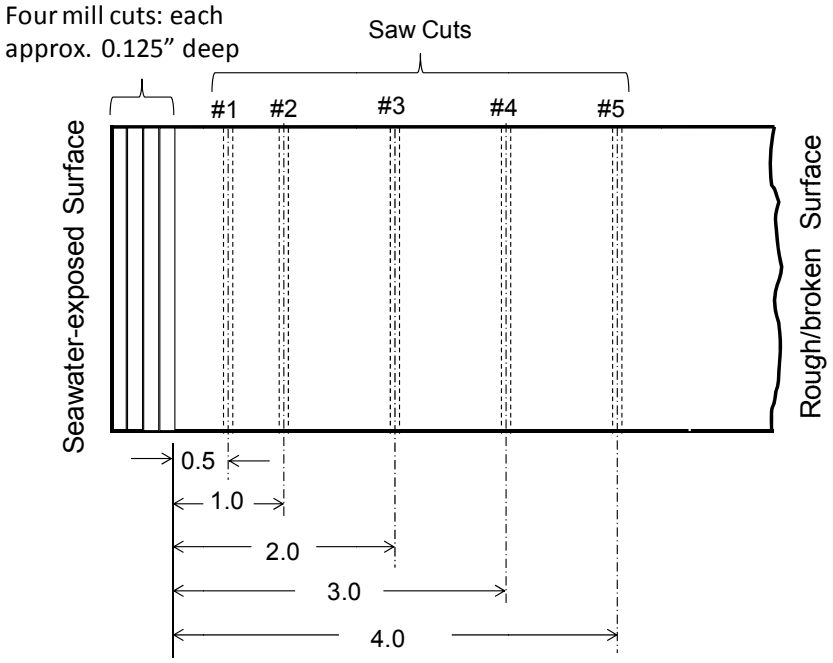

Figure 39. Core slicing scheme.

Figure 40. Core mounted on mill table.

Each powdered sample was divided into three equal portions for chloride analysis. Chloride analysis of the milled samples of Core #3 was conducted at the University of South Florida Corrosion Lab, and analysis of all remaining samples at the FDOT State

Materials Office. Although the USF analysis of the milled samples of Core # 3 was conducted in accordance with FDOT FM 5-516, there was high inconsistency among the triplicate results, likely due to subsequently discovered improper functioning of the silver/sulfide electrode used in the analysis.

The degree of inconsistency was evaluated by the ratio of the difference between the maximum and minimum observed chloride content to the average chloride content of the triplicate fractions at each depth. Results are shown in Figure 41. The ratio approached or exceeded 1 (indicating a 100% scatter) in two cases for Core #3, while it was about 1/3 or less in all other cases. Consequently, the results from those two cases were declared outliers and not used for profile evaluation.

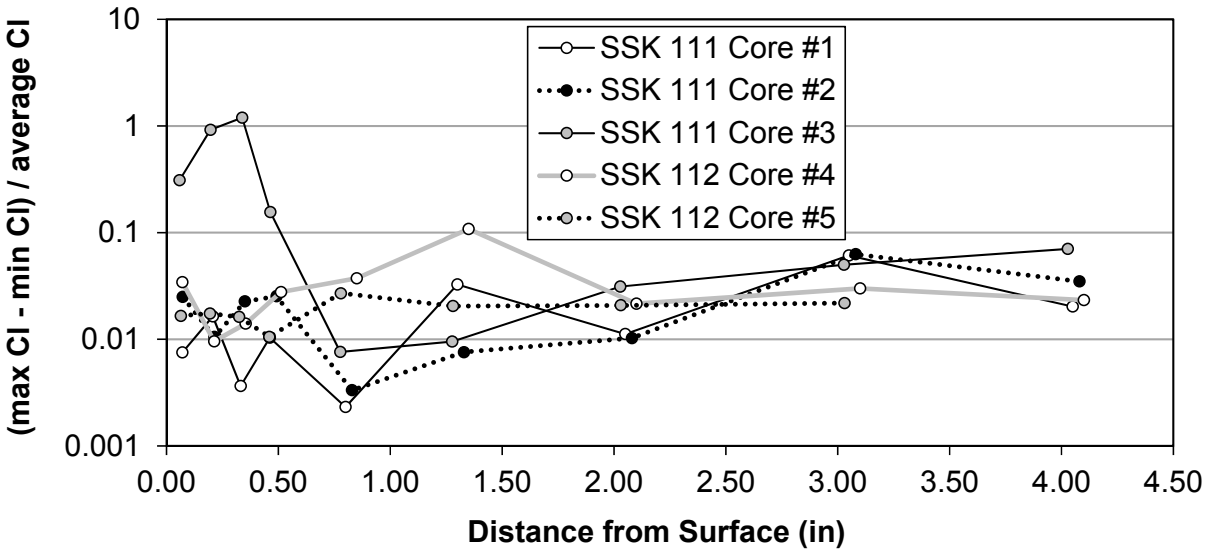

Figure 41. Ratio of the difference between the maximum and minimum chloride concentration values to the average chloride concentration value.

The resulting chloride profiles shown in Figure 42 indicated a decrease with depth as expected. It is noted that the results of the analysis of Core #s 1 and 5 ("on-crack" cores) presented higher low-depth chloride content than the other cores. However, even in those cases, the chloride content was less than ~½ of the values often seen in the splash-evaporation zone (e.g., 30 to 40 lb·yd^{-3}), consistent with the expectation of a more moderate surface chloride content in fully submerged concrete.

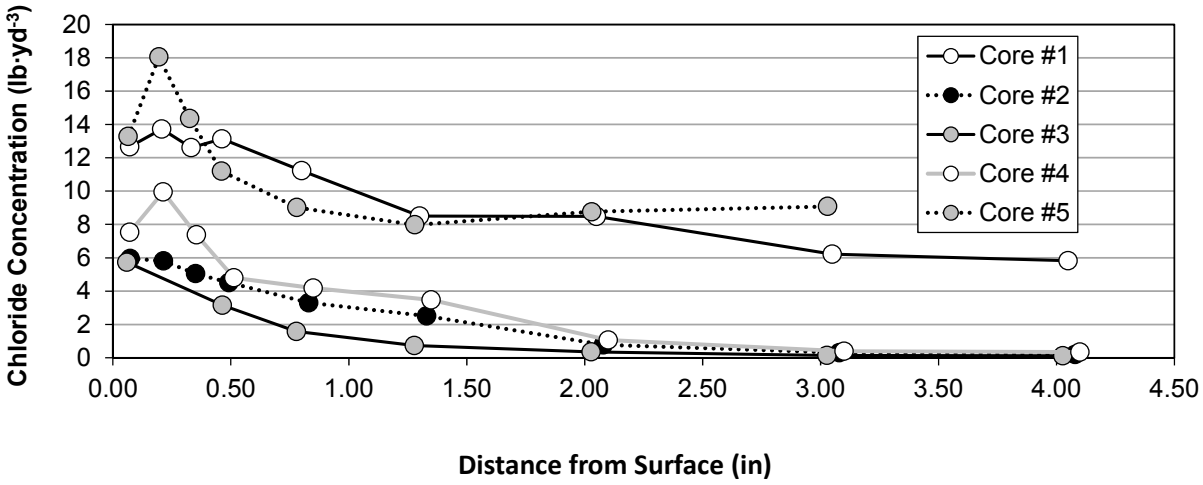

Figure 42. Chloride concentration as a function of distance from the outer/exposed surface.

Importantly, the on-crack cores showed not only greater surface chloride content than the others but also a much lower relative decrease of concentration with depth; concentrations at a depth of 4 inches for core #s 1 and 5 were approximately half of that at the surface, while for core #s 2, 3, and 4 it was more than 10 times smaller than at the surface. This behavior is typical of enhanced chloride penetration at cracks, which had been documented earlier for splash-evaporation regimes at Sunshine Skyway. This effect is illustrated in Figure 43 comparing the chloride concentration profiles of various pairs of cores. The chloride content is shown in logarithmic scale to better emphasize relative concentration trends.

In addition to the data for cores analyzed in this study, pairs of data are shown for cores that were extracted from a cracked region of the structure ("on-crack") and a companion core for each that was extracted from adjacent un-cracked ("sound") concrete. Each core in core pairs 1, 2, and 3 was extracted from Sunshine Skyway Bridge in 1997, as documented in Tables 3 and 5 in a previous FDOT report [11].

These observations support evidence of strongly enhanced chloride penetration in the submerged chamber wall of the Sunshine Skyway footers.

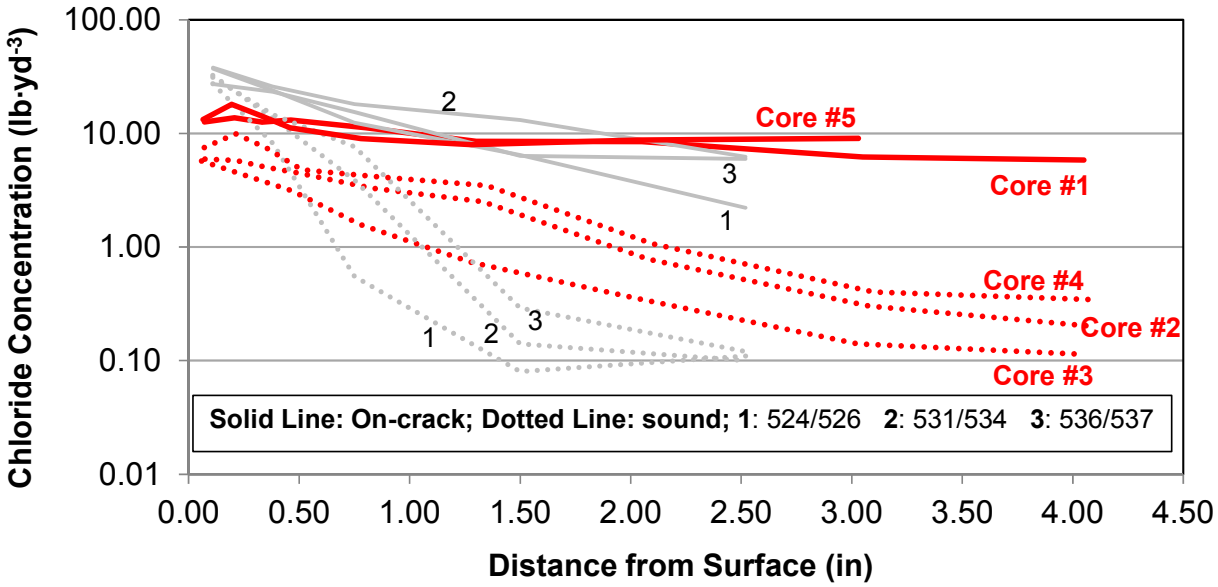

Figure 43. Comparison of chloride penetration in cores: on-crack and from sound concrete. Red lines indicate results from the current cores extracted from the chamber wall of Sunshine Skyway pier footers 111 and 112. The data associated with core pairs 1, 2, and 3 (extracted in 1997) and the numbers next to each pair (core designation codes) were taken from Sunshine Skyway splash-evaporation regimes in Sagüés et al. [11], Table 5. The two cores from each pier were taken from locations in close proximity to each other.

Hydraulic Transport

To evaluate the extent to which water can be exchanged between the general pier footer environment and the inside chamber of each pier footer, data was collected during the refilling of the chambers. Each chamber was filled to the top of its manhole opening and the water level was subsequently monitored and recorded at discrete points in time. Figure 44 (top and bottom) shows the water level at two points of observation for Pier 112. Figure 45 shows the water level evolution for both piers, revealing that in each case there is rapid and comparable water leak to the outside upon the action of a water head between the manhole water surface and the surrounding bay water surface. The head was on average ~7 ft during the early part of each test. Considering the manhole dimensions and the pressure head, the corresponding volume per water head-second in each case was determined to be on the order of 2 ft^3/ft-hour.

Figure 44. Top: Water level 30 minutes after filling, Pier 112. Bottom: Water level approximately 2 hours after filling, Pier 112.

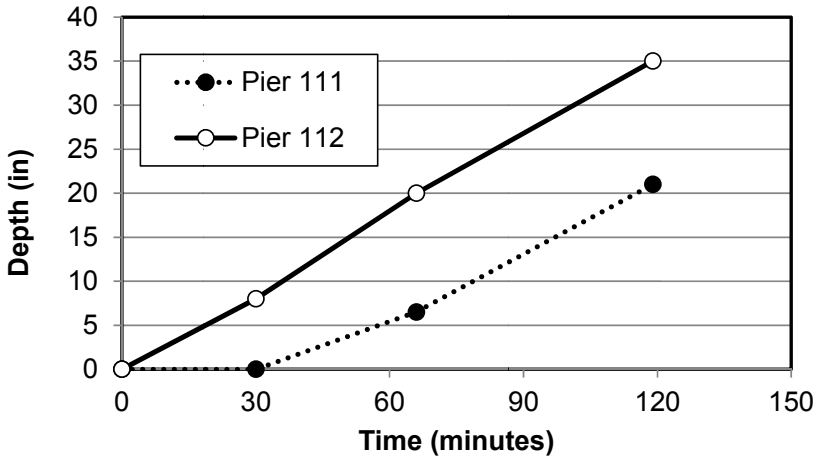

Figure 45. Water depth from manhole opening as a function of time.

Such leak rate is, on first approximation, sufficient to explain the development of substantial fresh water replenishment over a period of several years if rainwater is efficiently channeled to the manhole opening during frequent rain events. It is noted that the manhole cover is not watertight and that a preexisting channel may facilitate ingress. Observation of water flow during rain events is recommended as a means to ascertain whether this mechanism of water dilution is taking place.

2.2.4.3 Methods and Results - Second Field Study (2014)

Resistivity of water contained in the Sunshine Skyway pier footers was once again measured at 3 ft intervals between the manhole cover deck and footer bottom (floor) of each (North and South) pier footer during the biannual footer inspection on November 7, 2014. This work replicated similar work conducted in 2012 and described above (see also the 7th Quarter Progress Report, BDK84 TWO 977-16). Neither oxygen nor temperature could be recorded in this survey due to the failure of the probe shortly after the measurements were started. The water resistivity results are presented in Figure 46 along with the values recorded during October 2012 for comparison.

Both surveys (2012 and 2014) revealed general agreement between resistivity profiles in the North and South piers. Both surveys also revealed relatively high resistivity values of approximately 2,000 Ω-cm near the surface (i.e., water/atmosphere interface) of each footer (indicative of low-salinity as would be found in freshwater) and much lower values of approximately *25* Ω-cm (roughly equivalent to those typically observed in Tampa Bay) in the water near the floor of each footer. The results indicate however a notable change in the depth at which the transition from high to low resistivity values took place. As shown in Figure 46, the transition observed in 2014 appears to be approximately three feet higher (i.e., closer to the surface) than that in the 2012 survey.

In 2012 it was suggested that the existence of a resistivity gradient could be explained by the apparent introduction of rainwater (essentially high-resistivity freshwater) into the pier footers incrementally in time and the subsequent incomplete mixing with the seawater already contained in the footers. In light of this explanation, the difference between 2012 and 2014 might be attributable to the difference in duration of the freshwater infiltration period. The 2012 survey had taken place four years after removal/refilling with water drawn from the bay (2008) whereas the 2014 survey took place only two years after the most recent refilling. When compared with previous results, the results from the 2014 study suggest that the transition depth might increase with time and would further suggest that a profile made in 2016 will be more similar to that of 2012.

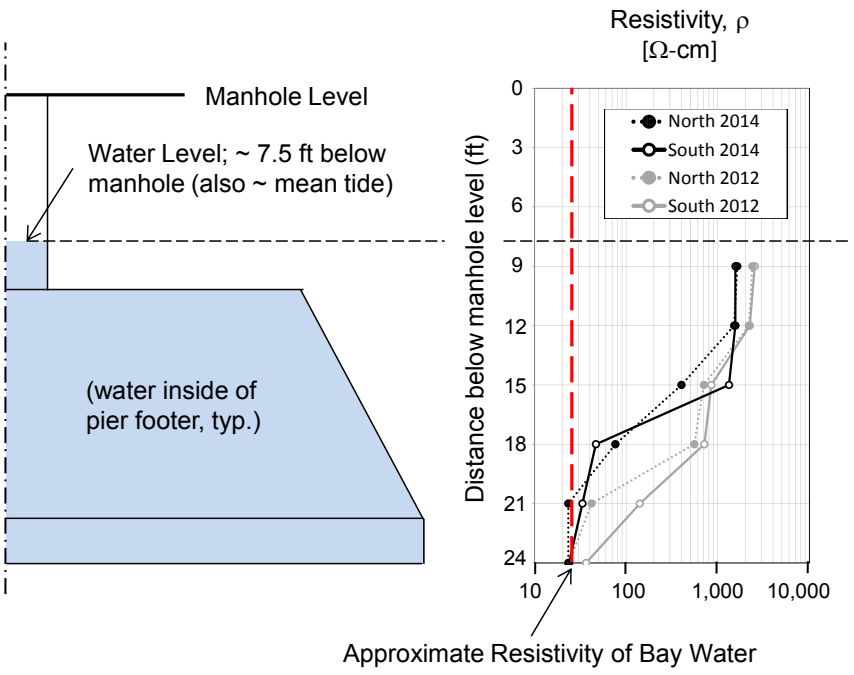

Figure 46. Resistivity of pier footer water; November 7, 2014

As indicated above, the failure of the dissolved oxygen probe prevented the acquisition of some of the desired data but this time an additional test, Biochemical Oxygen Demand (BOD) was conducted. The interest in BOD testing was inspired by the low oxygen values observed in 2012 which implied the existence of a chemical or biological mechanism which had consumed or was actively consuming the oxygen in the water in the footers. It was expected that the presence and nature of such a mechanism could be characterized and quantified via the measurement of the footer water's BOD.

Accordingly, water specimens were collected near the surface and near the floor of each footer (the latter conducted by the divers inspecting the footers) and subsequently analyzed. The greatest BOD values in both footers averaged only 4.8 mg/L which is similar to values that are obtained when sampling a "relatively unpolluted stream". [20] This would suggest that no strong chemical oxygen consumption mechanism was present there, but it is noted that tests of this type, at least in seawater, may tend to underestimate the BOD. [21].

2.3 Field Examination–Discussion of All Sites

2.3.1 Bridge Pilings

Table 7 is a comparative summary of the observations detailed earlier for the three structures from which decommissioned piles were extracted and examined.

Table 7. Summary of Bridge Piling Examination Observations

Bridge Designation	A Skyway Fishing Pier	B Pinellas Bayway Drawbridge	C Sunrise Key Bridge
FDOT bridge number	139002	150050	865725
Water chloride content (ppm)	18,504 [14]	19,144 [22]	20,000 (est)
Bridge construction date	1952	1962	1949 (est)
Element assessment date	2011	2013	2015
Age at time of assessment (years)	59	51	66 (est)
Structural element type	Square Pile	Square Pile	Square pile
Element size (cross section, in × in / m × m)	20 × 20 / 0.6 × 0.6	22 × 22 / 0.65 × 0.65	12 × 12 / 0.3 × 0.3
Number of piles assessed	2	1	1
Steel reinforcement type	#8 rebar / 2.54 cm diam.	0.5 inch / 1.26 cm prestressing strand	#5 rebar / 1.59 cm diam.
Number of reinforcement elements in cross section	8	20	4
Submerged length of each pile portion (linear ft / m)	19 / 5.8	23 / 7.0	17 / 5.2
Pile length below mudline (linear ft / m)	1.5 / 0.5	7 / 2.1	13 / 4.0
Length of submerged steel (linear ft / m)	304 / 93 [1]	460 / 140	68 / 21
Length of submerged steel directly examined (linear ft / m)	88 / 26.8 [1]	14 / 4.3	68 / 20.7
Fraction of submerged steel length directly examined	0.29	0.03	1
Length of examined submerged steel exhibiting corrosion (linear ft / m)	5.25 / 1.6 [1]	1.7 / 0.5	0.83 / 0.25
Fraction of examined submerged steel length exhibiting corrosion	0.06	0.12	0.012
Maximum corrosion penetration depth observed (in / mm)	0.082 / 2.1	.04 / 1.0 (est)	0.08 / 2.0
Maximum local corrosion-related cross sectional area loss (%)	29	20 (est)	23
Maximum depth below waterline of observed corroded region (ft / m)	18 / 5.5	12 / 3.7	13 / 4.0
Average cover depth (in / cm)	3 / 7.6	3.1 / 7.9	3.5 / 8.9
Average concrete resistivity in submerged region (kΩ-cm)	4.2	2.6	-
Concrete porosity (%)	16	13	-
Maximum measured concrete chloride concentration at reinforcement depth ($lb \times yd^{-3}$ / $kg \times m^{-3}$)	23 / 13.6	36 / 21.4	-

[1] Total for both piles; nominal amount disregarding H-piles and stirrup steel.

The most notable finding from the field examination of piles was the evidence of severe localized corrosion in the submerged zone of the piles, substantiating concerns indicated earlier in this report. The corrosion was not limited to the close proximity of the water level, but was also found in the submerged pile regions, including the region below the mudline. Considerations for interpreting those observations are presented in the following text.

The porosity and resistivity data, where available and when considered together, were indicative of high concrete permeability, consistent with the expected behavior from the concrete design guidelines prevalent during the epoch of construction [11].

The chloride content at the steel depth was high, reflecting the high permeability of the concrete, and amply exceeded the typically accepted corrosion threshold value that plain steel exhibits when it is in the passive state and at potentials typical of atmospheric exposure [23-25]. Given the high concrete permeability, the high chloride concentrations at the steel depth were likely to have been reached quite early in the service period of the piles, consistent with the nearly flat chloride profiles encountered on autopsy. Despite the chloride levels, submerged-zone steel exposed for examination was generally free of any severe corrosion except for the isolated strongly corroding regions affecting only a small % of the examined steel length. That observation agrees with the expectation, detailed in the Introduction, that the average rate of corrosion below water should be very small due to limited oxygen access to support the cathodic reaction. While the overall average was indeed low, the corrosion rate was however high in the small fraction of the surface where it took place.

The findings supported the hypothesis, also noted in the Introduction, that the effect of the small but finite cathodic reaction taking place on the entire submerged region (plus any additional coupling to cathodic regions above water) could be enough to sustain appreciable anodic activity over small regions. That effect would be facilitated if electrolytic coupling was made more efficient by a low electric resistance path between anodic and cathodic regions. As shown in the modeling section, the highly conductive seawater forms much of that path but some of it is through concrete. The concrete in the present cases exhibited low resistivity values, near the low end of the range typically reported for reinforced concrete [4], thus allowing effective coupling as well.

The localization of the corrosion also indicates that the majority of the steel that did not show appreciable corrosion must have been either in the active condition, and corroding at a very low rate, or alternatively have retained its initial passive character despite the presence of high chloride content on its surface.

To justify the first alternative (all submerged steel in the active condition) it would be necessary to explain why corrosion rate is so much greater (and sustained over long periods) on some regions than on others when no protective film is present in either. Such explanation could be made for example by invoking the fact that the corroding regions are associated with local concrete deficiencies [2,26] such as cracks, that somehow (for example by allowing faster removal of iron ions from the corroding region) enhance the rate of the anodic reaction compared to that of the rest of the steel surface.

Otherwise or synergistically, the stability of the local corrosion pattern could be proposed to be due to migration-enhanced chloride ion accumulation (to balance the ejection of positive metal ions at the anodic region) and local pH depression by associated hydrolysis [27], both phenomena acting to somehow strongly increase the anodic reaction rate over that of an also active region residing elsewhere. Such mechanisms nevertheless require that the corrosion at the rest of the surface should be dramatically smaller than in the affected region, even in the presence of severe chloride contamination. Suppression of corrosion there could be proposed to be due to macrocell coupling to the severely corroding regions, which would polarize negatively the steel in the rest of the steel assembly. However, such coupling would still leave the less corroding regions at a potential less negative than that of the more corroding spots, so for a given exchange current density of the anodic reaction the former would be the spots corroding faster, which was not the case. It would be necessary then to invoke mechanisms (as exemplified above) strong enough to yield a dramatically higher anodic reaction rate for a given potential at one set of active steel regions, than for other regions that are at an even more positive potential. These conditions constrain the plausibility of this alternative.

The second alternative (preservation of passivity over much of the submerged region) appears in comparison to the first to be more easily justified. In this scenario, before significant chloride buildup at the steel cover depth, the steel assembly is in the passive condition. The steel potential is at a value not very different from that of steel in an atmospheric regime, as the anodic reaction overall occurs at the very slow rate associated with anodic passive dissolution, hence demanding very little oxygen consumption and resulting in a relatively elevated mixed potential value. [24] As time progresses, chloride buildup at one given spot on the steel assembly causes the chloride threshold to be exceeded there. Given the prevalent value of the potential, the threshold value would be comparable to that of atmospherically exposed concrete [28]. The event localization could be due to a variety of causes, which may include but are not limited to a local concrete deficiency or slightly faster local chloride transport, somewhat greater surface chloride at the concrete surface near that spot, lower local threshold due to variability in the steel-concrete interface, and combinations of these and other circumstances. As a result of the local activation, the corrosion rate there increases dramatically over the original passive dissolution rate, while the rest of the assembly remains in the passive condition. That configuration results in local chloride buildup and acidification by the mechanisms noted above but also in a pronounced drop of steel potential that affects also the rest of the steel assembly to an extent and distance from the spot that depends on the steel polarization characteristics of the steel and on the extent of electrolytic coupling possible. That potential drop has the effect of increasing the chloride threshold of the still passive steel as in a classic cathodic prevention scheme [5,23-25,29], thus stabilizing its passive condition so the corrosion rate remains low. Conversely, corrosion at the active steel is aggravated by this coupling (in addition to adverse changes in the local chemical composition noted above) as it elevates the local potential, increasing the rate of the anodic reaction. The small corroding region / large passive zone configuration is thus stable and consistent with the observed behavior. As time progresses, chloride buildup at the steel surface increases.

If the chloride concentration becomes high enough, it may exceed the previously increased threshold and new corroding spots may appear. These spots will always tend to prevent corrosion in the rest of the steel assembly resulting in a localized and sustained state where corrosion is limited to a relatively small fraction of the steel assembly.

The scenario based on the second alternative in the above discussion has been articulated quantitatively in Chapter 3, Predictive Model Development and Implementation. As shown there, the model realizations successfully emulated the findings from the field examinations and were generally supportive of the plausibility of this interpretation.

2.3.2 Submerged Footers

The main footers of the Sunshine Skyway Bridge[1], which feature a unique design, were subject to in-depth FDOT inspection in 2012. The inspection offered the opportunity to explore some of the factors that indicate the possibility of corrosion in the submerged zone. Of special interest was the fact that the reinforcement in that bridge is epoxy-coated. Epoxy-coated rebar is no longer specified for use by FDOT but has been used in over 300 FDOT structures.

Observations pertaining to this project were conducted only in the main footer chambers, which have been normally filled with water since construction in the mid 1980's. Filling with water was intended as a beneficial action to prevent evaporative chloride enrichment at the concrete surface (to delay corrosion initiation) and slow down oxygen ingress to the reinforcement (to make the overall corrosion rate slow after initiation of corrosion).

The 2012 examination provided evidence of additional potentially beneficial effects of water flooding in the chambers. First, the fill water was found to be nearly anoxic, so not only was oxygen transport slow through water saturation of the concrete (the initially expected beneficial effect), but also the driving force for transport (oxygen concentration at the surface of the concrete minus that near the rebar) was greatly reduced. Second, and as confirmed during the 2014 follow-up measurements, the water resistivity over much of the chamber depth was much greater than that of the bay water. That greater resistivity was indicative of much reduced salt content and hence lowered tendency to initiate and sustain corrosion of steel, and also possibly a lesser tendency to support corrosion macrocells that would be detrimental after corrosion initiation.

The mechanism whereby the chamber water became nearly anoxic is expected to involve biological demand in a partially closed system, but the BOD tests performed were not clearly informative regarding the plausibility of that mechanism. The mechanism for reduced salt content in the chamber space appears to be replacement

[1] Full name: Bob Graham Sunshine Skyway Bridge

by rainfall and drainage into the manhole, facilitated by efficient hydraulic transport between the chamber and the exterior to allow for the initial saltwater to be pushed outwards by the increasing freshwater head. The measurements reported earlier support that hypothesis. A report by Figg Bridge Inspection, Inc. [30] addresses plausible means for rainfall concentration in that zone and supports the above interpretation.

Observations of the corrosion condition of reinforcing steel were limited to 5 cored holes that were made available as part of the bridge examination conducted by FDOT engineers and contractors. As indicated in Table 6, only one (centered on a crack) out of the 5 cores showed any indication of rebar corrosion. Rebar exposed by the other on-crack core and the three off-crack cores did not show signs of corrosion, although in all cases where coating adhesion was examined it was found to be deficient (as it is commonly the case for epoxy coated steel bars in Florida bridges [2]). Analysis and modeling of chloride penetration in the cores indicated that penetration to the rebar depth was found to be important only in the case of the on-crack core examined. The profiles also show an appreciable but still moderate level of surface chloride in the concrete, consistent with the submerged condition (no evaporative buildup) and with some extent of dilution by freshwater. The corresponding chloride diffusion coefficient for the sound concrete cores is consistent, together with the high concrete resistivity measured, with the concrete being of low permeability [2] which is as expected from the high performance mixture proportions specified for this bridge [2].

While the evidence obtained is from only a small number of locations, the results suggest that, given the low permeability of the concrete in the footer chambers, premature rebar corrosion may be a concern only at crack locations. The observation of corrosion in one of the two crack locations examined validates that concern. Corrosion at those locations should be aggravated to some extent by macrocell coupling with steel exposed at epoxy coating breaks in the rest of the assembly, and experiencing electric interconnection with the affected spot. Previous work has shown that such aggravation can be severe if the extent of coating breaks is high (for example, exposing as much as 2% of the underlying steel) [31]. An earlier survey of epoxy coated rebar condition in the Sunshine Skyway Bridge indicated 0.57% bare area exposed [32]. A report on work performed by a contractor during the 2012 inspection indicated a high degree of electric continuity (89% [30]) for the epoxy coated rebars in the footer chambers. Hence some key factors for macrocell corrosion aggravation of the crack-intersecting rebar are present, via mechanisms analogous to those considered in the previous subsections for pilings.

Continuing monitoring of the crack locations is recommended, as well as implementation of future corrosion control measures when needed. Part of the work performed by contractors in 2012 was to prepare the system for eventual implementation of cathodic protection [30], by fitting a number of contact rods. Given the high degree of rebar continuity observed that method of corrosion control may have good prospect for success if implemented.

3 PREDICTIVE MODEL DEVELOPMENT and IMPLEMENTATION

3.1 Predictive Modeling

The discussion in Section 2.3 examined alternative interpretations of the factors that resulted in the development and sustained presence of localized corrosion in the submerged zone. The alternative deemed to be most likely postulated normally passive steel surface, with localized active spots, a pattern that is sustained via macrocell coupling between active and passive regions. That pattern tends to delay activation of the passive regions due to an increase there of the corrosion threshold on polarization to more negative potentials. That hypothesis was selected for quantitative testing by creating models based on the hypothesis and comparing the model predictions with the field observations results. Given favorable comparison, the models can serve as powerful tools to forecast corrosion damage progression in existing structures (for better marshalling maintenance resources), as an aid for design of new structures, and as a means to assess the benefit of corrosion control alternatives, such as cathodic protection. The modeling was conducted in two stages.

The Stage 1 model assumed that a stable corrosion zone pattern was already in place and determined the resulting local corrosion rates. Assuming for simplicity that the pattern was unchanging, the resulting rates were integrated over a service life on the order of those of the examined extracted piling, and the resulting predicted steel loss was compared to that observed in the field. The model determined oxygen distribution, potential distribution, and corrosion current densities in a notional submerged reinforced concrete column of given geometry and material property values. The initial model simulations focused on a base case and on examining the effect of variations in oxygen diffusion, concrete resistivity, and surface area on the result. The geometry and material properties of the modeled column were based on a similar column of a related study from the literature. [6] The output of the Stage 1 model represented steady state conditions of structural elements experiencing active corrosion and did not consider any aspects of the initiation period such as chloride concentration on the concrete surface, chloride diffusivity, etc. The Stage 1 model provided estimates on the order of magnitude of foreseeable corrosion rates, and those were found to be generally consistent with those observed in the field, thus supporting the validity of the working assumptions noted earlier.

In Stage 2, the Stage 1 model was expanded to provide not only the expected corrosion rates under a given nearly steady steel activation pattern, but also the time evolution of the pattern as the structure ages. The model introduced the effect of macrocell coupling by incorporating recently developed Potential Dependent Threshold (PDT) features. Results of preliminary Stage 2 model simulations were also found to be consistent with the field observations and with the expected age evolution of the structures examined in the field, again supporting the likelihood of the hypotheses stated earlier. Consequently, the Stage 2 model was adopted for examination of the expected corrosion damage evolution that may exist under various concrete property scenarios, and also to estimate the potential for success and requirements of a galvanic cathodic protection system to

control corrosion of submerged steel, as well as other beneficial effects in the near-tidal zone.

3.2 Stage 1 Model: Behavior for an Established Corrosion Distribution Pattern

3.2.1 Background and Assumptions

The model addressed a notional partially submerged cylindrical steel-reinforced concrete column (0.525 m radius and 12 m height). The rebar cage was simulated by an arrangement of interconnected hoop elements made of 2 cm diameter bars separated by 0.062 m on center as indicated in Figure 47. Clear cover depth was 0.105 m. The waterline was placed at the midpoint of the total height and assigned elevation z = 6 m. The half above the waterline including the top end was regarded as having an electrically insulated surface, and the lower submerged half was regarded as having a surface with a single floating potential, given its direct contact with relatively high conductivity seawater. For simplicity, the bottom end of the column was regarded as an electrically insulated surface. For conservation of charge, the net electrolytic current integrated on the rest of the submerged surface was set to zero.

The selected dimensions, values, and variation schemes largely matched those of a previously modeled (finite difference (FD) simulation) column [6] except as noted below and the output of the present model was compared with the results of that FD model to verify consistency. The resistivity of the concrete and the oxygen diffusion coefficient of the modeled concrete were set at values below the waterline that were not elevation-dependent, reflecting the assumption that the concrete in this region was uniformly wet. For the region above the waterline it was assumed that increasingly drier conditions with elevation led to both higher resistivity and oxygen diffusivity.

Consequently and following previous work [6] both the concrete resistivity and the logarithm of the oxygen diffusivity were made to vary linearly with height above the waterline as indicated in Figure 47. Oxygen concentration C_O at all points on the column's exterior surface was assigned a constant value and oxygen flow through the top and bottom surfaces of the column was not allowed. A steel-to-concrete surface area ratio (i.e., steel placement density factor SF) of 1 (i.e., approximately 1 m^2 of steel surface area for every 1 m^2 of column exterior concrete surface area), typical for structures of this type, was used.

Corrosion of the reinforcing steel was modeled as resulting from both an anodic reaction

$$Fe \rightarrow Fe^{++} + 2e \qquad \text{(iron oxidation)} \qquad \text{eq. 1a}$$

and a cathodic reaction summarized by

$$O_2 + 2H_2O + 4e \rightarrow 4OH^- \qquad \text{(oxygen reduction)} \qquad \text{eq. 1b}$$

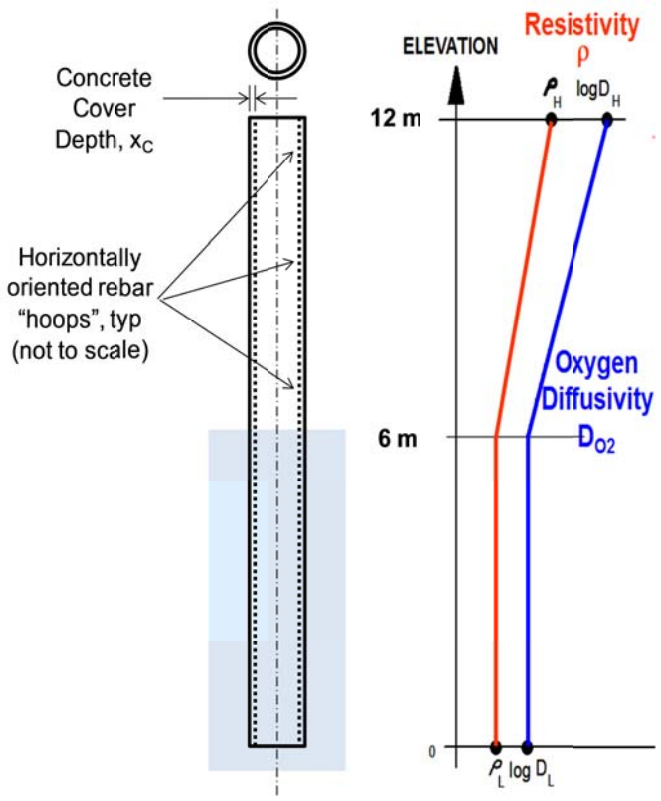

Figure 47. Concrete column model schematic diagram, concrete resistivity profile, and oxygen diffusivity profile.

The surface of each individual piece of rebar was designated as passive or active, according to the specifications of various simulation scenarios and other details described below. Polarization behavior for active dissolution was determined by a simplified adaptation of Butler-Volmer kinetics as in previous work [6] and is described by:

$$i_a = i_{0a}\, 10^{(E_s - E_{0a})/\beta a} \qquad \text{eq. 2}$$

where parameters consistent with treatment of a similar system [6] are defined and quantified in Table 8 [2]. On passive steel regions the anodic current density reflected slow passive dissolution at a potential-independent value i_p:

$$i_a = i_p \qquad \text{eq. 2a}$$

[2] The values of i_{oa} and i_{oc} were modified to adjust for differences in the geometric representation of the steel surface area; these values differ from those in the reference [6].

The cathodic reaction was assumed for simplicity to take place at similar rates on both active and passive steel regions, given by:

$$i_c = - i_{0c}(C_{SO}/C_O)10^{(E_{0c}-E_s)/\beta c} \qquad \text{eq. 3}$$

The signs for anodic and cathodic current densities were chosen to follow the usual convention. The oxygen mass flux associated with oxygen reduction at all rebar surfaces was equal to $i_c / 4F$ [mol / m^2·s]. The coupling between oxygen transport and the cathodic reaction at the steel surface was given by

$$i_c = - 4FD\ |dC/dn| \qquad \text{eq. 4}$$

where C is the concentration of oxygen in the concrete [3] and n is the distance along a line normal to the rebar surface. The current density distribution in the concrete domain is described by Ohm's law

$$i = -\rho^{-1}\ \nabla(E) \qquad \text{eq. 5}$$

and in that domain both i and C are also subject to their respective continuity equations

$$\nabla\ (\rho^{-1}\ \nabla(E) = 0 \qquad \text{eq. 5a}$$

$$\nabla\ (D\ \nabla\ C)= 0 \qquad \text{eq. 5b}$$

Equations 2 to 5 were solved simultaneously to yield the electric potential and the oxygen concentration anywhere in the concrete domain, which then were used to obtain the corresponding values of the reaction current densities at the steel surface.

[3] Consistent with previous modeling work [6] oxygen concentration is expressed in terms of estimated oxygen content of the pore water of the concrete, and the value of D is adjusted accordingly depending on the literature source used.

Table 8. Parameter Descriptions and Values

Parameter	Description	Value
β_a	Activation Tafel Slope for the anodic reaction	60 mV
β_c	Activation Tafel Slope for the cathodic reaction	160 mV
C_O	Oxygen concentration at the external concrete surface	3×10^{-7} mol/cm^3
C_{SO}	Oxygen concentration at the steel surface	(calculated)
D_L	Oxygen Diffusivity below the waterline	1×10^{-5} cm^2/s
D_H	Highest value of oxygen diffusivity above the waterline	1×10^{-3} cm^2/s
E_{0a}	Redox potential for the Fe/Fe^{++} +2e system	-780 mV_{SCE}
E_{0c}	Redox potential for the $OH^-/O_2 + 2H_2O$ +4e system	160 mV_{SCE}
E_s	Potential of steel with respect to electrolyte	(calculated)
i_{0a}	Exchange current density for the Fe/Fe^{++} +2e system	3.75×10^{-8} A/cm^2
i_{0c}	Exchange current density for the $OH^-/O2 + 2H2O$ +4e system	1.25×10^{-9} A/cm^2
i_p	Passive anodic current density	0.01×10^{-6} A/cm^2
X_C	Concrete cover	10.5 cm
ρ_L	Concrete Resistivity below the waterline	2 kΩ-cm
ρ_H	Concrete Resistivity above the waterline	10 kΩ-cm

The model simulations assumed that the steel above water was subject to corrosion in a splash zone that extended vertically upward from the waterline to a level 2 m above it. Simulation scenario number 1 (see Table 9), which was regarded as the base case, designating as active all rebar in both the splash zone and submerged region, and designating as passive all rebar in the rest of the column above the waterline. Active and passive area designations for the other scenarios are presented in Table 9. Note that the indicated surface areas of active steel in the submerged region (nominal percentages) were selected arbitrarily to provide adequate detail over the span of possible percentages.

Table 9. Distribution of Active and Passive Regions with 1:1 Steel-to-Concrete Surface Area Ratio (i.e., SF = 1)

Simulation Scenario Number	Condition of Steel in Splash Zone	Surface Area of Active Steel in Submerged Region (Nominal Percentage)
1	active	100
2		30
3		10
4		3
5		1
6	passive	100
7		30
8		10
9		3
10		1

All scenarios except for 1 and 6 represent cases that involve discrete active regions of the rebar assembly (i.e., a limited number of rebar hoops) centered at a point halfway between the bottom of the column and the waterline. Active region size (i.e., nominal percentage) was the simple ratio of the number of arbitrarily selected bars to the total number of below waterline bars (i.e., 95). These scenarios represent idealized conditions of localized depassivation that could arise for example given lower rebar cover depth, poor concrete consolidation, or preexisting cracks in the specified region. Upon initiation of corrosion in the region, the adjacent areas would tend to stay longer in the passive condition as a result of the newly anodic region providing a form of cathodic prevention [5,29] and thus the corrosion pattern could be treated as being stable for at least part of the structure's life. This issue is addressed in greater detail in section 3.3, Stage 2 Model.

Note that scenarios 1-5 designated all rebar in the splash zone as active. Scenarios 6-10 designated the rebar in the splash zone as passive to simulate cases in which the splash zone had been protected by means such as impermeable coatings or alternatively rehabilitated after removal of chloride contaminated concrete and replacement with new concrete. In all scenarios the simulation yielded data that was used to determine the maximum anodic current density in the active regions.

The model was developed using a COMSOL Multiphysics® platform. As a sensitivity test, additional exploratory cases were performed where the number of steel bars was doubled (SF = 2) and the exchange current density of the Faradaic reactions halved, all other variables remaining the same.

3.2.2 Results

Figure 48 shows a graphical example of the computation results for Case 1. Potential (E) and oxygen concentration (O_2) profiles are shown as color gradients for the column cross-section. Note that the consistent red color (Figure 48, middle) below the top of the splash-evaporative zone indicates that the potential is low (i.e., very negative) everywhere below that level as all steel was designated as active. Note also that the consistent dark blue color at rebar depth in the same region (Figure 48, right) indicates that oxygen concentration approaches zero as all oxygen is consumed in the cathodic reaction. The color-coded trends correspond to expected results, as diffusion-limited oxygen reduction below water leads to oxygen depletion inside the column in that region and potential is more negative in the submerged region than near the top. The results were also in general agreement with those obtained in a previous simplified modeling effort [6].

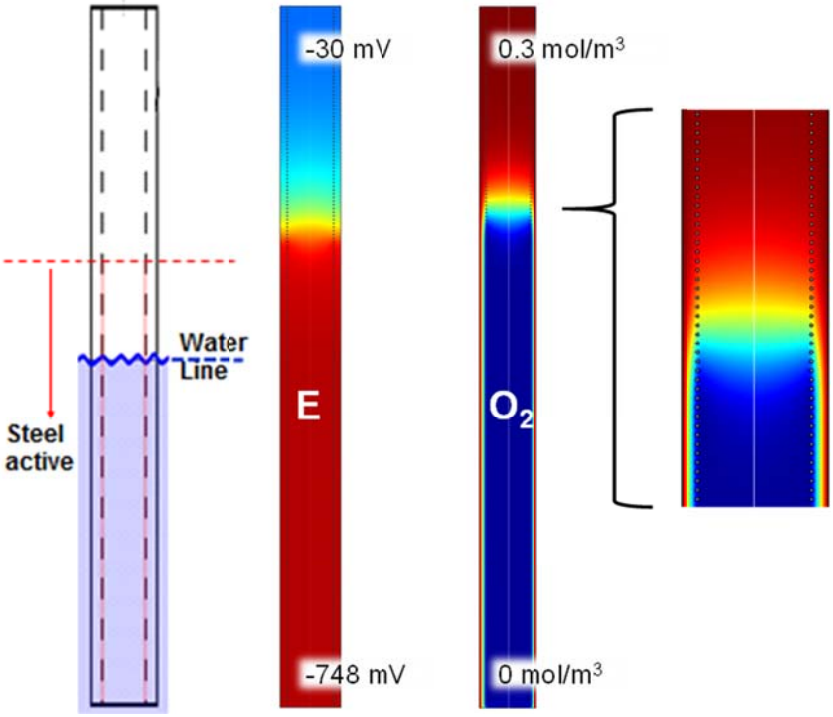

Figure 48. Potential and oxygen concentration configuration for base case (Case 1).

Figure 49 (top) shows oxygen diffusion flux streamlines from the outer surface of the concrete (where C_O = 0.3 mol/m^3) to the region near the bars (shown in cross-section). Oxygen can be seen to travel normal to the column surface until reaching the region in

close proximity to the steel bars. At this point it proceeds directly to the bar surface for the cathodic reaction at the bar surface. Note also that essentially all the O_2 is consumed by the cathodic reaction occurring at the bars and that virtually no O_2 reaches a depth much greater than the "inner" edge of the bars. Figure 49 also shows (bottom) color-mapped steady state distribution of oxygen concentration.

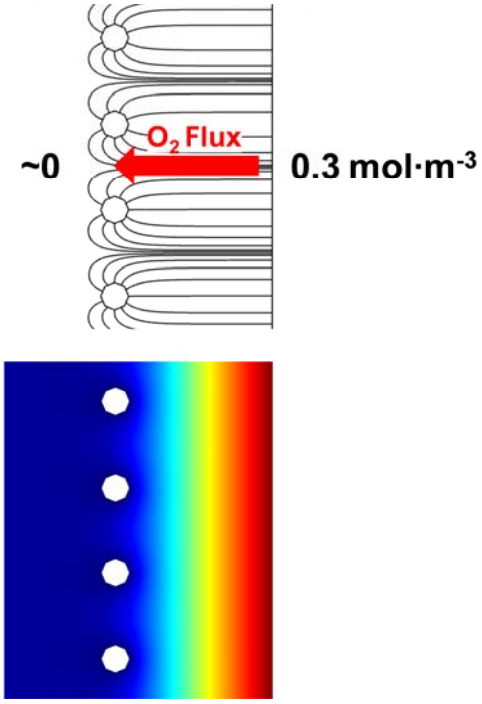

Figure 49. Top: Streamlines that indicate the oxygen diffusion path between the outer concrete surface and the surfaces of individual rebars. Bottom: Color variation representation of the oxygen concentration between the outer concrete surface and steel bars (i.e., magnified view of the edge of the column in the submerged region depicted in Figure 48)

Based on the potential and oxygen concentration distributions generated by the model simulations, the anodic current density was calculated and averaged on the circumference (i.e., cross-sectional perimeter) of each individual rebar hoop in the column. The result was plotted as a function of column elevation as indicated in Figure 50 and

Figure 51. The corresponding E and O_2 profiles are shown using the same color coding scheme used in Figure 48. The corrosion rate corresponding to the anodic current densities was calculated for each scenario and averaged over the active steel in the submerged region.

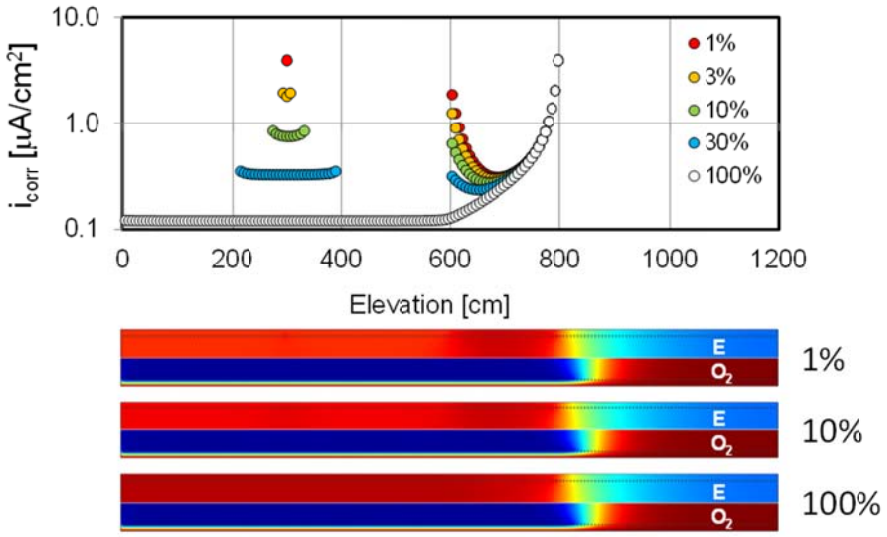

Figure 50. Top: Predicted corrosion current densities associated with active rebar (of indicated percentage) centered at z = 3 m and in the splash zone (z = 6 to 8 m); Bottom: Electrical potential and oxygen concentration profiles in each scenario color coded as in Figure 48. Note localized dark regions of high anodic current density in the electrical potential profiles

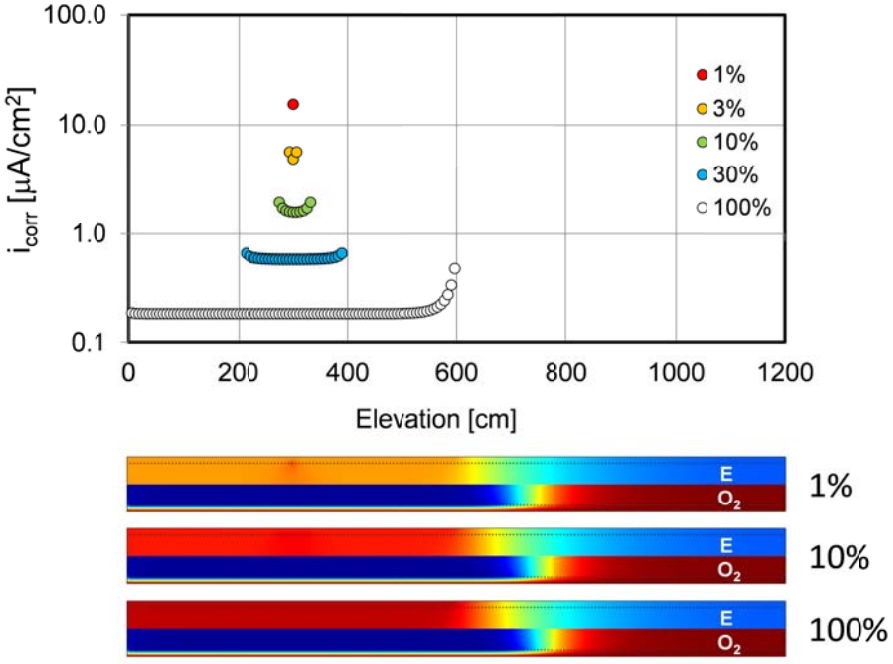

Figure 51. Top: Predicted corrosion Current Densities associated with Active Rebar (of indicated percentage) Centered at z = 3 m; Bottom: electrical Potential and Oxygen Concentration profiles in each scenario color coded as in Figure 48. Note localized dark regions of high anodic current density in the electrical potential profiles.

Figure 52 shows each result plotted as a function of its associated active rebar percentage below the waterline. The results observed in the case of uniform depassivation in both scenarios 1 and 6 (corrosion current density ≈ 0.1-0.2 $\mu A/cm^2$ and corresponding corrosion rate ≈ 1.2-2.3 $\mu m/yr$) agree well with results observed in prior work [6,13]. In contrast, the local anodic current density/corrosion rate was much higher (by up to two orders of magnitude) in cases that involved highly localized anodes (e.g., scenarios 2-5 and 7-10) even though the overall cathodic reaction rates were small. The corrosion rate enhancement was proportionally greater as the active zone involved smaller fractions of the steel surface. Clearly, while the overall amount of cathodic reaction remained nearly the same and was diffusion-limited, the concentration of the balancing anodic reaction in increasingly smaller areas led to the much higher corresponding local corrosion rates. The macrocell action is facilitated in part by the strong coupling between anodic and cathodic regions provided by the highly conductive seawater surrounding the submerged region, represented by the equipotential treatment of the submerged surface.

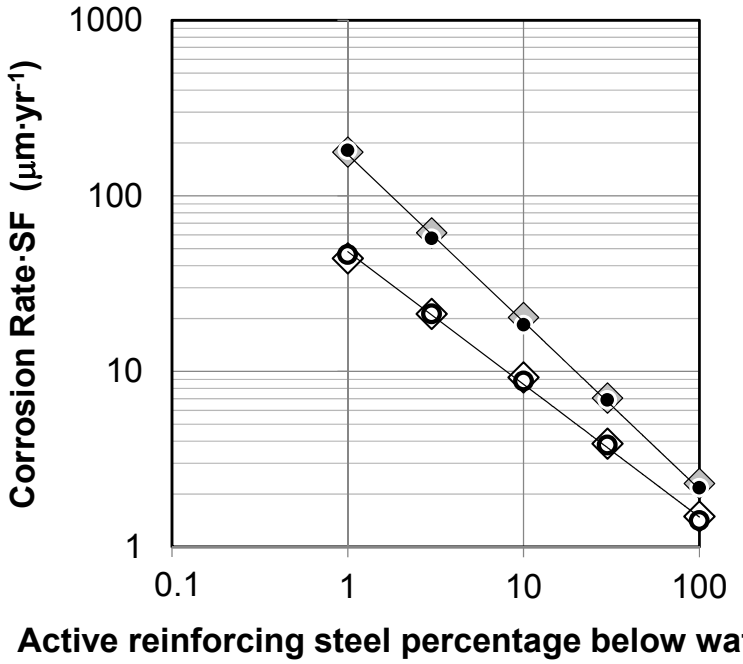

Figure 52. Corrosion rate of actively corroding steel in submerged zone as a function of active rebar percentage. Open symbols: cases with activation above waterline. Filled symbols: no activation above waterline, resulting in higher corrosion rates in submerged zone. Circles: Main calculations with SF = 1. Diamonds: exploratory SF = 2 cases with adjusted parameter values, scaled as indicated in the text for appropriate comparison.

Figure 52 also shows the results for the exploratory cases where the steel placement density was doubled (in conjunction with lowering the exchange current densities to obtain approximately the same overall macrocell current levels). Since in the submerged zone nearly limiting diffusional conditions predominated, for a given rebar

cover the corresponding value of the total available oxygen reduction current would remain about the same regardless of the value of SF. Hence the resulting submerged zone corrosion rates for SF = 2 would be expected to be approximately half of those observed for SF=1. This expectation was confirmed by the corrosion rate results of the SF = 2 simulations, which upon multiplication by the SF fell in line with the corrosion aggravation trends obtained in the main series of calculations. Thus, these tests indicated that the main conclusions from the model analysis were not unduly sensitive to system choice.

Of significant interest is that each simulation involving passive rebar in the splash zone indicated a higher maximum anodic current density than that of the corresponding simulation with active rebar in the splash zone. The assumption of passive rebar in the splash zone effectively simulates cases where successful corrosion abatement was implemented in that part of the column. As noted in Chapter 1, Introduction, corrosion in the splash zone would be expected to mitigate corrosion in the submerged zone due to beneficial galvanic coupling. Conversely, absence of corrosion above water would be expected to have the opposite effect, so aggravation of corrosion in the submerged zone could ensue. The model outcomes were consistent with those expectations.

Overall, the modeling results supported the hypothesis that very severe localized corrosion can arise in the submerged portion of the piles if the corrosion is localized and the rest of the steel assembly is in generally passive condition. The values of the model-calculated corrosion rates in Figure 52 and those obtained in the various field examinations (Figure 14, Table 7) are generally consistent with each other and further supportive of the overall interpretation noted earlier for these phenomena.

3.3 Stage 2 Model: Evolution of Corrosion with Structure Age

3.3.1 Background and Assumptions

The Stage 1 modeling explained how localized corrosion in the submerged zone could reach severe levels even though on average the amount of corrosion in the same zone was minor. The model however addressed only a steady state condition, without consideration of how or where corrosion-related damage could progress as the structure ages. Stage 2 modeling was intended to help project how damage develops and progresses with time and to provide a quantitative assessment of the extent of corrosion control that may be achieved with alternative protective measures.

As indicated in the Introduction, while active corrosion below water can escape detection, it can also be effectively suppressed for some time by a mechanism that involves localized increases in the chloride threshold value. The chloride threshold was found in particular to increase when potentials become appreciably more cathodic than the open circuit potential in atmospheric air-exposed concrete. [23,24,29,33,34] The observations may be abstracted as indicating that that the value of the chloride threshold, C_T increases as the result of cathodic polarization according to

$$\log\left(\frac{C_T}{C_{T_0}}\right) \sim \frac{E_{T_0} - E}{|\beta_{C_T}|} \qquad \text{eq. 6}$$

where C_{T_0} is the chloride threshold at the baseline potential E_{T_0}, and B_{C_T} is the so-called cathodic prevention slope.

Galvanic coupling between steel in the submerged zone and steel in the tidal and evaporation zones (which might have started corroding earlier in the life of the structure) can effectively make the potential of the submerged steel more negative via macrocell action. This could elevate the chloride threshold and thus, under some conditions, retard the initiation of corrosion below water (cathodic prevention). [4,23,24,29]

Even after corrosion eventually initiates in the submerged region its severity could be mitigated by galvanic coupling with corroding steel in the atmospheric air-exposed region. In both instances the extent of corrosion above water would be increased and corrosion in the submerged zone would be decreased. However this protective mechanism for the submerged zone is not operational if the steel in the tidal and evaporation zones is in the passive condition. Thus, as noted in the Stage 1 Model discussion, corrosion control measures (e.g., use of thicker concrete cover and less permeable concrete) for the above-water region may paradoxically aggravate corrosion in the submerged zone, at least early in the structure life.

Potential Dependent Threshold (PDT) features were added to the existing partially submerged reinforced concrete column model to account for the corrosion-preventing effect of active steel regions on passive regions in the rest of the structure. The model was subsequently used to simulate corrosion initiation under various conditions during service lives of approximately 100 years.

The addition of PDT features to the Stage 1 model involved: 1. Simulating the ingress of chloride ions via diffusion into the bulk of the notional concrete column, 2. Monitoring chloride concentration near each discrete segment of the rebar cage, 3. Recognizing points in time when the chloride concentration in each discrete region exceeded the chloride threshold in that region, 4. Modifying the electrochemical condition of the steel surface (i.e., changing it from “passive” to “active”) in that region where the threshold was exceeded, and then recalculating the resulting, new potential profile with associated new chloride threshold profile. 5. Allowing the chloride diffusion penetration in the system to further evolve until the new local threshold is exceeded in another region, changing steel character there to “active”, and repeating the process. [24]

As in Stage 1, actively corroding and passive regions were both assigned anodic current density but unlike Stage 1 which didn’t involve cathodic protection (CP), the actual anodic current density differed according to the corrosion status and polarization nature of the steel. In the actively corroding regions, the anodic current density was calculated according to eq. 2. In passive regions with sufficient anodic polarization, the anodic current density was assigned a small, constant, potential-independent value i_p (see Table 8) that represented residual passive dissolution. In passive regions subject

to cathodic polarization such that steel potential was made negative enough to cause an incipient active condition, the anodic current density was calculated as described below.

Steel in alkaline media without aggressive ion contamination does not exhibit a pronounced passivation current density peak [35]. The value of i_a for nominally passive steel was therefore approximated by eq. 2, using the local E_S, when the calculated value of ia was less than i_p. The threshold value V_T at which this happens can be calculated by determining the potential at which i_a, calculated using eq. 2, equals the value of i_p. Using the above baseline parameter values, V_T was determined to be -0.814V. The value of i_a for nominally passive steel therefore reverts to that given by eq. 2 in locations where potential is more negative than V_T, resulting in very small anodic current densities.

On executing the Stage 2 model realizations it was found that under the above conditions the local mixed potential tended to stay above the hydrogen evolution range, even upon combination with a strongly polarized cathodic reaction under cathodic protection. Hence, the cathodic reaction selection in these simulations was limited to oxygen reduction. This choice neglects for simplicity any hydrogen evolution that may be taking place at the corroding spot, where the medium has a lower pH than the rest [36].

3.3.2 System Modeled and Scope of Calculations

The physical system modeled had dimensions and configuration similar to those used for the Stage1 calculations. As indicated there, the system is a relatively large substructure column with a steel placement pattern that would correspond to densely-placed steel hoops for computational simplicity. In this arrangement rotational symmetry can be assumed and there are no longitudinal elements. As before, the default number and size of the rebar making up the hoops were chosen to simulate a total steel placement density comparable to that encountered in a typical substructure column or pile, namely on the order of 1 ft^2 of steel surface per ft^2 of external concrete surface. All hoops were declared to be electrically interconnected as would be the case of a rebar mat with multiple shorts created by tie wires.

From a macroscopic electrochemical standpoint, the configuration adopted is close enough to that of an actual system. This results in nearly the same overall current distribution that would be encountered in an actual rebar mat if corrosion were to occur uniformly around the perimeter of the column.

The calculations were intended to reveal overall trends of corrosion evolution and possible behavior under cathodic protection. The adoption of a cylindrical geometry and simulation of rebar reinforcement does not prevent application of the computation results to, for example, square cross-section piles with prestressing strands having the same concrete cross-section, length, and steel placement density and concrete and environmental regimes. For piles with length, cross-section, and other properties that

differ significantly from those assumed in the calculations, the general trends identified here would still largely apply. In such cases, detailed calculations with the specific properties of interest could provide more quantitatively relevant information for those cases as implementation of changes is fairly straightforward with the modeling platform used. Other issues relevant to model simplifications and possible future model improvement are noted in Section 4.2.

The elevation-dependent concrete property and environmental chloride concentration are shown in Figure 53. The shape of those profiles reflect typical conditions in Florida marine bridge substructures and the chosen patterns for concrete resistivity and oxygen diffusivity followed the rationale discussed in the Stage 1 model description. The surface concentration chloride profile, introduced here for Stage 2, shows high chloride accumulation just above the waterline representing evaporative salt concentration, as discussed in detail in previous publications [6,11,32]. For initial calculations the chloride concentration on the exterior surface of the column was set as a simple time-invariant function of elevation: uniform below the waterline (i.e., elevation 0 to 600 cm; C_{sB}=9 kg/m^3); rising sharply to a peak at the waterline (C_{sP}=20 kg/m^3) and then decreasing linearly to zero at the top of the column (i.e., elevation 1,200 cm; C_{sT}=0 kg/m^3; see brown line in Figure 53). For the main sequence of realizations the chloride profile was assigned statistical variability, as described later. Table 10 lists the values assigned to the model parameters and the variations of those parameters addressed in the main sequence of cases examined. The steel polarization and cathodic prevention parameter values are based on those used in previous investigations [24], with some differences from the values chosen for Stage 1 to better match those sources. The key concrete properties of resistivity and chloride diffusivity were assigned various alternative values representing a broad range of conditions. Those values included combinations typical of less protective, highly permeable, and highly conductive concrete (i.e., high chloride diffusivity, low resistivity cases) such as that encountered in some of the Florida Keys bridges that experienced early corrosion in the 1980's [32], and in some of the older bridges whose piles were examined in this project. The combinations also included values characteristic of highly protective concrete (i.e., low chloride diffusivity, high resistivity cases) approaching conditions encountered with the use of FDOT Class V concrete with low water to cement ratio, high cement content, and pozzolanic admixtures [11]. For completeness, cases with medium ("Med" in the table and figures) parameter values and combinations of contrasting resistivity and chloride diffusivity properties were included as well. The matrix of combinations explored is detailed in Table 11.

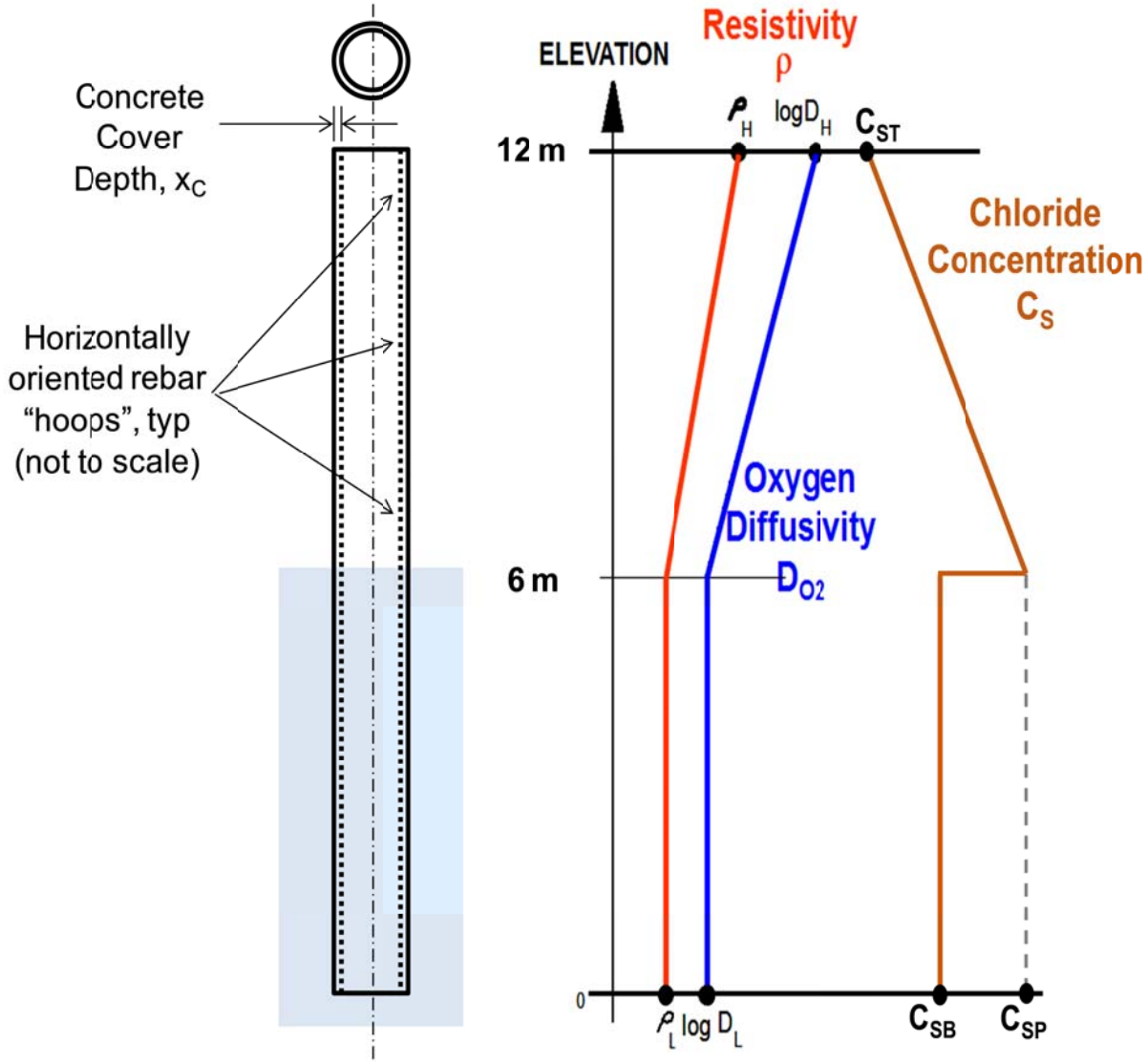

Figure 53. Chloride concentration profile at exterior surface of concrete (brown) used for Stage 2 calculations. Other pattern shapes are same as those in Stage 1 simulations.

Table 10. Parameter values used in the Stage 2 simulations

Parameter	Description		Value
β_a	Activation Tafel Slope for the anodic reaction		60 mV
β_c	Activation Tafel Slope for the cathodic reaction		140 mV
β_{CT}	Cathodic prevention Slope		0.55 V
C_O	Oxygen concentration at the external concrete surface		3×10^{-7} mol/cm^3
C_{SO}	Oxygen concentration at the steel surface		(calculated)
C_{sB}	Chloride concentration at concrete surface, bottom		9 kg/m^3
C_{sP}	Chloride concentration at concrete surface, waterline		20 kg/m^3
C_{sT}	Chloride concentration at concrete surface, top		0 kg/m^3
C_{T0}	Baseline chloride threshold value at E_{T0}		1.78 kg/m^3
D_L	Oxygen diffusivity below the waterline		1×10^{-5} cm^2/s
D_H	Highest value of oxygen Diffusivity above the waterline		1×10^{-3} cm^2/s
D_{Cl}	Chloride diffusivity	Low	8.3×10^{-9} cm^2/s
		Med	2.5×10^{-8} cm^2/s
		High	7.5×10^{-8} cm^2/s
E_{0a}	Redox potential for the Fe/Fe^{++} +2e system		-780 mV_{SCE}
E_{0c}	Redox potential for the $OH^-/O_2 + 2H_2O$ +4e system		160 mV_{SCE}
E_s	Potential of steel with respect to electrolyte		(calculated)
E_{T0}	Baseline steel potential value at C_{T0}		-0.100 V
i_{0a}	Exchange current density for the Fe/Fe^{++} +2e system		3.75×10^{-8} A/cm^2
i_{0c}	Exchange current density for the OH^-/O2 + 2H2O +4e system		1.4×10^{-10} A/cm^2
i_p	Passive anodic current density		0.01×10^{-6} A/cm^2
x_C	Concrete cover		7.5 cm
ρ_L	Concrete Resistivity below the waterline (three cases)*	Low	3.5 kΩ-cm
		Med	10.5 kΩ-cm
		High	31.5 kΩ-cm
ρ_H	Concrete Resistivity above the waterline (three cases)*	Low	17.5 kΩ-cm
		Med	52.5 kΩ-cm
		High	157.5 kΩ-cm

* Note that each case modeled used both a ρ_L and a ρ_H value linked according to the description "High", "Med", or "Low ". Example: "High" resistivity cases used ρ_L = 31.5 kΩ-cm and ρ_H = 157.5 kΩ-cm. The "High", "Med", or "Low" designation for D_{Cl} was independent of that used for resistivity.

Table 11 - Cases evaluated.

Case Number		1	2	3	4	5	6	7	8	9	10	11	12	13	14	15	16	17	18
Concrete Resistivity*	High	●	●	●							●	●	●						
	Med				●	●	●							●	●	●			
	Low							●	●	●							●	●	●
Chloride Ion Diffusivity*	High	●			●			●			●			●			●		
	Med		●			●			●			●			●			●	
	Low			●			●			●			●			●			●
Submerged Sacrificial Anode Cathodic	N	●	●	●	●	●	●	●	●	●									
	Y										●	●	●	●	●	●	●	●	●

* The descriptions "High", "Med", and "Low" correspond to parameter values indicated in Table 10. All cases were examined for the randomly altered surface chloride pattern (see text); selected cases used the simple pattern shown in Figure 54.

The simulations covered a 100-year service period. Prior to initiating each simulation (i.e., commencement of service life), the chloride concentration in the bulk of the concrete column was set to zero, approximating the typically very low native chloride content. When the simulation begins, chloride ions start to diffuse from the outer concrete surface toward the embedded rebars, as illustrated in Figure 54, using for the initial trial the simple surface chloride profile (as in Figure 56, without random variability).

Chloride concentration at rebar depth (which approximates the shape of the simple surface concentration profile) was plotted for nine-year intervals over the course of the simulation as shown in Figure 55 (top). Local chloride threshold, which varies with local potential, was evaluated at 30-day time steps per the procedure indicated above, but plotted for simplicity only at the point in time that it was first exceeded by local chloride concentration.

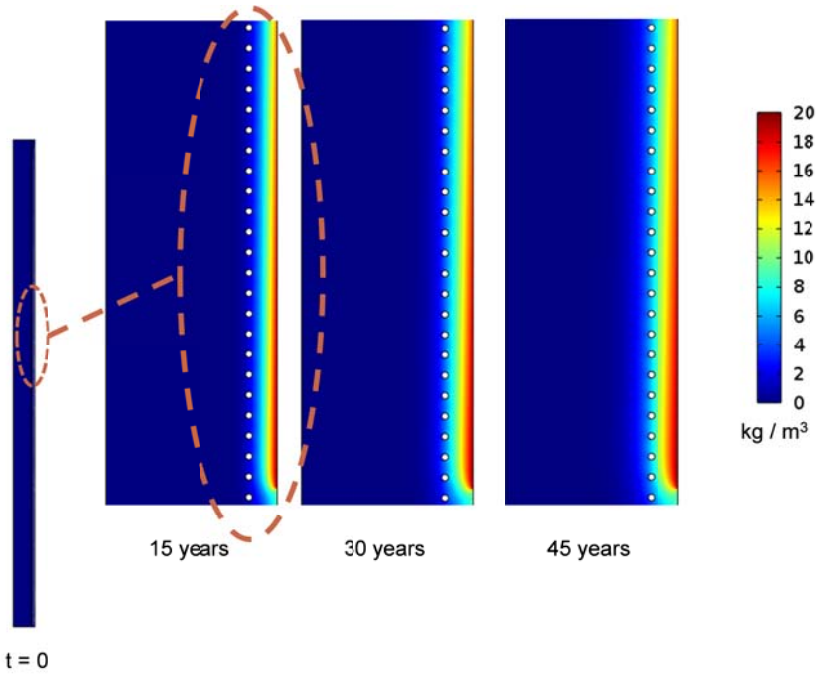

Figure 54. Chloride concentration penetration as function of column age focusing on a region just above the waterline, for a simple surface chloride profile without random variability. Concrete property parameters correspond to the medium chloride ion diffusivity cases in Table 11, simulating a moderately permeable concrete. The scale at right is color coding for the chloride ion concentration.

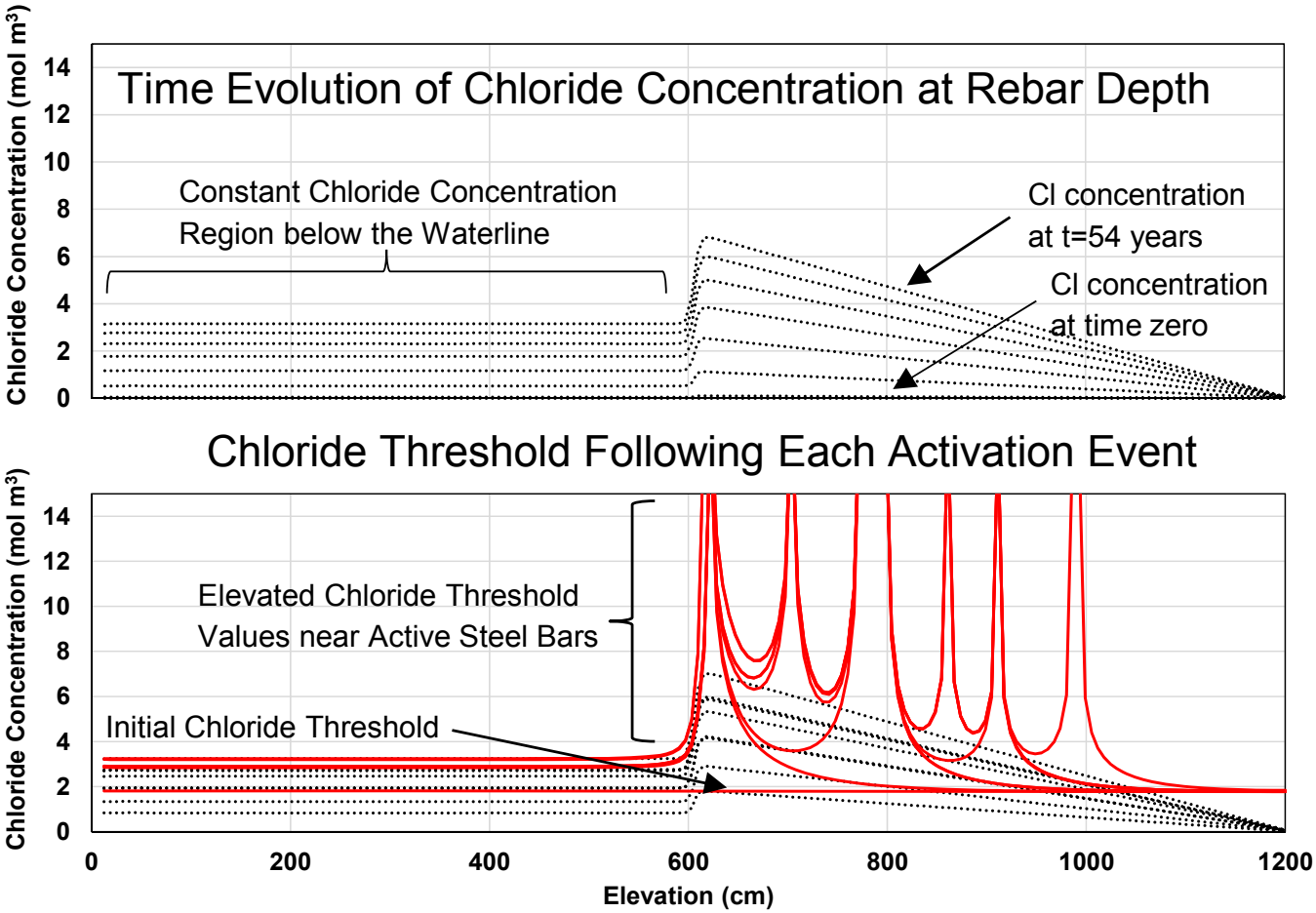

Figure 55. Time evolution of chloride concentration (top) and chloride threshold following each activation event (bottom). Medium chloride ion diffusivity for a simple surface chloride profile without random variability.

The first threshold attainment occurred as expected near elevation 600 cm and is indicated in Figure 55 (bottom) by the intersection of initial chloride threshold curve (lowest red solid line) and the peak of the chloride concentration line (dotted black line). At this point, the rebar at that location was designated active and this accordingly caused a subsequent change in potential distribution in the column. This activation event cathodically polarized nearby bars and thus effectively increased the local chloride threshold as shown by the peak in the next highest red line.

Subsequent threshold attainments yielded additional activation events and corresponding cathodic protection of nearby rebars as shown by other red lines in Figure 55 (bottom). The model kept track of both the resulting corrosion rate at each elevation and the accumulated corrosion penetration P at the rebar surface. For elevations above water, it is assumed that when P reaches a critical value P_{Crit} the accumulation of corrosion products at the rebar-concrete interface will cause cracking of the concrete cover. This criterion has been used successfully in prior modeling efforts [24] where a value P_{Crit} = 100 μm was adopted based on literature observations [37]. Given the rebar size and center-to-center distance used in the simulations, damage in the form cracking and related delamination/spall associated with one rebar reaching the

cracking criterion was quantified as affecting a region of elevation with height *h* around the entire circumference of the column. The value *h* was assigned a value equal to the center-to-center rebar distance, approximately 6.3 cm. Accordingly, the fraction of the external concrete surface having reached the declared damage condition at a given time was simply equal to the number of rebar hoops for which the condition was reached, divided by the total number of rebar hoops. The resulting value as time evolves, expressed as a percentage, is defined as the Damage Function (DF) of the column. For initial presentation of the modeling results, accumulation of corrosion damage in the submerged region was computed using the same criterion as that in the above-water region. Recognizing that corrosion products in the submerged region can be fluid and not result in cracking, hence delaying damage declaration until a greater amount of corrosion has accrued, an alternative damage criterion for bars in the submerged region was considered and is described in greater detail below.

Preliminary calculations were performed using column dimensions and parameters similar to those used in a previous investigation of the PDT concept that implemented a simplified corrosion computation method [24]. The DF results obtained with the present sophisticated FEM model were found to be quite close to those obtained in the previous investigation, serving as a positive check of the functionality of the present implementation.

For the main body of the model realizations explored here, the chloride concentration at the surface of the concrete, Cs was assumed to exhibit a degree of random spatial variability, representing the fluctuations that may be expected in an actual system. The variations were assumed to involve a coefficient of variation (standard deviation divided by average) of 0.25 (25%) around the simplified elevation trend shown in Figure 56 (top). The 25% value was chosen as an example to be on the order of the variability encountered in Cs values in previous investigations of FDOT marine substructure [11].

The profile with surface concentration variability was constructed by selecting elevations evenly separated by 0.5 m, starting from the bottom of the column (a total of 25 values) and multiplying the initial Cs value at each point by the sum (*1+ random adj)* where *random adj* is a number generated by a one-time application of the Microsoft Excel function NORMSINV(RAND())×0.15. As chloride concentration was assumed to vary linearly between local minima and maxima, the value of Cs at any point on the exterior surface of the column elevation was obtained by interpolation of the values declared at the selected points used in the above procedure.

The resulting pattern was used in the entire main sequence of realizations. Figure 56 (bottom) exemplifies the resulting pattern of chloride concentration at the concrete surface and the buildup as function of time at the rebar depth for both the simplified initial surface profile and the randomly altered pattern. The altered pattern captures situations in the submerged portion where corrosion initiation occurs slightly earlier than in the rest, thus generating local anodes and enabling exploration of the implications of PDT behavior.

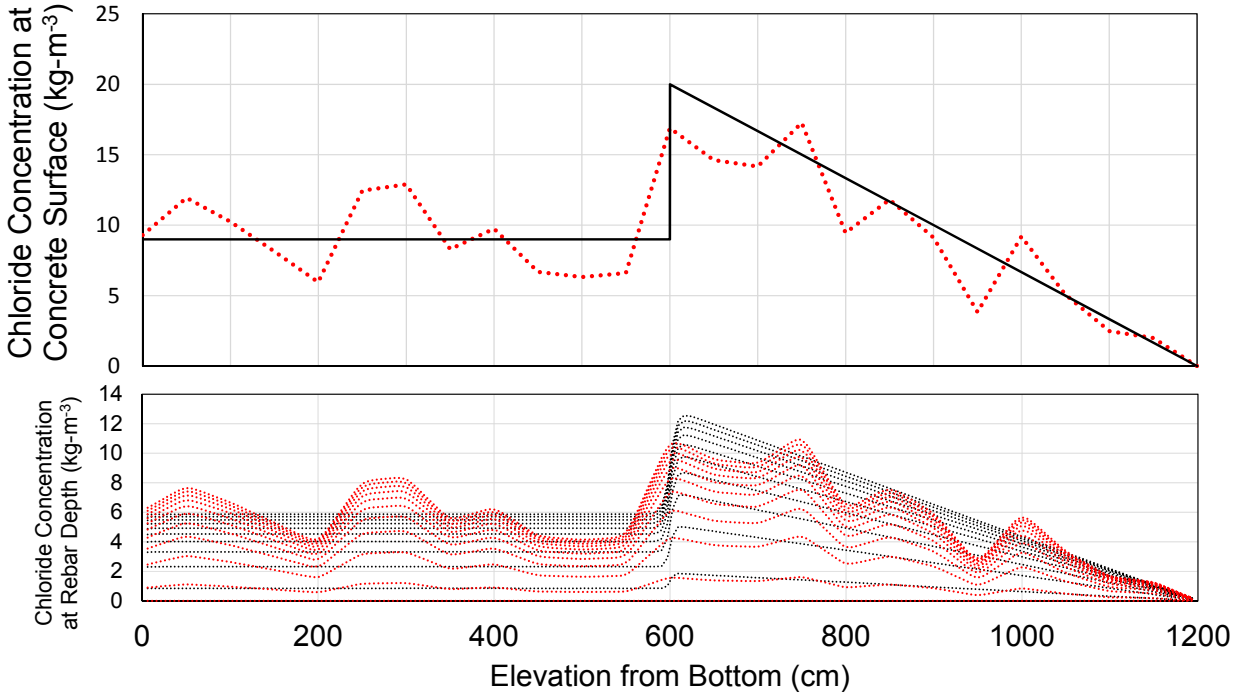

Figure 56. Top: Pattern of chloride concentration at the concrete surface for both the simplified initial surface profile (black solid line), and for the randomly altered pattern (red dotted line). Bottom: Evolution of the concentration profile at the rebar depth for both cases, illustrated for 10-year intervals for a medium chloride diffusivity realization.

In addition to simulating corrosion evolution in a column without intervention, the model was used to examine the effectiveness of corrosion control measures in the submerged zone and low elevation regions of the above-water zone, by means of notional sacrificial anode cathodic protection (SACP). Implementation of this feature represented what would have been accomplished, in practical terms, by installing a stainless steel connecting stud to the rebar assembly at the time of construction, and then installing an anode in contact with seawater at the time that the column was put into service. Given the low resistivity of seawater and the relatively low current densities present in these systems, it was assumed that the connection of the anode resulted in creation of an equipotential condition at the submerged surface of the column, with an operating potential value E_{Prot} characteristic of the anode used. For these realizations the anode was assumed to be a commercial zinc anode with E_{Prot} = -1.05 V (vs CSE). The DF for the SACP cases was then calculated using the same approach as for the freely corroding system, and the reports were reported together for comparison.

3.3.3 Results

It should be emphasized that the model used here, as that for Stage 1, involves a number of assumptions and simplifications, so that projections for specific cases inevitably involve uncertainty from both conservative and non-conservative treatment issues. Nevertheless the model results provide important insight on the corrosion

behavior of the system and on the feasibility of corrosion control. The following findings and discussion are included in that light.

3.3.3.1 Projections for Freely Corroding Systems

The time evolution of corrosion that results from the Stage 2 model assumptions and parameters is illustrated in Figure 57 for Case 1, with the randomly altered *Cs* pattern. For the particular parameter values in this case the potential in the concrete domain is a sensitive indicator of corrosion condition of the nearby steel. More negative potential (redder color) is for the present example indicative of nearby anodic activity, in the fashion of the indications obtained by potential surveys under ASTM C-876[4]. Given the Cs profile shown in Figure 56, the first activation events happened near the waterline. As Case 1 corresponds to a situation of high concrete resistivity, preventive polarization from that early corrosion did not extend strongly to the submerged region. Consequently and as that region had some of the largest Cs values, the next activation events took place there. That situation is manifested by the potential map in Figure 57 for 9 years. As time progressed and chloride content at the steel depth increased, other activation events took place both above and below the waterline and potentials over the submerged zone and some of the splash zone reflected that situation by becoming increasingly negative. The corrosion in the submerged zone remained limited to only a few of the locations through the entire simulated period. As it will be shown subsequently, development of corrosion in the submerged zone became even more restricted when concrete resistivity was low and preventive coupling with corroding regions in the atmospheric zone was more effective.

The DF results for the main series of cases listed in Table 11 are shown in Figure 58. The DFs for the cases without SACP show the typical time trends expected for this kind of system [24] when chloride diffusivity has been assumed, for simplicity, to be the same at all elevations. There is an initial period without any significant damage corresponding to the initial chloride ion buildup at the rebar depth before the corrosion threshold is reached at the point of highest surface concentration. As noted above, in the Cs profile shown in Figure 56, that point is near the waterline and the first activation event occurs there. Corrosion rates are localized and high at that point since no active steel exists elsewhere and the rest of the system is cathodic. The first manifestation of damage occurs therefore quite early there, at a time when the sum of the time-to-activation and the time for metal wastage reaches P_{Crit}. That time is shortest for the cases of lowest resistivity, where the sacrificial macrocell coupling of that first corroding steel to the rest of the rebar assembly is most efficient.

[4] It is noted that if extensive passivity breakdown exists in the submerged zone, as in some of the cases in Figures 50 and 51, the potential value becomes less sensitive of an indicator of corrosion activity.

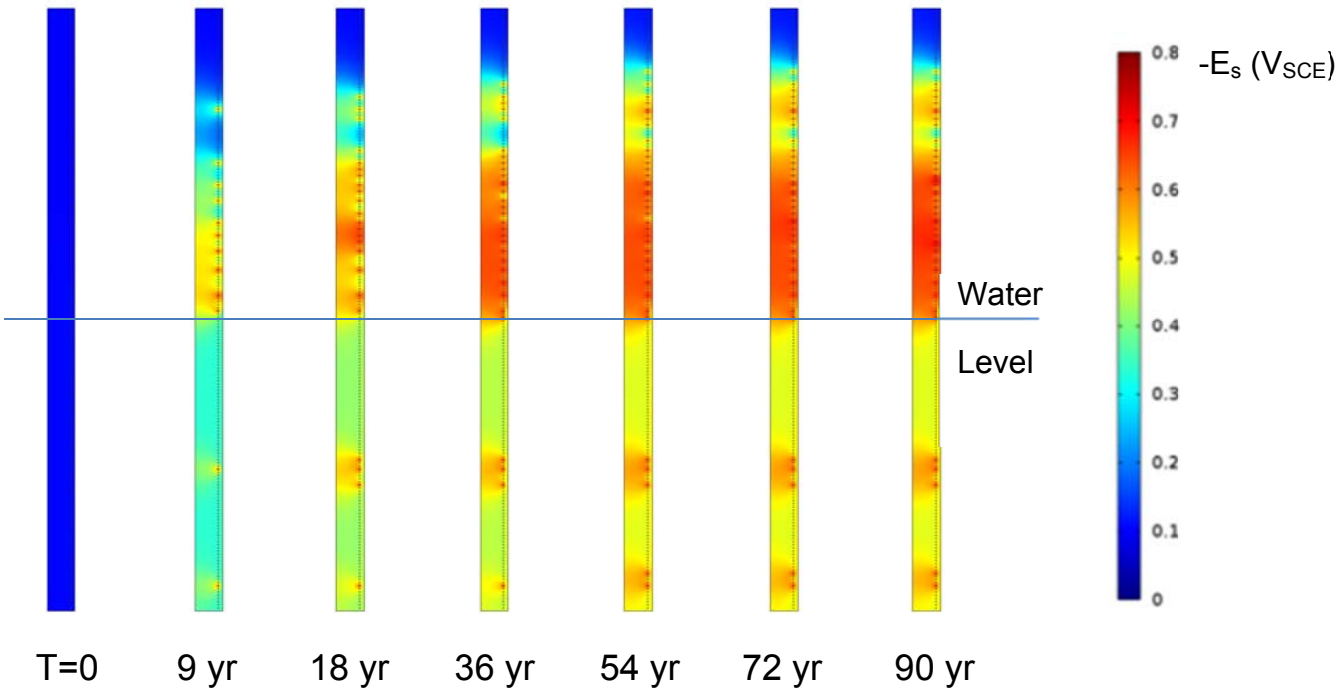

Figure 57. Potential distribution evolution with time for Case 1 (Table 11) with the randomly altered C_S pattern. Note early onset of corrosion in the submerged zone. Potential maps are shown on the vertical column cross section with the cylindrical symmetry axis on left.

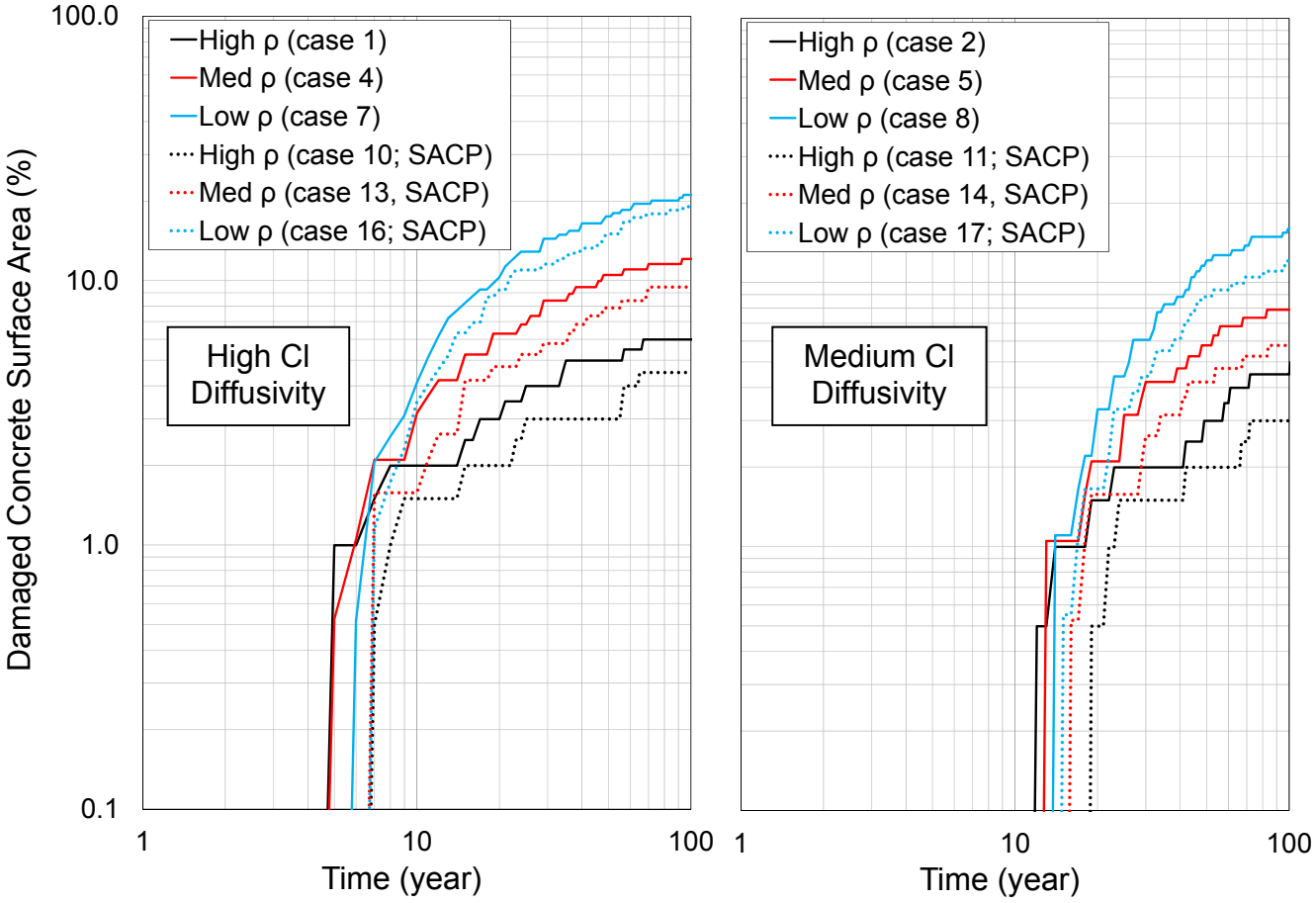

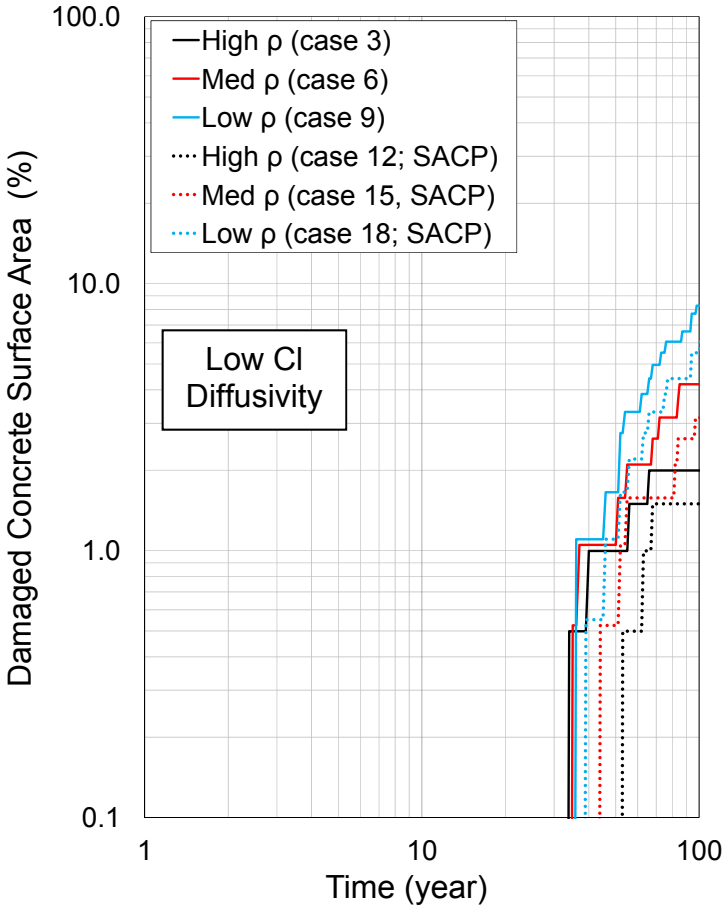

Figure 58. Damage function outputs for the entire column using the above-water damage declaration criterion. Numbers in parentheses are keyed to cases listed in Table 11. The three charts represent damage under three different chloride diffusivities.

As time progresses the initial pattern of dependence of damage on resistivity noted above tends to be reversed. The corrosion preventive effect of the first corroding zone on the rest of the assembly, which results in a delay of the second activation event, is stronger when low resistivity permits more efficient macrocell coupling between corroding and not corroding regions. That effect continues in the chain of subsequent events. Hence as evidenced by comparing the DF plots for a given chloride diffusivity, the long term damage progression becomes (paradoxically) less pronounced with decreasing concrete resistivity.

The dependence of the damage progression on chloride diffusivity is straightforward; the lower the chloride diffusivity the slower the time scale of initial and subsequent activation events. Accordingly the DF plots are displaced to the right as the diffusivity decreases. The time scale of the simulations, 100 years, results in DF projections that agree with typical observations in Florida bridges [11,24,32]. As shown in those sources, for the rebar cover value assumed (7.5 cm), structures with chloride diffusivity on the order of 10^{-7}, 10^{-8}, and 10^{-9} cm^2/s are expected to begin showing some signs of deterioration at times on the order of one decade, a few decades, and from several decades to over 100 years respectively. The DF projections indicate that very conspicuous damage (several % of the column surface exhibiting delamination or spall symptoms) can be expected at structure ages on the order of two times longer than those for appearance of the first signs of damage.

Most of the damage projected in the cases analyzed takes place above the waterline, as is to be expected due to the greater chloride concentration there. A detailed view of the evolution of the part of the corrosion affecting only the submerged region is illustrated in Figure 59.

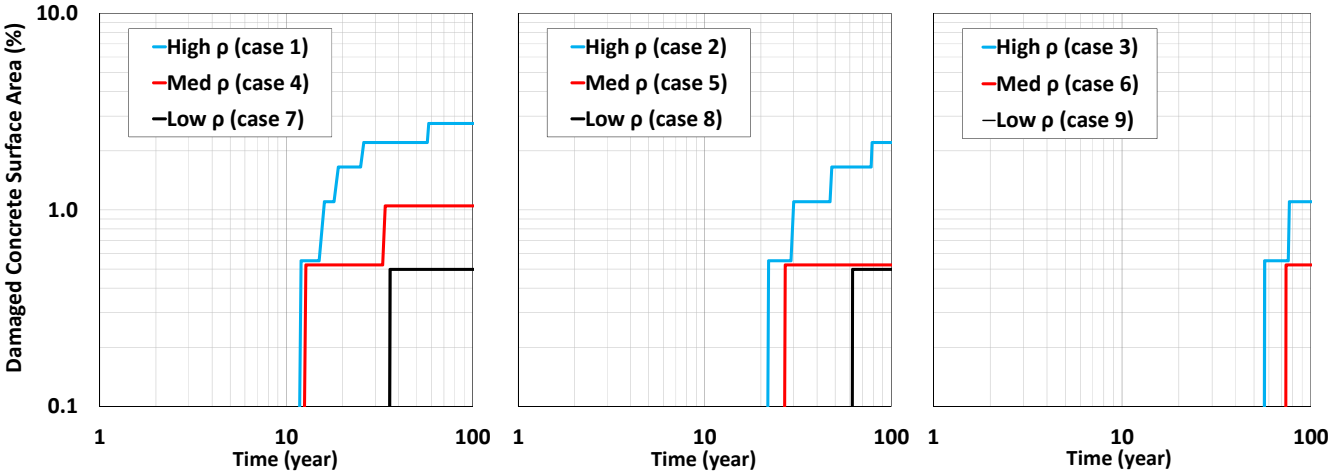

High Chloride Diffusivity Medium Chloride Diffusivity Low Chloride Diffusivity

Figure 59. Damage function output for the submerged portion only, using the alternative damage declaration criterion discussed in the text. The percentages indicated are of the entire column surface; percentages of submerged portion are twice as high. Application of SACP projected complete suppression of corrosion damage in the submerged zone so curves for those cases are not shown.

In this region, an alternative specialized damage declaration criterion has been used. The declaration takes into account that below water the mode of deterioration is not likely to be concrete cracking due to accumulation of solid corrosion products, but rather either loss of bond between rebar and concrete, or simple rebar mechanical failure under acting stresses, both due to steel loss of cross-section by corrosion. A precise determination of the extent of steel loss that could enable either situation is not available. As a working assumption however a conservative estimate may be made whereby bond loss or other adverse mechanical deterioration takes place if rebar cross-section is reduced by corrosion to a level comparable to the low end of rebar production tolerance, e.g., about 5% less than the initial cross-section].

As can be seen, the model projects damage by that criterion on the order of a few percent after several decades of service, in general agreement with the field observations noted in Chapter 2. This observation provided some degree of validation of the modeling approach used and encouraged the use of the model to examine the prospect of success of possible corrosion control methods. That examination is presented in the next section for the case of SACP.

3.3.3.2 Projections for Cathodically Protected Columns

Figure 58 shows the projected DF for the SACP cases in dotted lines with the same line color as the corresponding cases without SACP. Application of the anode significantly delays the projected appearance of first damage in most cases, and also reduces the total amount of projected damage over the long term. Even though the anode is placed in contact with the seawater only, an appreciable extent of the beneficial effect reaches above water, especially at the low elevation zones where the electrolytic conductive path via the column concrete is shortest, and also for the cases where the resistivity of the concrete is lowest. Important to the subject of this project, application of the anode completely prevented the onset of corrosion below water for the entire 100 year simulation period for the entire set of scenarios investigated. Consequently, no DF projection curves for the SACP cases appear in Figure 59.

The electrical current demand on the anode by the large column modeled here (with about 200 sq. ft. of surface below water) was found to be only on the order of 40 mA, a value that changed little with age as new regions on the column surface (all above water) became active. The small current value is consistent with the amount expected to be sufficient to sustain the cathodic reaction at the small limiting current density determined by the water-saturated concrete condition (and consequently small oxygen diffusivity) and a relatively thick rebar cover. For a zinc marine anode with a typical consumption rate of 24.6 lb /year [39], the wastage would be on the order of 1 lb/year, so modest size commercially available anodes such as those used for FDOT jacket rehabilitation systems [38] could conceivably last for long time periods (e.g., decades) in regular piles before needing replacement.

The model-projected benefits provided by SACP (assuming that it starts at the time of construction) include not only virtual elimination of submerged zone corrosion but also a significant reduction of the rate of corrosion damage progression in the low elevation zone above water. A potentially adverse effect could be increased susceptibility to hydrogen embrittlement (HE) of high strength strand in prestressed piles. The operating potential for a zinc anode (assumed to be -1,050 mV SCE in the simulations) is about 100 mV more negative than the potential above which the likelihood of HE is deemed to be greatly reduced [18,41,42]. However, the model calculations indicate that submerged steel potential (at least in the High resistivity cases) is about 35 mV less negative than the assumed anode potential, accordingly reducing the excursion into adverse polarization regimes. Also, typical instant-off steel potential values observed in FDOT substructure field installations with zinc galvanic anodes rarely exceed -900 mV [40], likely due to anode polarization and electrolyte plus metallic circuit resistances, factors only partially accounted for in the present model. Hence the risk from excessive cathodic polarization, while meriting some consideration in future work, does not appear to be a high priority concern.

To further explore that issue, sensitivity to anode potential was evaluated with special model subcases for three cases of particular interest: (1) low concrete resistivity, high chloride diffusivity (Case 16) e.g., old-specification concrete; (2) high concrete

resistivity, low chloride diffusivity (Case 12) e.g., modern-specification concrete; and (3) high concrete resistivity, high chloride diffusivity (Case 10) e.g., modern-specification concrete with deficiency(ies). Damage functions for various anode potentials (-600 mV, -750 mV, -900 mV, and -1,050 mV) are shown in Figure 60. As the figure shows, corrosion suppression below water and in the near waterline region, as projected by the model, was still very effective even if the operating anode potential is much less negative (even at -600 mV) than the -1,050 mV default value used. Furthermore, damage function sensitivity to anode potential within the range explored was shown to be small so the findings seem to be robust with the provisions on model uncertainty noted earlier.

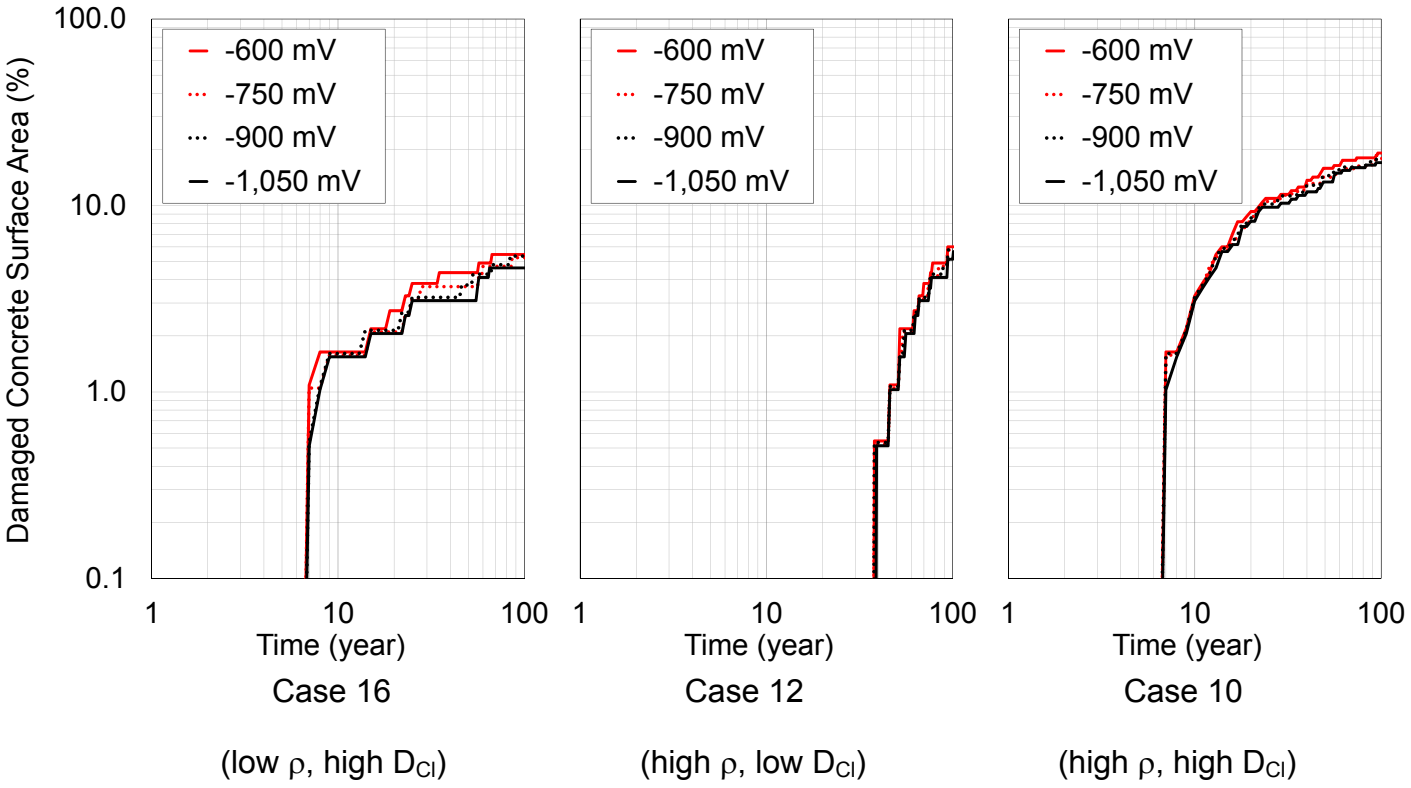

Figure 60. Damage functions based on anode potentials of -600, -750, -900, and -1,050 mV for selected cases. Note minimal sensitivity of damage projections to anode potentials in the given range.

4 SIGNIFICANCE OF FINDINGS AND PATH FORWARD

4.1 Significance of Findings

The most noteworthy findings of this project have been the identification of severe localized steel corrosion in submerged piling of FDOT bridges, and the development of understanding of the underlying phenomena, producing a predictive model suitable to assess corrosion control alternatives. Conventional expectations for corrosion in the submerged region rightfully indicated that in the absence of strong external cathodic regions the overall rate of corrosion would be very low, due to limited oxygen delivery to the surface of the steel. That situation however is true only on the average, and does not preclude the development of small regions of intense corrosion coupled to the remaining part of a generally passive steel assembly. Because of the resulting large cathode-to-anode ratio, even a very small amount of average cathodic reaction can be enough to support a high corrosion rate on small lengths of the steel in the submerged zone.

Chapter 2 documented such instances of severe corrosion affecting only a small percentage of the steel in ~60 year old field extracted piles while the rest of the steel assembly was essentially not corroded. An instance of localized corrosion was present even in epoxy coated rebar in a normally submerged footer chamber at the nearly 30 year-old Sunshine Skyway Bridge. While in that case cathodic action over much of the rest of the rebar assembly is impeded by the presence of the coating, the combined effect of many small imperfections in the coating can supply appreciable cathodic current when aggregated over the very large area of the same structural element.

The modeling effort in Chapter 3 showed quantitatively that the observed corrosion in the piles is fully consistent with the electrochemical mechanism described above, when plausible material properties and polarization parameters are input. The Stage 1 modeling provided insight by indicating that the corrosion below water could be aggravated if some otherwise successful corrosion control methods, such as use of thicker concrete cover and low permeability concrete, would suppress corrosion in the immediate tidal and low elevation atmospheric region. Those regions, where damage is conspicuous and tends to happen early, have received most of the attention in the past. In the absence of corrosion, those regions could support significant external cathodic action (not countered by the suppressed anodic reactions) and be available to enhance corrosion below water. Hence, it is possible that the present accepted strategy of substructure corrosion control, based on extending the length of the initiation stage through high concrete quality and thick cover, may have the unintended effect of greater vulnerability in the submerged zone. This type of effect is likely to become increasingly important as more ambitious durability goals, for example 100 years or more, become the norm.

The above issues were addressed in part by the Stage 2 modeling, which examined the time evolution of corrosion in a generic column/pile for scenarios generally representative of the range of conditions encountered in FDOT bridges. The calculations indicated that the vulnerability to submerged zone corrosion, for a given

rate of chloride penetration in the concrete, tended to be more manifested if the concrete resistivity was high. This behavior is somewhat counterintuitive, as corrosion is usually expected to be more severe if low concrete resistivity permits more efficient macrocell coupling between anode and cathodes. However, higher resistivity also tends to effectively isolate the candidate new anodic sites (while they are still in the passive condition) from previous, already active anodic regions. That isolation diminishes macrocell coupling which in that case is actually beneficial by making the potential of the candidate sites more negative, thus preventing or delaying new corrosion initiation events. Those previous corroding regions could include other submerged zone corroding spots, or the region immediately above water as noted earlier. As the best performing concrete formulations used by FDOT (e.g., Class V concrete) have also high resistivity, the condition noted above may be of special interest when considering behavior after the structure has accrued a long service life.

From the standpoint of damage development with time, the Stage 2 model projections suggest that substantial incidence of submerged zone corrosion could take place already during the first few decades of service for the most permeable concretes in the present FDOT bridge inventory. For medium quality concrete the damage is projected to develop after several decades of service. For the modern, highest quality concretes in sound condition the damage prognosis indicates some concern only at times on the order of the present 75-year design service life. However, it is noted that those projections have not evaluated the case of cracked concrete. If cracks were to occur for example during pile driving, chloride penetration and hence corrosion initiation at the crack/steel intersection could happen very fast. Thus, the damage development at cracks below water in otherwise high quality concrete may resemble that of the high resistivity, but medium or even high chloride diffusivity concrete. Thus, the possibility of topical severe corrosion at the spots affected by cracking could not be ignored under those circumstances.

The Stage 2 model also permitted evaluating the effectiveness and feasibility of controlling submerged zone corrosion by means of a sacrificial cathodic protection anode. The results were encouraging, projecting virtual suppression of submerged zone corrosion and some additional benefit in reducing corrosion in the immediate tidal zone above water. The projected rate of anode consumption was low enough to indicate that application of a regular modestly sized and priced commercial anode could offer effective corrosion control over a period of decades before need for replacement.

4.2 Path Forward

The project developed information on the rate and modality of corrosion loss of reinforcement of submerged components, developed a modeling tool to assess how corrosion will develop in new and existing structures, and established good prognosis for a candidate means of control of that corrosion. This information can be highly useful for the development of corrosion control strategies toward increasing the durability of the extended FDOT bridge inventory. That development can benefit from the following future actions offered here for subsequent discussion and consideration by FDOT. The

list is not exhaustive and other areas of potential benefit should be considered upon future examination of this report:

1-Assessment of the structural and economic implications of the degree and type of corrosion considered here. The main modality of deterioration in the submerged zone is not likely to be cracking of the concrete cover, as is the case of above-water corrosion. Instead, loss of rebar or strand cross-section with consequent loss of strength and bond is likely to be of more consequence. Hence there is strong need for defining an alternative limit state (i.e., other than visible external cracks and spalls) for submerged reinforced concrete. The amount of the material loss and its evolution with bridge age can be projected using the Stage 2 model or variations thereof, as will be noted below. However, evaluation of the weakening structural effect of losing cross-section to a given extent over a given small length of steel was not within the scope of this project. Now that the presence of that corrosion has been established it is of importance to assess the extent of that effect for various relevant pile configurations, dimensions, and modes of service loading. Both structural and engineering economic issues should be investigated. Assessment is needed to establish the importance of submerged zone corrosion relative to other modes of aging of structures, and thus prioritize future FDOT needs and solutions for this issue.

2-Consideration of need and means to fit sacrificial anode cathodic protection in new piling. As part of and based on the outcome of the structural and economic analysis, the feasibility of fitting new piling with provisions for installation of cathodic protection anodes and interconnection of strands should be evaluated. The analysis should include examination of pile design, and practice for best location for possible external contacts based on pile size and configuration. Should the analysis of this and the prior issue find it to be in order, guidelines should be formulated for when and how to effect incorporation of cathodic protection anodes in new or existing piling.

3- Next generation modeling. As in any modeling effort, sweeping assumptions and simplifications have been made in the Stage 2 model in the interest of practicality and of addressing the issues clearly requiring the most immediate attention. The following areas represent some of the more pressing issues that merit attention toward creating a more realistic picture of the system of interest in next generation models:

> 3a: Effect of preexisting concrete cracking. This feature is not implemented directly at present except in a qualitative basis, by replacing a given chloride diffusivity designation e.g., “Low” by “Medium” or “High”. A quantitative treatment by assuming a given incidence of cracking and topically fast chloride penetration rates should be implemented for more informative analysis. The treatment used by Lau [2] and Busba [26] may serve as an initial step.
>
> 3b: Statistical dispersion of more system properties. The present model addresses stochastic distribution of the surface chloride concentration only. For a more realistic representation of damage projection variability of other parameters (especially concrete cover) should be introduced. These features

would capture more accurately and more conservatively the early stages of damage development, and improve rational selection of corrosion control alternatives and more accurate cost benefit analyses. The approach recently developed for FDOT in Project BDK84 977-09 [43] is an example of a procedure that could be adopted for this purpose. Additional realizations with variations of the stochastic distribution themselves (e.g., alternative versions of the pattern in Figure 56) should be conducted as well and the results averaged accordingly.

3c: Three-dimensional (3-D) representation. The present model assumes cylindrical geometry for simplicity, resulting in a simulated ring-pattern of damage that is only a coarse representation of actual systems. A next generation model capturing more realistic features should use a full 3-D geometry, which would have the added benefit of more precisely simulating corrosion damage development in square piles. This transition should be coupled with the statistical variability of parameters approach to better simulate the random development of corrosion damage. The next generation model should also account in more detail for the tidal zone of the piling, which in the present model is roughly simplified as a sharp transition from submerged to above-water regimes.

4-Increased base of field observations. Due to limited opportunities during the execution period, this project examined only piles of relatively aged FDOT bridges, mostly with highly permeable concrete. As new opportunities arise, samples of extracted pilling from a wider variety of FDOT bridges should be sought and examined adopting whenever practical the methodology established in this investigation. Of special interest would be decommissioned piles made with more recent, less permeable concrete formulations representative of present and future FDOT construction.

5 CONCLUSIONS

1. Severe corrosion of steel can occur in the submerged portions of reinforced concrete structures in marine environments. Field studies of decommissioned piling from Florida bridges revealed multiple instances of strong corrosion localization, showing appreciable local loss of steel cross-section. An instance of localized corrosion was also found in a submerged pier footer chamber at the Sunshine Skyway Bridge.

2. Quantitative understanding of the phenomenon and its causes has been developed and a predictive model was created based on that understanding. Corrosion rate estimates and the extent of corrosion localization from the field observations are consistent with the results of the predictive model.

3. The following factors were found to affect the likelihood and severity of corrosion of steel in submerged reinforced concrete structures and members:

    - Localization: Cathodic reaction rates under oxygen diffusional limitation that are negligible in cases of uniform corrosion can support substantial corrosion rates in cases of localized corrosion.

    - Extent of electrochemical macrocell coupling between different zones of the piling: Mutual prevention or aggravation of corrosion may take place depending on factors such as electric resistivity of the concrete. Eliminating corrosion in the evaporative/splash zone could in some cases increase corrosion vulnerability of steel in the submerged region.

4. Results indicate need for defining an alternative limit state (i.e., other than visible external cracks and spalls) for submerged reinforced concrete, and for determination of the possible structural consequences of this form of corrosion in future work.

5. The predictive model developed under this project serves as a tool for exploring the progression of corrosion with structure age as function of designs with alternative concrete properties. For piling without deficiencies built with modern concretes currently specified by FDOT the prognosis for long term durability is good. However, deficiencies such as cracking that may allow for fast local chloride penetration that may induce early damage in the submerged zone.

6. The modeling tool projected that with use of sacrificial anode cathodic protection corrosion in the submerged zone could be virtually eliminated, together with significant reduction of the rate of corrosion damage progression in the low

elevation zone above water. Continuation work should be conducted to assess the technical feasibility and cost/benefit aspects of incorporating anodes, or provisions for anode placement, in future specification guidelines for bridge piling and other submerged elements.

7. It is recommended that as new opportunities arise, samples of extracted pilling from a wider variety of FDOT bridges should be sought and examined adopting whenever practical the methodology established in this investigation. Of special interest would be decommissioned piles made with more recent, less permeable concrete formulations representative of present and future FDOT construction.

8. It is also recommended that a next generation modeling tool be developed in continuation work for more accurate assessment of the extent and consequences of corrosion in submerged substructure. New features of importance to be incorporated should include effect of preexisting cracking, statistical dispersion of more system properties, and three dimensional representation of the system.

REFERENCES

[1] Sagüés, A., Lau, K., Powers, R. and Kessler, R., "Corrosion of Epoxy Coated Rebar in Marine Bridges. Part I- A 30 Year Perspective", *Corrosion*, Vol. 66, p. 065001 (2010).

[2] Lau, K., Sagüés. A. and Powers, R., "Corrosion of Epoxy Coated Rebar in Marine Bridges. Part II- Corrosion in Cracked Concrete ", *Corrosion*, Vol. 66, p. 065002 (2010).

[3] Beaton, J.L., Spellman, D.L., and Stratfull, R.F., *Corrosion of Steel in Continuously Submerged Reinforced Concrete Pile*, Report No. M&R 635116, California Division of Highways, Sacramento, CA, (1967).

[4] Bertolini, L., Elsener, B., Pedeferri, P., and Polder, R. Corrosion of Steel in Concrete: Prevention, Diagnosis, Repair. Wiley-VCH, Weinheim, Germany (2004).

[5] Sagüés, A.A., Kranc, S.C., and Lau, K. "Service Life Forecasting for Reinforced Concrete incorporating Potential-Dependent Chloride Threshold." *Corrosion/2009*, Paper No. 09213. NACE International, Houston, TX p. 22 (2009).

[6] Kranc, S.C. and Sagüés, A.A., "Computation of Reinforcing Steel Corrosion Distribution in Concrete Marine Bridge Substructures", *Corrosion*, Vol. 50, p.50 (1994).

[7] Raupach, M., "Chloride-induced macrocell corrosion of steel in concrete—theoretical background and practical consequences", *Construction and Building Materials*, Vol. 10, p. 329 (1996).

[8] Kranc, S.C. and A.A. Sagüés "Computation of Corrosion Distribution Of Reinforcing Steel in Cracked Concrete", in Proc. International Conference on Corrosion and Rehabilitation of Reinforced Concrete Structures, Orlando, FL, Dec. 7-11, 1998, CD ROM Publication No. FHWA-SA-99-014, Federal Highway Administration (1998).

[9] Gjorv, O., "Steel corrosion in concrete structures exposed to Norwegian marine environment", P.K. Mehta Symposium on Durability of Concrete, Proc. of the Third CANMET/ACI International Conference on Durability of Concrete, Nice, France. American Concrete Institute, Detroit, MI. p. 243 (1994).

[10] Espelid, B. and Nilsen, N., "A field study of the corrosion behavior on dynamically loaded marine concrete structures", in Concrete in Marine Environments, Proc., 2nd. Int. Conference, V.M. Malhotra, Ed., SP-109. American Concrete Institute, Detroit, MI. p. 85 (1988).

[11] Sagüés, A.A., Kranc, S.C., Presuel-Moreno, F., Rey, D., Torres-Acosta, A, and Yao, L., *Corrosion Forecasting for 75-Year Durability Design of Reinforced Concrete*, Final Report to Florida D.O.T. WPI 0510805. University of South Florida, Tampa, FL (2001) Available online at www.dot.state.fl.us.

[12] Polder, R.B., Peelen, W.H.A. and Leegwaer, G., Tailor Made Concrete Structures, Walraven, and Stoelhorst, Eds. Taylor and Francis Group, London, England. p.187 (2008).

[13] Coppola, L., Fratesi, R., Monosi, S., Zaffaroni, P., and Collepardi, M., "Corrosion of Reinforcing Steel in Concrete Structures Submerged in Seawater", Third CANMET/ACI International Conference on Performance of Concrete in Marine Environment, SP 163-5. pp. 127, 134, 138 (1996).

[14] "Corrosion Condition Evaluation of Bridge Substructure Bridge Nos. 139002, 139003, 159007, and 159008", Florida Department of Transportation Corrosion Research Laboratory, Gainesville, FL (2002).

[15] Angst, U., Vennesland, O., and Myrdal, R., "Diffusion Potentials as Source of Error in Electrochemical Measurements in Concrete", *Materials and Structures,* Vol 42. pp. 365-375 (2009).

[16] Sagüés, A.A., Moreno, E., Morris, W., and Andrade, C., "Carbonation in Concrete and Effect on Steel Corrosion", FDOT State Job No. 99700-3530-119, WPI 0510685 pp. 39, 52, 58. University of South Florida, Tampa, FL (1997).

[17] Cáseres, L., Sagüés, A.A., Kranc, S.C., and Weyers, R.R., "In-Situ Leaching Method for Determination of Chloride in Concrete Pore Water", *Cement and Concrete Research*, Vol. 36, p. 492 (2006)

[18] Broomfield, J. "Corrosion of Steel in Concrete: Understanding, Investigation and Repair, Second Edition" CRC Press 2006.

[19] Kranc, S.C. "Decreased Corrosion Initiation Time of Steel in Concrete Due to Rebar Obstruction of Diffusional Flow", with A.A. Sagüés and F.J. Presuel-Moreno, *ACI Materials Journal*, Vol 99,No.1, pp 51-54, 2002.

[20] USGS TWRI Book 9–A7 (Third Edition) Five-Day Biochemical Oxygen Demand (11/2003), p. 11. Available online at (https://water.usgs.gov/owq/FieldManual/Chapter7/NFMChap7_2_BOD.pdf).

[21] Simon, F.A., et al. Improvement of the analysis of the biochemical oxygen demand (BOD) of Mediterranean seawater by seeding control. Talanta 85, pp. 527-532 (2011).

[22] Florida Department of Transportation, Bridge Environment Data, Last updated June 29, 2015. Available online at http://www.dot.state.fl.us/statematerialsoffice/administration/resources/library/publications/bridge/environment.pdf.

[23] Presuel-Moreno, F.J., Sagüés, A. A., Kranc, S.C. "Steel Activation in Concrete Following Interruption of Long Term Cathodic Polarization", *Corrosion*, Vol. 61, p.428 (2005).

[24] Sagüés, A.A., Sánchez, A.N., Lau, K., and Kranc, S.C., “Service Life Forecasting For Reinforced Concrete Incorporating Potential-Dependent Chloride Threshold”, *Corrosion*, Vol. 70, pp. 942-957 (2014).

[25] Sánchez, A.N. and Sagüés, A.A., “Chloride Corrosion Threshold Dependence on Steel Potential in Reinforced Concrete”, Paper No.4118, *Corrosion/2014*, NACE International, Houston (2014).

[26] Busba, E. and Sagüés, A.A., “Localized Corrosion of Embedded Steel in Cracked Reinforced Concrete Pipes”, *Corrosion*, Vol. 69, pp. 403-416 (2013).

[27] Fontana, M. Corrosion Engineering, third edition. NewYork, NY: McGraw-Hill, (1987).

[28] Sagüés, A.A., Sánchez, A.N., Lau, K., and Kranc, S.C., “Service Life Forecasting For Reinforced Concrete Incorporating Potential-Dependent Chloride Threshold”, *Corrosion*, Vol. 70, pp. 942-957 (2014).

[29] Pedeferri, P., Cathodic Protection and Cathodic Prevention, *Construction and Building Materials,* 10(5): p. 391-402 (1996).

[30] Figg Bridge Inspection, Inc. “Sunshine Skyway Bridge Specialty Engineers Report” January 23, 2013.

[31] Sagüés, A.A., Perez-Duran, H., and Powers, R., “Corrosion Performance of Epoxy-Coated Reinforcing Steel in Marine Substructure Service”, *Corrosion*, Vol 47, p.884, (1991).

[32] Sagüés, A.A., Lee, J.B., Chang, X., Pickering, H., Nystrom, E., Carpenter, W., Kranc, S.C., Simmons, T., Boucher, B., Hierholzer, S., *Corrosion of Epoxy Coated Rebar in Florida Bridges*, Final Report to Florida D.O.T. WPI 0510603, University of South Florida, Tampa, FL, 135 pp. (1994).

[33] Alonso, C., Castellote, M., and Andrade, C. "Chloride threshold dependence of pitting potential of reinforcements" Electrochimica Acta, vol. 47, pp. 3469-3481 (2002).

[34] Alonso, C., Castellote, M., Andrade, C., and Castro, P. “Chloride threshold values to depassivate reinforcing bars embedded in a standardized OPC mortar”, *Cement and Concrete Research*, vol. 30, pp. 1047-1055 (2000).

[35] Li, L., and Sagüés, A.A., “Chloride Corrosion Threshold of Reinforcing Steel in Alkaline Solutions – Cyclic Polarization Behavior”, *Corrosion*, Vol. 58, p.305 (2002).

[36] Enos, D. G., Williams, A. J., and Scully, J. R. “Long-Term Effects of Cathodic Protection on Prestressed Concrete Structures: Hydrogen Embrittlement of Prestressing Steel”, *Corrosion*, Volume 53, Number 11, Pages 891-908 (1997).

[37] Torres-Acosta, A. and Sagüés, A.A., “Concrete Cracking by Localized Steel Corrosion - Geometric Effects”, *ACI Materials Journal*, Vol. 101, p.501 (2004).

[38] Florida Department of Transportation., “Technical special provision for cathodic protection of integral pile jacket system” Specification 4570000, (2010).

[39] Roberge, P., “Corrosion Engineering: Principles and Practice”, McGraw-Hill, New York (2008).

[40] Presuel-Moreno, F. and Hartt, W., *Protection of Reinforced Concrete Bridge Substructures using Submerged Bulk Anodes, Final Report to Florida D.O.T., Project BD546-3*, Florida Atlantic University, Boca Raton, FL (2009). Available online, www.dot.state.fl.us.

[41] Hartt, W. H., Kumria, C.C., and Kessler, R.J., “Influence of Potential, Chlorides, pH, and Precharging Time on Embrittlement of Cathodically Polarized Prestressing Steel”, *Corrosion Journal*, Volume 49, Number 5, pp. 377-385 (1993).

[42] Hartt, W., Poeydomenge, A., Stauder, A. and Scannell, W., *Long-term effects of cathodic protection on prestressed concrete bridge components*, Report No. FHWARD-98-075, Published by NTIS, (1998).

[43] Sánchez, A.N. and Sagüés, A.A., *Modeling Reinforced Concrete Durability*, Final Report to Florida Dept. of Transportation, Report No. BDK84 977-09, 73 pp. (2014).